6-2-2011

Model based assessment of potential impacts of climate change on the flow of the main headwaters of the Nile River: Equatorial Lakes Region and Blue Nile Basins

Fisseha G. Berhane
fishcivilmu@yahoo.com, fishcivilmu@yahoo.com

Model based assessment of potential impacts of climate change on the flow of the main headwaters of the Nile River: Equatorial Lakes Region and Blue Nile basins

by

Fisseha Berhane

A Thesis

Submitted to the Graduate Faculty of

The University of Connecticut

In partial fulfillment of the

Requirement of the degree of

Master of Science

Natural Resources and the Environment

May 2011

APPROVAL PAGE

Master of Science Thesis

Model based assessment of potential impacts of climate change on the flow of the main headwaters of the Nile River: Equatorial Lakes Region and Blue Nile basins

Presented by

Fisseha Gebremariam Berhane, B.Sc.

Major Advisor _____
Dr. Richard Anyah

Associate Advisor _____
Dr. Xiusheng Yang

Associate Advisor _____
Dr. Glenn Warner

The University of Connecticut

2011

Abstract

Berhane Fisseha. Model based assessment of potential impacts of climate change on the flow of the main headwaters of the Nile River: Equatorial Lakes Region and Blue Nile basins (Under the direction of Dr. Richard Anyah).

Spatially and temporally detailed assessment of the hydrologic processes of the main sources of the Nile River headwaters (Blue Nile basin and Equatorial Lakes Region) is vital for basin-wide scale management to cope with the pressing water problems due to burgeoning populations, a growing demand for electricity, irrigation for food production and possible climate change.

The main objectives of this study were to use a physically-based, semi-distributed hydrological modeling system (Soil and Water Assessment Tool-SWAT) to study the hydrological processes of the Blue Nile and Equatorial Lakes Region subbasins, and investigate the potential impacts of climate change in the Blue Nile basin based on regional surrogate climate change scenarios (SCCS).

The lack of weather data is the main hindrance for hydrologic research in the Nile River basin. The distribution of the available weather and discharge observation stations is quite uneven. Moreover, the quality of the data is not reliable, and there are often large amounts of missing data. Required weather data for SWAT model, including daily precipitation, daily maximum and minimum temperature, were stochastically generated from the Climatic Research Unit (CRU) gridded monthly weather dataset using Monthly to Daily Weather Converter (MODAWEC). As it is difficult to manually calibrate such a

complex model with many parameters, the Sequential Uncertainty Fitting (SUFI2) algorithm was used for calibration and to quantify uncertainty.

The model over the Blue Nile calibrates reasonably well bracketing 90% of the observed river discharge and introducing an R^2 of 0.93 and Nash-Sutcliffe (NS) of 0.93 for calibration and R^2 of 0.92 and NS of 0.92 for validation. The Equatorial Lakes Region has many lakes and data about the regulated lake Victoria were not found. This resulted in poor model performance. The study showed that downscaled gridded monthly weather data can be used in data scarce areas like the Nile basin where the measuring gages are small in number (not with the recommended density of observation stations), unevenly distributed and sometimes with much missing and erroneous data. The final goal of this study is to achieve an accurate representation of the monthly water balance with SWAT. It is unrealistic to model daily water flows using generated daily weather data. The study showed that SWAT can be used to study environmental change impacts on water resources and the competition for water resources by different sectors in the Blue Nile basin.

Surrogate climate change scenarios (SCCS) were used as input to the calibrated SWAT model to investigate the possible impacts of potential climate change on the hydrology of the Blue Nile basin. The surrogates were approximated using Intergovernmental Panel on Climate Change (IPCC-2007) data. Surrogates for A2, B1 and A1B were considered. The period from 1960-2000 was used as baseline and has been used to determine the changes and the effect of the surrogate climate changes. A simulation study of climate change effects on the basin demonstrates that the hydrology of the basin is very sensitive to

climate change with 104%, 33% and 77% of the baseline increase to the surface runoff, lateral flow and water yield, respectively, for the A2 scenario surrogate.

ACKNOWLEDGMENTS

I am thankful to National Science Foundation for financial support for this study. I am also grateful to my major advisor Dr. Richard Anyah for his supervision and unreserved professional and material help. I would also like to acknowledge Dr. Glenn Warner and Dr. Xiusheng Yang for their invaluable and constructive guidance.

I am indebted to Dr. Mekonnen G/Micael, Dr. Daba Gedafa, Menberu Bitew, Dr. Dawit Zeweldi, Feyera Hirpa, Vincent Owanda, among others for their support.

I sincerely thank my wife Freweiny for always being there for me. My son Athanasius, you are my joy.

Last but not least, I thank Almighty God for His limitless blessings, love and care.

TABLE OF CONTENTS

LIST OF FIGURES

LIST OF TABLES

CHAPTER ONE

1.0 INTRODUCTION

Climate change associated with increased emissions of greenhouse gases (GHGs) is of great concern as its impacts on hydrological systems threaten the availability, supply and sustainability of water resources. Climate issues are interwoven with many elements of our livelihoods and need deliberate and multi-dimensional efforts to avert their adverse effects.

The impacts of climate change are expected to be more devastating within the Nile River basin countries that primarily depend on the available water resources to support their dominant agro-based economic and social developments. Disasters from climate/weather related phenomena such as floods, droughts and landslides can also be amplified in the Nile River basin due to accelerated population increase, poor land use practices, unsustainable farming practices, and deforestation, among others. Furthermore, the riparian countries have limited capacity to adapt to projected climate change and have weak disaster preparedness capabilities as well as early warning systems for mitigation measures.

Many previous studies show that many parts of the Nile River basin, which provides an invaluable source of livelihood to over 300 million people, are sensitive to climatic variations (Conway and Hulme, 1996; Yates and Strzeperk, 1996, 1998a, b; Conway, 2005; Kim *et al*., 2008; Beyene *et al*., 2009). This implies that climate change will have considerable impact on the water resources. The average climatic conditions in the Nile River basin and their variability and frequency are expected to change.

Mohamed et al., (2005) stated that in many river basins steady climatic conditions are no longer considered a valid assumption for sustainable water resources management. They stressed that appropriate water resources planning and management at river basin level is viable only by considering the complete water cycle in the basin, including both the land surface and atmospheric processes. Spatially and temporally detailed assessments of hydro-climatic processes of a basin are essential for rational decision-making in water resources planning and management. Further changes and uncertainties in the allocation of Nile River water resources may have significant effects on local and regional economies, agricultural production, energy availability, and environmental quality (Conway et al. 1993; Yates *et al*., 1998; Hulme *et al*., 2005; Beyene *et al*. 2009).

The Nile River basin consists of 10 countries: Burundi, Eritrea, Ethiopia, Kenya, Rwanda, Sudan, Uganda, Tanzania, Democratic Republic of Congo and Egypt. The portion of the sub-Saharan Africa that depends entirely on the Nile River for its water supply is particularly susceptible to hydrologic changes that might be associated with warmer climate (Beyene *et al*., 2009). The Nile River Basin is faced with very high population growth rates which makes flooding and droughts difficult to cope with. In the face of the increasing pressures on water supplies due to dwindling resources, competitive uses as well as other transboundary social, political and legislative conditions are becoming a big challenge and potential source of conflicts in the basin.

The burgeoning populations, a growing demand for electricity and irrigation for food production together with climate change impacts call for robust basin-wide, far-sighted, management alternatives. Hence, understanding the hydrologic processes of the main

sources of the Nile River headwaters: Blue Nile and Equatorial Lakes Region, and their sensitivities to potential climate change is vital for basin-wide scale management.

1.1 Justification and Objectives

There is an imbalance in the primary producers and consumers of the Nile basin's water resources, with Egypt and the Sudan being completely dependent on the Nile water as their primary water source. The water demand in Egypt alone is said to increase (Conway, 1993) while the other riparian countries are increasing their share of the Nile water usage for different sectors. This situation now requires all the riparian countries to have basin-wide scale management of the Nile water resources which requires comprehensive understanding of the hydrologic cycle, and interactions of climate and hydrology in the basin.

In this study we are motivated by two main objectives. The first objective is to apply a semi-distributed hydrologic model to perform a suite of simulations aimed at understanding the hydrological processes influencing the primary sources of the Nile River headwaters: Equatorial Lakes Region and Blue Nile basin. It is important to understand the hydrology of the catchments, particularly the physical processes occurring within the catchments and the influenced water balances within the sub-catchments. The second objective is to study the response of the hydrological (physical) processes in the Blue Nile basin to extreme climatic conditions, climate variability and potential climatic changes under various scenarios. This can give valuable insight how the Nile River flow will respond to climate change since the Blue Nile basin is the main contributor of the

Nile River flow, which in return can inform better management and development of water resources within the riparian countries.

Water resources planning studies, which typically are conducted for time horizons of several decades, require consideration of ongoing global climate change and uncertainties in the signature of future climate change (Beyene *et al.,* 2009*).* Planning of water resources without full understanding of the impact of climate change can no longer be sustainable. With mainly agro-based economies, climate change has important consequences on the socioeconomic stability and sustainability of the Nile River basin riparian countries. Therefore, in depth understanding of the potential climate change impacts on the water resources is critical for sustained socioeconomic development in the region. The near certainty of increased future water demand in the riparian countries (notwithstanding uncertainty of magnitude of increase in demand) contrasts with the uncertainty of climatically-induced changes in the water supply of the Nile River basin (Strzepek et al., 1995; Conway et al., 1996; Yates et al., 1998a; Strzepek et al., 2000; Beyene et al., 2009*).* Hence, there is still need to undertake comprehensive study to examine the mechanisms associated with dynamical and physical processes influencing the hydrology of the Nile River basin, especially in a changing climate. Consequently, the central theme of this thesis research focuses on:

(a) Application of a semi-physically-based, semi-distributed hydrological modeling system (Soil and Water Assessment Tool-SWAT) to study the hydrological processes of the Blue Nile and Equatorial Lakes subbasins

(b) Investigation of potential impacts of climate change in the Blue Nile basin, based on surrogate climate change scenarios.

1.2 Study Area

Joining Lake Victoria with the Mediterranean Sea and stretching for over 35^{o} latitude, the Nile River is the longest river in the world with a latitudinal gradient of flow from the southern hemisphere to the northern hemisphere (Figures 1 and 3-a). It flows 6650 km before it reaches the Mediterranean Sea. Its main sources are the Ethiopian plateau and the Equatorial Lakes Region (Figures 3-a and 4-b). The Nile River basin is formed by three tributaries: the Blue Nile, the White Nile which consists of the Equatorial Lakes Region and Sobat, and the Atbara (Tazebe *et al*., 2007), see Figure 4-b. The upper Blue Nile basin which has an area of approximately 174,000 km^2 (Figure 3) and the portion of the Equatorial Lakes Region upstream of the outlet at lake Albert with an approximate area of 410,024km^2 (Figures 4-a, 22) are considered in this study.

Mohamed *et al*., (2005) stated that the relative contribution to the mean annual Nile River water at Aswan of 84.1 Gm^3 is approximately 4/7 from the Blue Nile, 2/7 from the White Nile (of which 1/7 is from Sobat) and 1/7 from Atbara River (Figure 4-b). They also added that the Ethiopian catchment (Sobat, Blue Nile and Atbara River) contributes to about 6/7 of the Nile water resources at Aswan.

Beyene *et al., (*2007) stated that the headwaters of all the tributaries of the Blue Nile are in the highlands of Ethiopia, and the bulk of their runoff (70% on average) occurs between July and September.

The Nile River basin covers areas with large topographical variations, orographic complexities and different geographical features and climatic regimes (Figure 3, a and b).

The lakes in the basin (Figure 1) account for more than 84,300 km^2. The area covered by swamps is an additional 69,700 km^2 (Biswas, 1994; Beyene et al., 2010).

1.3 Literature survey of previous studies

Precipitation over the Nile River basin is largely governed by the movement of the Inter-Tropical Convergence Zone (ITCZ), but modulated significantly by topography. In general, precipitation increases from north to south, and with elevation. Precipitation is virtually zero in the Sahara desert, and increases southward to about 1200–1600 mm/yr in the Ethiopian and Equatorial Lakes Plateaus (Mohamed *et al*., 2005; Beyene et al., 2010).

The climate of the Blue Nile basin is of tropical highland monsoon type with one rainy season between June and September and a dry season from October to March. The rainfall is controlled by the northward and southward movement of the ITCZ. Moist air masses are driven from the Atlantic and Indian oceans during the rainy season (June to September). From October through May the ICTZ shifts southward and dry conditions prevail.

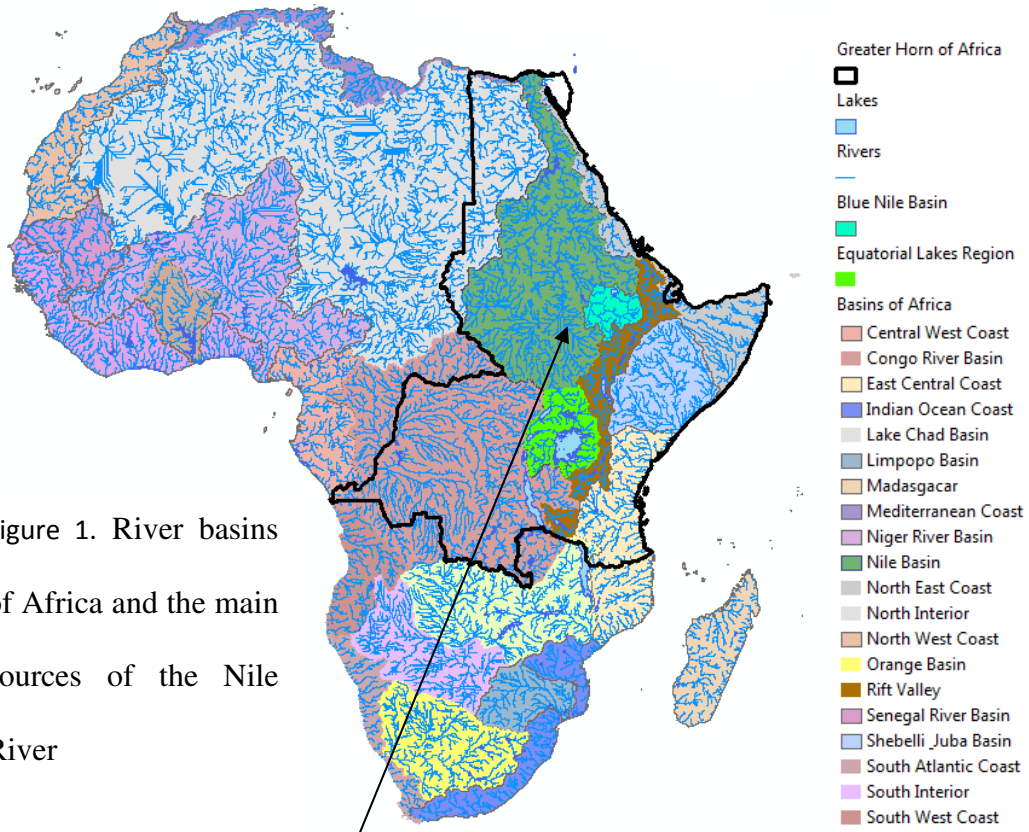

Figure 1. River basins of Africa and the main sources of the Nile River

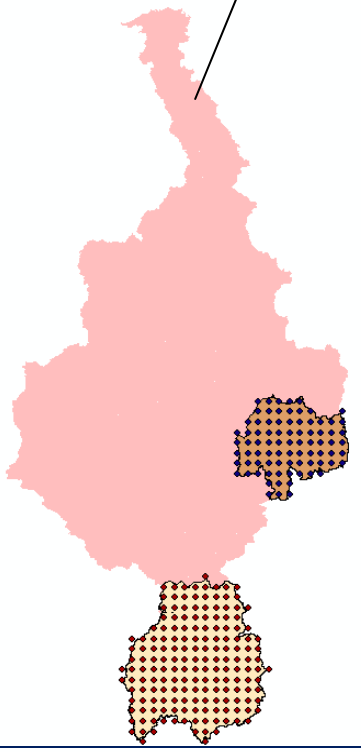

Figure 2. Data point locations in the Blue Nile and Equatorial Lakes Region from CRU for precipitation and temperature input to SWAT

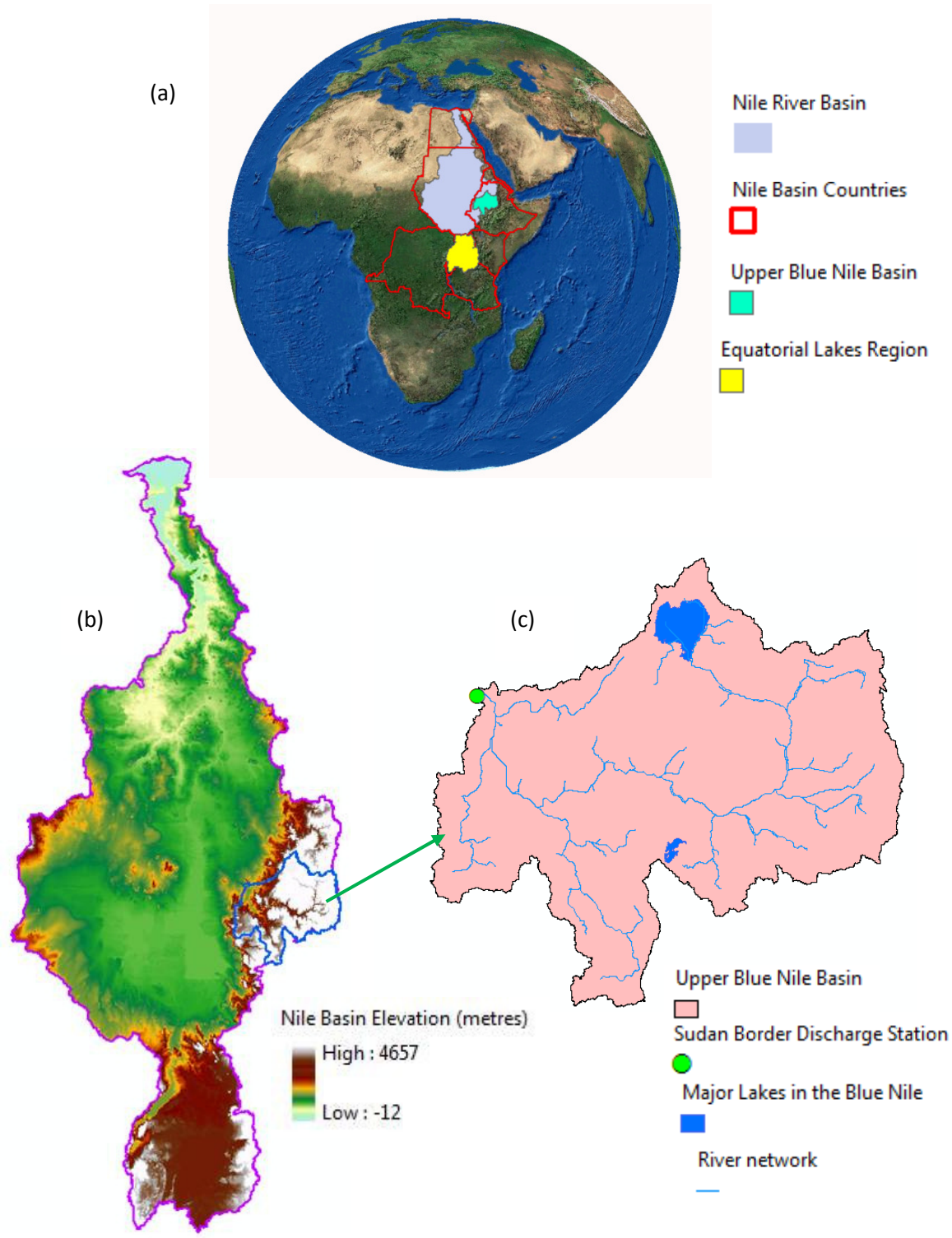

Figure 3. The geographic location of the study area (a), Nile River basin topography (b); upper Blue Nile basin and gauge station used for calibration and validation (c)

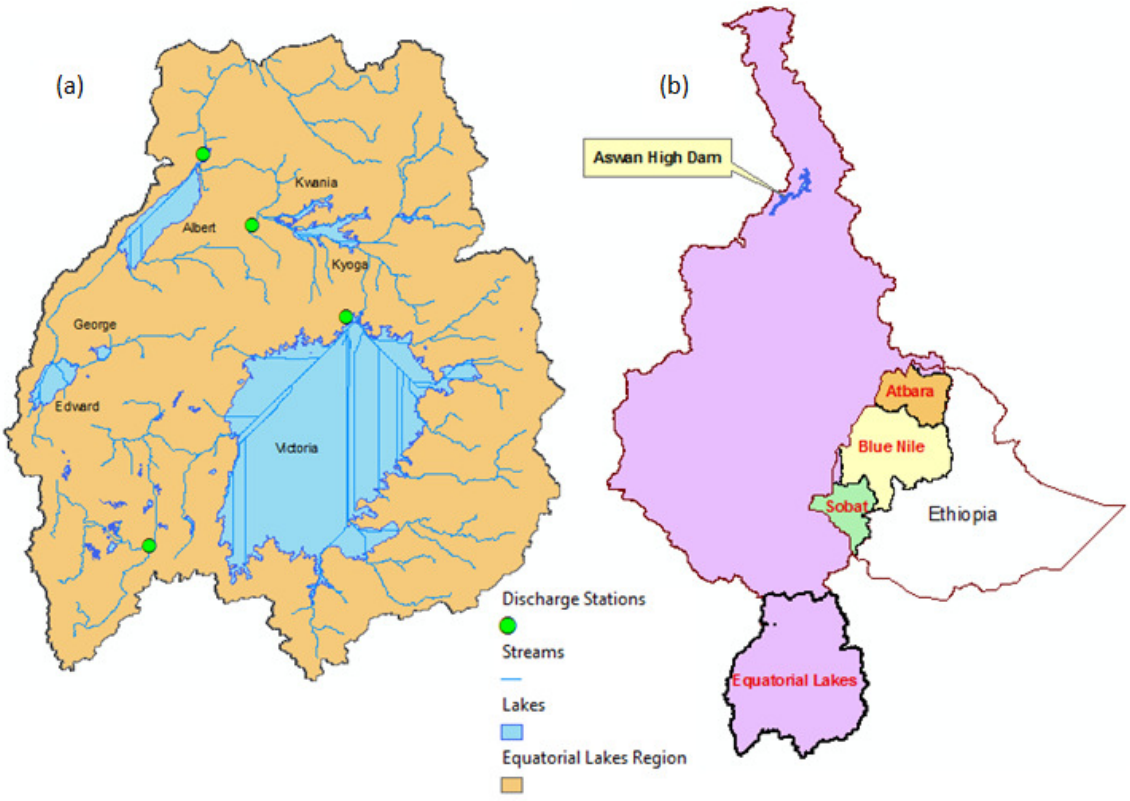

Figure 4. Discharge gauge stations, streams and lakes in the Equatorial Lakes Region (a); the main sources of the Nile River basin (b)

The effects of climate variability in the Ethiopian Highlands and Lake Victoria are shown to have caused significant interannual and interdecadal variability in the Nile River flows (Conway, 2005). He noted that, although there is low convergence among GCM simulations of rainfall, climate scenarios of rising temperatures are more consistent and could lead to large increases in evaporation because of the large expanses of open water and irrigated agriculture in the Nile River basin.

Conway (2000) studied the spatial and temporal characteristics of climate in the region of central Ethiopia that comprises the upper Blue Nile basin by constructing a 99-year basin-wide area average time series of rainfall (1900-1998) from 11 gauges each with over 25 years length of record. He indicated that rainfall is highly seasonal with roughly 70% of the annual rainfall occurring between June and September. He also showed that annual rainfall generally declines from over 2000 millimeters in the south-west to less than 1000 millimeters in the north-east, although effects of the complex topography, rain shadow effects and local moisture sources complicate this pattern. The basin-wide series in the Blue Nile shows association with the Southern Oscillation Index (SOI), and the basin-wide rainfall series and the Blue Nile river flow are strongly correlated (Conway, 200). He noted that the River flow of the Blue Nile is, therefore, influenced by the same factors as rainfall over the region, namely association with the strength of the Indian Monsoon and the behavior of the SOI.

Kim *et al.,* (2008) evaluated the impacts of climate change on both hydrologic regimes and water resources of the upper Blue Nile basin in Ethiopia using the outcomes of multiple general circulation models (GCMs) to perturb the baseline climate scenario representing the current temperature and precipitation patterns. They used a two-tank hydrologic model. They suggested that the climate in most of the upper Blue Nile River basin is likely to become wetter and warmer in the 2050s (2040-2069), and mid-to-long-term droughts are likely to become less frequent in the entire basin although uncertain with the accuracy of GCMs and limited data availability for the hydrologic model. Elshamy et al. (2009) analyzed the output of 17 general circulation models (GCMs) included in the 4th IPCC assessment report (IPCC, 2007) for the period of 2081-2098 for

the upper Blue Nile basin. They concluded that there is no consensus among the GCMs on the direction of precipitation change. They found that changes in annual precipitation range between -15% to +14% but more models reported reductions (10) than those reporting increases (7), though the ensemble mean of all models showed almost no change in the annual total rainfall. They noted that all models predict the temperature to increase between 2^{o}C and 5^{o}C and consequently the potential evapotranspiration to increase by 2-14% although uncertainties in the direction of precipitation. Their study shows that a reduced wet season runoff coefficient would prevail as a result of an increase in potential evapotranspiration without change in rainfall. Assuming no change or moderate changes in rainfall, their simulations indicated that the water balance of the upper Blue Nile basin may become more moisture constrained in the future.

In the Equatorial Lakes plateau, flows in the headwater regions are variable but are heavily damped by the storage provided by the swamps and lakes in that part of the basin, with large losses to evaporation and permanent spillage in some regions (Sene et al., 2001). From a hydrological modeling perspective, the Equatorial Lakes Region is more complex as compared to the Blue Nile because, in addition to the large variations in flows typical of the region (both seasonally and over longer time scales), it is also necessary to consider the complicated influence of the storage in the basin, and the impacts of climate change on the individual components in the water balance for each water body. Schuol et al. (2008) used the well-established, semi-distributed SWAT model, in combination with the GIS interface ArcSWAT and SUFI2 calibration procedure to quantify the freshwater availability for the whole African continent at a detailed subbasin level and monthly basis with uncertainty analysis. Though this study provided significant insights into continental

freshwater availability on a subbasin level and with a monthly time step, poorer model results were shown in the area of the great lakes of East Africa. Deogratias et al., 2007, used SWAT to model the hydrology of the Simiyu River catchment, a subbasin of the Equatorial Lakes Region, with detailed DEM, land use and soil data but found low level of model performance.

Sene et al., 2001, used different modeling studies to model climate change impacts on the White Nile, and showed a very rough indication of the likely magnitude of those impacts. Their overall conclusion from all methods is that climate change may lead to a slight increase in White Nile flows; and climate change scenarios for the Nile are dependent not only on the input climate and hydrological data and climate change scenarios, but also on the type of model used and its formulation.

This study seeks to model the hydrologic processes in the main headwaters of the Nile River basin: Equatorial Lakes Region and Blue Nile basins and compare potential impacts of climate change on the Blue Nile basin based on surrogate climate change scenarios using a semi-distributed hydrologic model. This is useful to study the sensitivity of the Nile River basin to potential climate change as the river is mainly affected by the response of the Blue Nile basin.

This study is organized as follows: chapter 1 covers the general introduction, highlighting potential climate change impacts on hydrology, study area and some previous studies on the hydroclimatology of the Blue Nile and Equatorial Lakes Region Nile River subbasins. Chapter 2 gives description of data used in this study, methodology, model calibration and validation. In chapter 3, we present our SWAT calibration and validation results over

the Blue Nile and Equatorial Lakes Region. In chapter 4 we present the sensitivity of the hydrology of the Blue Nile basin to potential climate change scenarios and finally summarize our results and draw conclusions in chapter 5.

CHAPTER TWO

2.0 Hydrologic Models

Hydrologic models use mathematical and empirical expressions that define quantitative relationships between inputs (e.g. temperature, precipitation) and outputs (e.g. discharge) for water resources studies. They are vital for decision makers who need to evaluate various management alternatives under different climate and land use/cover scenarios. The scope of hydrologic modeling and its applications has broadened dramatically over the past decades. They are used to determine the performance of watersheds under land use, climate extremes, variability and changes as well as under different management alternatives**.**

This can take the form of sensitivity analysis where baseline conditions of climate, land cover and streamflow are established, and then used to compare the effect on flow due to changes in precipitation, temperature, land cover and other climate variables. These analyses provide information on the direction and magnitude of flow changes, the processes responsible most for those change as well as providing insight as to which variables are most significant in predicting these changes.

Hydrologic models can be classified as:

a) Statistical models: they are purely a mathematical construct where processes that produce results are not considered. They fit regression curves to observed data.

Predictions of future events are made from enough previous observations. Examples include TP40, Flood frequency Analysis, Rating Curve, etc. Though these models are simple and easy to understand and convey information, they do not include process information and they may not be valid beyond the range of information.

b) Numerical Models: they use mathematical and empirical relationships to represent complex physical and dynamical processes within the earth systems. They are useful to analyze project alternatives and predict the effects of future changes, such as urban development, land use change, climate change, etc. Numerical models can be generally divided into three:

   I. Lumped models: these empirically based models integrate over some time and space scales. The high non-linear response of watersheds appears linear. Examples include Rational Method, TR-20, HEC-1, HSPF, etc. Though they are conceptually simple and easy to program and apply, they require substantial calibration data and they are not useful outside of the range of calibration.

   II. Physically based distributed parameter models: these are broken down into small time and space increments. The physical processes occurring in the watershed may be explicitly simulated, and then integrated to produce the watershed response. Examples in this category are GSSHA,

MIKE-SHE, ADH, etc. These types of models simulate physical processes. They explicitly include spatial heterogeneity. They can be used to analyze changing conditions such as land use changes, project alternatives, and climate change and they are extendible beyond the calibration range. However, they are data intensive and code development is difficult.

III. Hybrid hydrologic models: these are semi-distributed models. They are mixture of empirical and physics based approaches. They lie between lumped and distributed models. They have the advantage of increased spatial resolution and better process descriptions over simple lumped parameter models. They also maintain the computational advantage over fully distributed, physics based models. One such model is the Soil and Water Assessment Tool (SWAT), a semi-distributed model (Arnold *et al*., 1998), which has been used in this study.

2.1 Soil and Water Assessment Tool (SWAT) model

The model employed in our study is "Soil and Water Assessment Tool"(SWAT2009) [Arnold et al., 1998]. A number of studies have successfully applied SWAT for water quantity and quality issues for a wide range of scales and environmental conditions around the globe (e.g. Rosenthal *et al*., 1995; Srinivasan *et al*., 1998a,b; Rosenthal and

Hoffman, 1999; Spruill *et al*., 2000; Santhi *et al*., 2001; Qiu and Prato, 2001; Zhang *et al*., 2003; Chu and Shirmohammadi, 2004; Singh *et al*., 2005; Pohlert *et al*., 2005, 2006; Schuol et al., 2008; among many others) to study impacts of land cover change, management scenarios, and climate change and variability impacts on hydrology. The other advantage of applying SWAT over our study area is that it can run with a minimum number of parameters as detailed information of the parameters over the Nile basin is difficult to obtain.

In Africa, SWAT has been applied to quantify continental fresh water availability (Schuol *et al*., 2008). Their study provided significant insights into continental freshwater availability on a subbasin level and with a monthly time step. Setegn *et al*. (2008) used SWAT for hydrological modeling in the Tana basin, which is a subcatchment of the Blue Nile, Ethiopia. They found that the SWAT model can be used to investigate the impacts of various land use/cover, climate and management scenarios on the water resources of the catchment.

SWAT2009 is a publicly available model actively supported by the USDA (United States Department of Agriculture) – ARS (Agricultural Research Service) at the Grass-land, Soil and Water Research Laboratory in Temple, Texas, USA. It was developed from earlier models such as Simulator for Water Resources in Rural Basins model (SWRRB) (Williams et al., 1985; Arnold et al., 1990), Chemical Runoff, and Erosion from Agricultural Management System (CREAMS)(Knisel, 1980), Ground Water Loading Effects on Agricultural Management Systems (GLEAMS) (Leonard et al., 1987), and Erosion-Productivity Impact Calculator (EPIC)(Williams, 1975).

SWAT is a semi-physically based, computationally efficient river basin, or watershed-scale model that is used to predict the impact of land management practices on water, sediment and agricultural chemical yields in large complex watersheds with varying soil, land use and management conditions over long periods of time using readily available inputs (Neitsch et al., 2005).

We apply the latest version of the SWAT2009 (Arnold *et al.,* 1998) in the present study over the Blue Nile basin and Equatorial Lakes Region to investigate the effect of climate change on the hydrological processes and water resources of the basins. SWAT is a continuous time model and operates on a daily and subdaily time steps at a watershed scale to simulate multiple hydrological/physical processes involving water quality and quantity, including the transport and transforming processes of water, sand, and chemical substances. The model can be used to simulate the effect of climate and land cover changes by tuning the climatic and land cover input. The model operates at three spatial levels: basin, subbasin and Hydrologic Response Units (HRUs). A HRU is a lumped land area of the subbasin that can be represented by a unique combination of soil, land use and management combinations, and has no physical location in the subbasin. Input information for each subbasin is grouped into climate, HRUs, ponds/wetland, groundwater, and the main channel, or reach, draining the subbasin. Simulation of the hydrology of a watershed can be separated into the following:

a) Land phase: this controls the amount of water, sediment, nutrient and pesticide loadings to the main channel in each subbasin, depicted in Figure 6.

b) Channel phase: this is the movement of water, sediment, etc. through the channel network of the watershed to the outlet.

The computed runoff from each subbasin is routed though the river network to the main basin outlet by using, in our case, the variable storage method. The hydrologic model is based on water balance for the four storage volumes: snow, soil profile (0-2 m), shallow aquifer (2-20m) and deep aquifer (> 20 m). It considers precipitation, interception, evapotranspiration, surface runoff, infiltration, percolation, and sub-surface runoff (Schuol et al., 2008). In this study the Penman-Monteith equation (Montheith, 1965; Allen, 1986; Allen et al., 1989) is used to calculate potential evapotranspiration. The surface runoff from daily rainfall amounts is modeled using a modification of the USDA Soil Conservation Service (SCS) curve number method taking into account land use, soil type and antecedent soil moisture.

SWAT uses hydrologic response units (HRUs) that comprise specific land use, soil and slope characteristics to describe spatial heterogeneity in terms of land cover, soil type and slope class within a watershed. The model estimates relevant hydrologic components such as evapotranspiration, surface runoff, and peak rate of runoff, groundwater flow and sediment yield for each HRU.

The hydrologic model is based on a water balance equation for soil water content as follows (Arnold *et al*., 1998; Stone *et al*., 2001).

$$SW_t = SW_0 + \sum_{i=1}^{t} \left(R_{day} - Q_{surf} - E_a - w_{seep} - Q_{gw} \right) \qquad Eq.\,3-1$$

Where SW_t is the soil water content (mm H_2O) for the current day, SW_0 is the initial soil water content on day i (mm H_2O), t is the time (days), R_{day} is the amount of precipitation

on day i (mm H_2O), Q_{surf} is the amount of surface runoff on day i (mm H_2O), E_a is the amount of evapotranspiration on day i (mm H_2O), w_{seep} is the amount of water entering the vadose zone from the soil profile on day i (mm H_2O), and Q_{gw} is the amount of return flow on day i (mm H_2O).

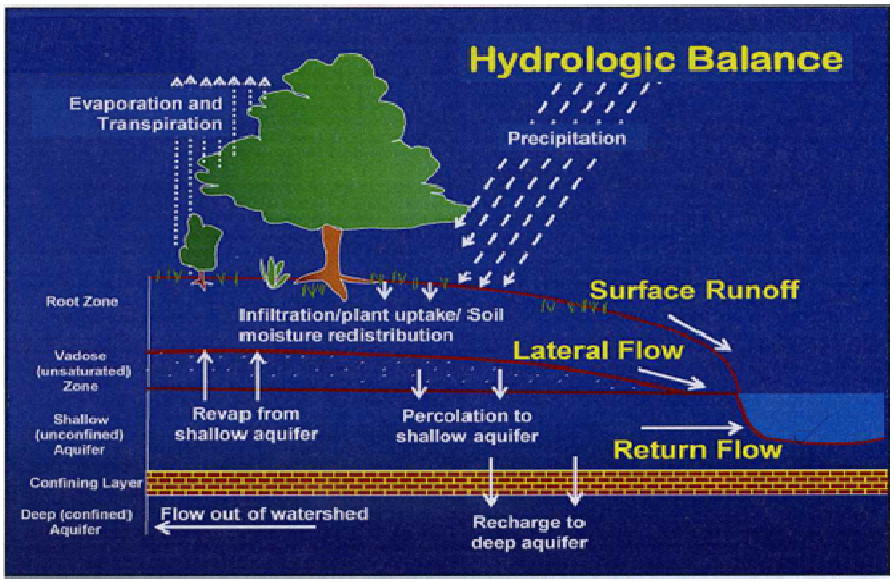

Figure 6. Schematic representation of the hydrologic cycle (Neitsch et al., 2005)

Schematic flow pathways for water movement in SWAT model is shown in Figure 7. The preprocessing of the SWAT model input (e.g. watershed delineation) is performed within ESRI ArcGIS 9.3 using the ArcSWAT interface.

2.1.1 Surface Runoff

Surface runoff occurs whenever the rate of water reaching the ground surface exceeds the rate of infiltration. SWAT provides the SCS curve number (SCS, 1972) and Green and Amp infiltration method (Green and Ampt, 1911). In this study SCS curve number procedure is used. The SCS has developed a method of determining excess rain by dividing precipitation into the following categories:

1) Direct runoff (Q) which shows up as runoff
2) Actual retention which is the depth of the abstraction
3) Initial abstraction which is the depth of rain that must fall before runoff starts

The SCS curve number equation is given by

$$Q_{surf} = \frac{(R_{day} - I_a)^2}{(R_{day} - I_a + S)} \qquad Eq.3-2$$

Where Q_{surf} is the daily surface runoff in millimeters (mm), R_{day} is the daily precipitation (mm), I_a is the initial abstraction which is commonly approximated as 0.2S, and S is the retention parameter.

Runoff will occur only when R_{day} is *greater than* I_a. Eq.3-2 by substituting 0.2S for I_a gives:

$$Q_{surf} = \frac{(R_{day} - 0.2S)^2}{(R_{day} + 0.8S)} \qquad Eq.3-3$$

The retention parameter S is given as

$$S = 25.4(\frac{1000}{CN} - 10) \qquad Eq.3-4$$

Where CN is the curve number for the day, which is a function of soil permeability, land use and antecedent soil water conditions. SWAT model defines three antecedent moisture conditions to determine the appropriate CN for each day using the CN-AMC (Curve Number – Antecedent Soil Moisture Condition) (USDA – NRCS, 2004) distribution based on the moisture content of the soil calculated by the model (Neitsch et al., 2005) employing eq. 3-5 and 3-6. This daily CN is then used to determine a theoretical capacity S (retention parameter) that can be infiltrated, given by eq. 3-4.

SCS defines three antecedent moisture conditions: I - dry (wilting point), II - average moisture condition and III - wet (field capacity).

$$CN_1 = CN_2 - \frac{20 \,.\, (100 - CN_2)}{(100 - CN_2 + \exp[2.533 - 0.0636 \,.\, (100 - CN_2)])} \qquad Eq.3-5$$

$$CN_3 = CN_2 \,.\, \exp[0.00673 \,.\, (100 - CN_2)] \qquad Eq.3-6$$

Where CN_1 is the moisture condition I curve number which is the lowest value the daily curve number can assume, CN_2 is the moisture condition II curve number, and CN_3 is the moisture condition III curve number. The various curve numbers for moisture condition 2 curve number available from tables are appropriate for slopes less than 5%. In areas where the slope is greater than 5%, the equation developed by Williams, 1995 was used

$$CN_{2s} = \frac{(CN_3 - CN_2)}{3} \,.\, [1 - 2.\exp(-13.86 \,.\, slp] + CN_2 \qquad 3.7$$

In which CN_{2S} is the moisture condition 2 curve number adjusted for slope, CN_3 is the moisture condition 3 curve number for the default 5% slope, CN_2 is the moisture condition 2 curve number for default 5% slope, and slip is the average percent slope of the subbasin.

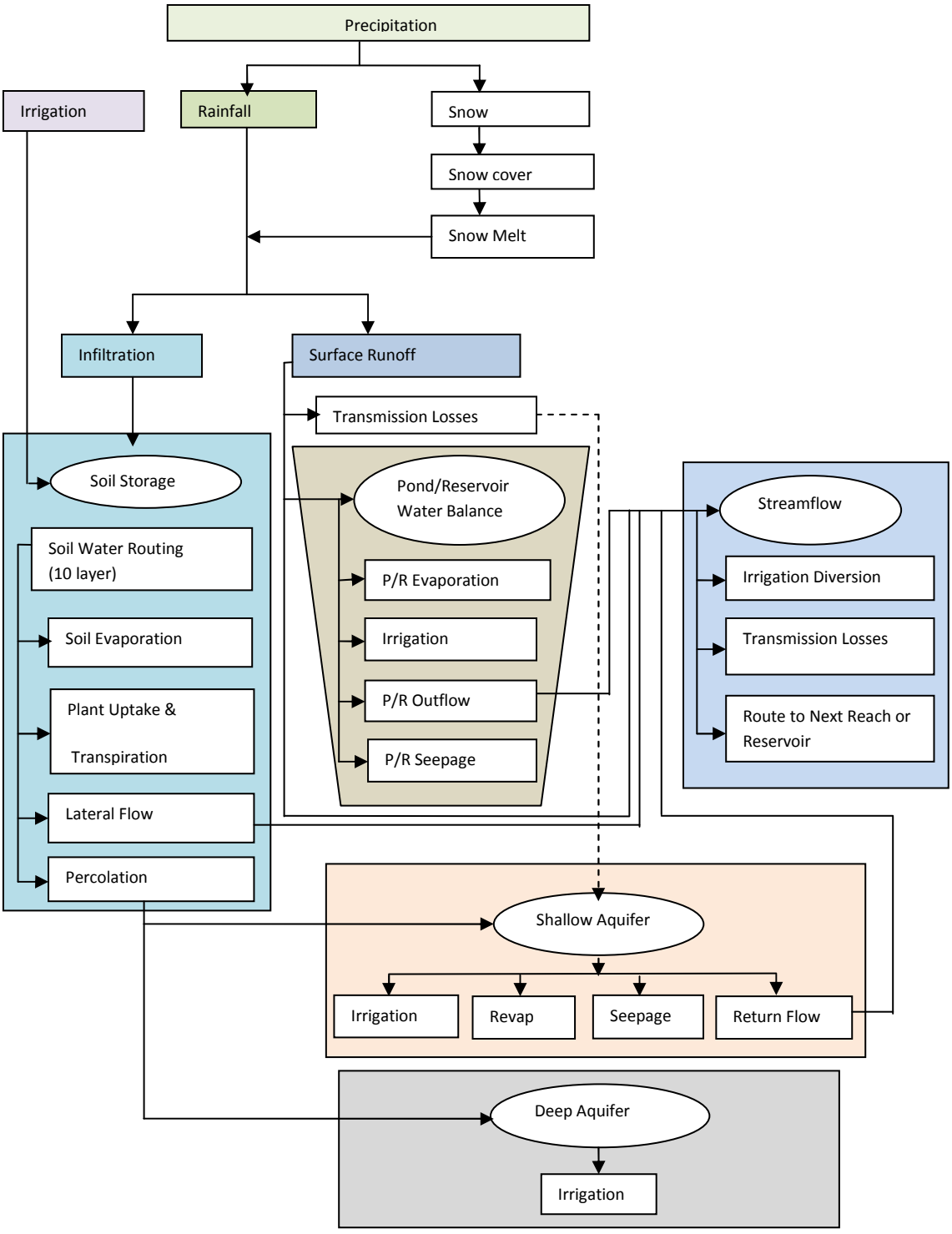

Figure 7. Schematic flow pathways for water movement in SWAT (Adapted from Neitsch et al., 2000).

SWAT calculates the peak runoff rate with a modified rational method given by Eq. 3-8.

$$q_{peak} = \frac{C \,.\, i \,.\, Area}{3.6} \qquad Eq.3-8$$

Where q_{peak} is the peak runoff rate (m^3/s), C is the runoff coefficient given by Eq. 3-9, i is the rainfall intensity (mm/hr), Area is the subbasin area (km^2)

$$C = \frac{Q_{surf}}{R_{day}} \qquad Eq.3-9$$

Where Q_{surf} is the surface runoff (mm H_2O) and R_{day} is the rainfall for the day (mm H_2O). The time of concentration, the amount of time from the beginning of a rainfall event until the entire subbasin area is contributing to flow at the outlet, is given by Eq. 3-10.

$$t_{conc} = t_{ov} + t_{ch} \qquad Eq.3-10$$

Where t_{conc} is the time of concentration for a subbasin (hr), t_{ov} is the time of concentration for overland flow (hr) given by Eq. 3-11 and t_{ch} is the time of concentration for channel flow given by Eq. 3-13

$$t_{ov} = \frac{L_{slp}}{3600.v_{ov}} \qquad Eq.3-11$$

Where L_{slp} is the subbasin slope length (m), v_{ov} is the overland flow velocity (m/s) given by Eq. 3-12

$$v_{ov} = \frac{q_{ov}^{0.4} \,.\, slp^{0.3}}{n^{0.6}} \qquad Eq.3-12$$

Where q_{ov} is the average overland flow rate (m^3/s), slp is the average slope of the subbasin (m/m) and n is the manning's roughness coefficient for the sub-basin.

$$t_{ch} = \frac{L_c}{3.6 \,.\, v_c} \qquad Eq.3-13$$

Where t_{ch} is the channel flow time of concentration, L_c is the average flow channel length for the subbasin (km) given by Eq. 3-14, v_c is the average channel velocity (m/s) given by Eq. 3-15.

$$L_c = \sqrt{L.L_{cen}} \qquad Eq.3-14$$

Where L is the channel length from the most distant point to the subbasin outlet (km), and L_{cen} is the distance along the channel to the subbasin centroid (km)

The average velocity is estimated from Manning's equation assuming a trapezoidal channel with 2:1 side slopes and a 10:1 bottom width-depth ratio

$$v_c = \frac{0.489.q_{ch}^{0.25}.slp_{ch}^{0.375}}{n^{0.75}} \qquad Eq.3-15$$

Where v_c is the average channel velocity (m/s), q_{ch} is the average channel flow rate (m^3/s), slp_{ch} is the channel slope (m/m), and n is Manning's roughness coefficient for the channel.

A portion of the generated surface runoff is released to the main channel in subbasins with a time of concentration greater than 1 day. Once surface runoff is calculated with the curve number method, the amount of surface runoff released to the main channel is calculated:

$$Q_{surf} = (Q_{surf}^{*} + Q_{stor,i-1}).(1 - \exp\left[\frac{-surlag}{t_{conc}}\right] \qquad Eq.3-16$$

Where Q_{surf} is the amount of surface runoff discharged to the main channel on a given day (mm H_2O), Q_{surf}^{*} is the amount of surface runoff generated in the subbasin on a given day (mm H_2O), $Q_{stor,\ i-1}$ the surface runoff lagged or stored from the previous day (mm

H_2O), surlag is the surface runoff lag coefficient, and t_{conc} is the time of concentration for the subbasin (hrs).

2.1.2 Evapotranspiration

Evapotranspiration is a collective term that includes all the processes by which water on the earth's surface is converted to water vapor. SWAT incorporates three potential Evapotranspiration estimation mechanisms: the Penman-Monteith method (Montheith, 1965; Allen, 1986; Allen et al., 1989), the Priestley-Taylor method (Priestley and Taylor, 1972) and the Hargreaves method (Hargreaves et al., 1985).

In this study the Penman-Monteith method was used because it is more appropriate for climate change studies. It is given by

$$\lambda E = \frac{\Delta.(H_{net} - G) + \rho_{air}.c_p.\left[e_z^o - e_z\right] / r_a}{\Delta + \gamma.(1 + r_c / r_a)} \qquad Eq.3-17$$

Where λE is the latent heat flux density (MJ/m^{2}d), E is the depth rate evaporation (mm/d), Δ is the slope of the saturation vapor pressure–temperature curve, de/dT (kpa/^{o}C) , H_{net} is the net radiation (MJ/m^{2}d) given by Eq. 3-19, G is the heat flux density to the ground (MJ/m^{2}d), ρ_{air} is the air density (kg/m^3), c_p is the specific heat at constant pressure (MJ/kg^{o}C), e_z^o is the saturation vapor pressure of air at height z (kPa), e_z is the water vapor pressure of air at height z (kPa), γ is the psychrometric constant (kPa/^{o}C), r_c is the plant canopy resistance (s/m), and r_a is the diffusion resistance of the air layer (aerodynamic resistance)(s/m) given by Eq. 3-18.

$$r_a = \frac{\ln\left[(z_w - d) \,/\, z_{om}\right] \ln\left[(z_p - d) \,/\, z_{ov}\right]}{k^2 u_2} \qquad Eq.3-18$$

Where z_w is the height of the wind speed measurement (cm), z_p is the height of the humidity (psychrometer) and temperature measurements (cm), d is the zero plane displacement of the wind profile (cm), z_{om} is the roughness length for momentum transfer (cm), z_{ov} is the roughness length for vapor transfer (cm), k is the von Kármán constant, and u_2 is the wind speed at height z_w (m/s).

$$H_{net} = H_{day}\downarrow - \alpha . H_{day}\uparrow + H_L\downarrow - H_L\uparrow \qquad Eq.3-19$$

Where H_{net} is the net radiation (MJ/m^2d), H_{day} is the short-wave solar radiation reaching the ground (MJ/m^2d), α is the short-wave reflectance or albedo, H_L is the long-wave radiation (MJ/m^2d) and the arrows indicate the direction of the radiation flux.

2.1.3 Percolation

SWAT calculates percolation for each soil layer in the profile. For water to percolate the water content must exceed the field capacity water content for that layer and the layer below must not be saturated. When the soil layer is frozen, no water flow out of the layer is calculated. The volume of water available for percolation in the soil layer is given by:

$$SW_{ly,\,excess} = SWly - FCly \quad \text{if } SWly > FCly \qquad \text{Eq. 3-20}$$

$$SW_{ly,\,excess} = 0 \quad \text{if } SWly < FCly \qquad \text{Eq. 3-21}$$

Where $SW_{ly,\,excess}$ is the drainable volume of water in the soil layer on a given day (mm H_2O), SW_{ly} is the water content of the soil layer on a given day (mm H_2O) and FC_{ly} is the water content of the soil layer at field capacity (mm H_2O).

The amount of water that percolates to the next layer is given by

$$w_{perc,ly} = SW_{ly,excess} \cdot \left[1 - \exp\left[\frac{-\Delta t}{TT_{perc}}\right]\right] \qquad Eq.3-22$$

where $w_{perc,\,ly}$ is the amount of water percolating to the underlying soil layer on a given day (mm H_2O), $SW_{ly,\,excess}$ is the drainable volume of water in the soil layer on a given day (mm H_2O), Δt is the length of the time step (hrs), and TT_{perc} is the travel time for percolation (hrs).

The travel time, which is unique for each layer, is given by

$$TT_{perc} = \left[\frac{SAT_{ly} - FC_{ly}}{K_{sat}}\right] \qquad Eq.3-23$$

Where TT_{perc} is the travel time for percolation (hrs), SAT_{ly} is the amount of water in the soil layer when completely saturated (mm H_2O), FC_{ly} is the water content of the soil layer at field capacity (mm H_2O), and K_{sat} is the saturated hydraulic conductivity for the layer (mm/h).

2.1.4 Lateral Flow

This kind of flow is significant in watersheds with soils having high hydraulic conductivities in surface layers and an impermeable or semi-permeable layer at a shallow depth. Perched water table, which is formed by vertically percolating rainfall and ponding

above the impermeable layer forming a saturated zone of water, is the source of water for lateral flow.

SWAT uses kinematic storage model, which simulates subsurface flow in a two dimensional cross-section down a steep hill slope, for subsurface flow developed by Sloan et al. (1983) and summarized by Sloan and Moore (1984).

$$Q_{lat} = 0.024 . \frac{\left[2 . SW_{ly,excess} . K_{sat} . slp\right]}{\phi_d . L_{hill}} \qquad Eq. 3-24$$

Where Q_{lat} is the lateral flow, $SW_{ly,\ excess}$ is the drainable volume of water stored in the saturated layer in millimeters (mm) (A soil is considered to be saturated whenever the water content of the layer exceeds the layer's field capacity water content), K_{sat} is the saturated hydraulic conductivity (mm/hr), *Slp* is the increase in elevation per unit distance equivalent to Tanαhill where Tanαhill is the slope of the hill slope segment, *Φd* is the drainable porosity of the soil layer (mm/mm), and *Lhill* is the hill slope length (m).

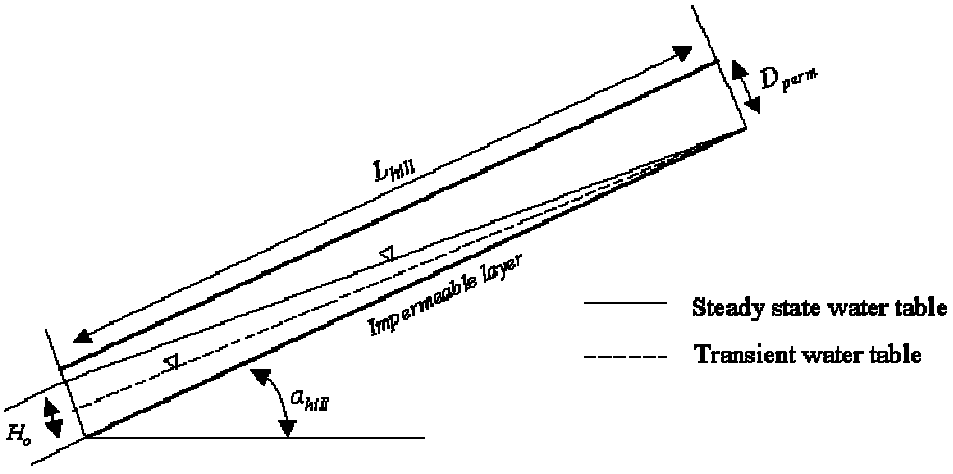

Figure 9. Behavior of the water table as assumed in the kinematic storage model (Neitsch et al., 2005)

The drainable volume of water stored in the saturated layer is calculated:

$SW_{ly,\,excess} = SWly - FCly$ if $SWly > FCly$ Eq. 3-25

$SW_{ly,\,excess} = 0$ if $SWly < FCly$ Eq. 3-26

The drainable porosity of the soil layer Φd is calculated as follows.

$\Phi_d = \Phi_{soil} - \Phi_{fc}$ Eq. 3-27

Where Φ_{soil} is the total porosity of soil layer in mm/mm and Φ_{fc} is the porosity of soil layer filled with water when the layer is at field capacity in mm/mm.

In large subbasins with a time of concentration greater than 1 day, only a portion of the lateral flow will reach the main channel on the day it is generated. The lag on lateral flow results is only a fraction of the lateral flow from each HRU reaching the stream. Thus the daily amount of lateral flow reaching the stream is calculated (Neitsch et al., 2005):

$$Q_{lat} = (Q'_{lat} + Q_{latstor,i=1}) \cdot (1 - \exp^{\left(-\frac{1}{TT_{lag}}\right)} \qquad Eq.3-28$$

Where Q_{lat} the amount of lateral flow discharged to the main stream in a day in mm, Q'_{lat} is the amount of lateral flow generated in the subbasin on a given day in mm, and *TTlag* is the lateral flow travel time (days).

The model will calculate lateral flow travel time or utilize a user-defined travel time. If drainage tiles are present in the HRU, lateral flow travel time is calculated (Neitsch et al., 2005) as follows:

$$TT_{lag} = \frac{tile_{lag}}{24} \qquad Eq.3-29$$

Where TT_{lag} is the lateral flow travel time (days) and $tile_{lag}$ is the drain tile lag time (hrs). In HRUs without drainage tiles, lateral flow travel time is calculated based on formulation by (Neitsch et al., 2005):

$$TT_{lag} = 10.4 \cdot \frac{L_{hill}}{K_{sat,mx}} \qquad Eq.3-30$$

Where L_{hill} is the hill slope length (m) and $K_{sat, mx}$ is the highest layer saturated hydraulic conductivity in the soil profile (mm/hr).

2.1.5 Ground Water

Soil water is held at negative pressure due to surface tension between water and moist soil particles, while ground water is under positive pressure, i.e. pressure greater than the atmospheric pressure. Water enters ground water due to infiltration/percolation and sometimes due to recharge from surface water bodies. Ground water systems are classified as unconfined (shallow) aquifer and confined (deep) aquifer. An aquifer is a geologic unit that can store enough water and transmit it at a rate fast enough to be hydrologically significant (Dingman, 1994). The upper boundary of unconfined aquifer is the water table, where as a confined aquifer is bounded above and below by geologic formations whose hydraulic conductivity is significantly lower than that of the aquifer.

The water balance for a shallow aquifer is given by:

$$aq_{sh,d} = aq_{sh,d-1} + w_{rchrg,sh} - Q_{gw} - w_{revap} - w_{pump,sh} \qquad Eq.3-31$$

Where $aq_{sh,d}$ is the amount of water stored in the shallow aquifer on day d (mm H_2O), $aq_{sh,d-1}$ is the amount of water stored in the shallow aquifer on day d-1 (mm H_2O), $w_{rchrg, sh}$ is the amount of recharge entering the shallow aquifer on day d (mm H_2O), Q_{gw} is the

groundwater flow or base flow into the main channel on day d (mm H_2O), w_{revap} is the amount of water moving into the soil zone in response to water deficiencies on day d (mm H_2O), and $w_{pump,sh}$ is the amount of water removed from the shallow aquifer by pumping on day d (mm H_2O).

The lag of the water that moves past the lowest depth of the soil profile to be shallow and/or deep aquifer recharge depends on the depth of the water table and the hydraulic properties of the vadose and groundwater zones. The recharge to both aquifers on a given day is given by:

$$w_{rchrg,i} = \left(1 - \exp\left[-1/\delta_{gw}\right]\right).w_{seep} + \exp\left[-1/\delta_{gw}\right].w_{rchrg,i-1} \qquad Eq.3-32$$

Where $w_{rchrg,i}$ is the amount of recharge entering the aquifers on day i (mm H_2O), δ_{gw} is the delay time or drainage time of the overlying geologic formations (days), w_{seep} is the total amount of water exiting the bottom of the soil profile on day i (mm H_2O), and $w_{rchrg,i-1}$ is the amount of water recharge entering the aquifers on day i-1 (mm H_2O). The total amount of water exiting the bottom of soil profile on day i is calculated:

$$w_{seep} = w_{perc,ly=n} + w_{crk,btm} \qquad \text{Eq. 3-33}$$

where w_{seep} is the total amount of water exiting the bottom of the soil profile on day i (mm H_2O), $w_{perc,ly=n}$ is the amount of water percolating out of the lowest layer, n, in the soil profile on day (mm H_2O), and $w_{crk,btm}$ is the amount of water flow past the lower boundary of the soil profile due to bypass flow on day i (mm H_2O).

Water entering into the deep aquifer from the shallow aquifer is calculated:

$$W_{deep} = \beta_{deep} \cdot w_{rchrg} \qquad \text{Eq. 34}$$

Where w_{deep} is the amount of water moving into the deep aquifer on day i (mm H_2O), β_{deep} is the aquifer percolation coefficient (this parameter is defined by the user as RCHRG_DP), and w_{rchrg} is the amount of recharge entering both aquifers on day i (mm H_2O). The amount of recharge to the shallow aquifer is given as follows:

$$W_{rchrg,sh} = w_{rchrg} - w_{deep} \quad \text{Eq. 3-35}$$

Where $w_{rchrg,sh}$ is the amount of recharge entering the shallow aquifer on day i (mm H_2O). Groundwater/base flow to the main channel is calculated:

$$Q_{gw,i} = Q_{gw,i-1} \cdot \exp\left[-\alpha_{gw} \cdot \Delta t\right] + w_{rchrg,sh} \cdot \left(1 - \exp\left[-\alpha_{gw} \cdot \Delta t\right]\right) \text{ if } aq_{sh} > aq_{shtrh,q} \quad \text{Eq. 3-36}$$

$$Q_{gw,i} = 0 \quad \text{if } aq_{sh} \leq aq_{shthr,q} \quad \text{Eq. 3-37}$$

Where $Q_{gw,i}$ is the groundwater flow into the main channel on day i (mm H_2O), $Q_{gw,i-1}$ is the groundwater flow into the main channel on day i -1 (mm H_2O), α_{gw} is the baseflow recession constant which is a direct index of groundwater flow response to change in recharge (Smedema and Rycroft, 1983), Δt is the time step (1day), $w_{rchrg,sh}$ is the amount of recharge entering the shallow aquifer on day i (mm H_2O), aq_{sh} is the amount of water stored in the shallow aquifer at the beginning of day i (mm H_2O) and $aq_{shthr,q}$ is the threshold water level in the shallow aquifer for groundwater contribution to the main channel to occur (H_2O).

When the shallow aquifer receives no recharge the above equation is simplified to:

$$Q_{gw,i} = Q_{gw,0} \cdot \exp\left[-\alpha_{gw} \cdot t\right] \quad \text{if } aq_{sh} > aq_{shthr,q} \quad \text{Eq. 3-38}$$

$$Q_{gw,i} = 0 \quad \text{if } aq_{sh} \leq aq_{shthr,q} \quad \text{Eq. 3-39}$$

Where $Q_{gw,i}$ is the ground water flow into the main channel at time t in mm, $Q_{gw,0}$ is the ground water flow into the main channel at the beginning of the recession (time = 0) in

mm, α_{gw} is the base flow recession constant defined by the user (ALPHA_BF), and t is the time elapsed since the beginning of the recession (days).

The maximum amount of water that may be removed from the shallow aquifer into the overlying unsaturated zone is calculated:

$$w_{revap,\,mx} = \beta_{rev} \cdot E_o \qquad \text{Eq. 3-40}$$

where $w_{revap,mx}$ is the maximum amount of water moving into the soil zone in response to water deficiencies (mm H_2O), β_{rev} is the revap coefficient, E_o is the potential evapotranspiration for the day (mm H_2O). The actual amount of revap that will occur on a given day is calculated:

$$w_{revap} = 0 \qquad \text{if } aq_{sh} \leq aq_{shthr,rvp} \qquad \text{Eq. 3-41}$$

$$w_{revap} = w_{revap,mx} - aq_{shthr,rvp} \qquad \text{if } aq_{shthr,rvp} < aq_{sh} < (aq_{shthr,rvp} + w_{revap,mx}) \qquad \text{Eq. 3-42}$$

$$w_{revap} = w_{revap,mx} \qquad \text{if } aq_{sh} \geq (aq_{shthr,\,rvp} + w_{revap,mx}) \qquad \text{Eq. 3-43}$$

where w_{revap} is the actual amount of water moving into the soil zone in response to water deficiencies (mm H_2O) which is allowed to occur only if the amount of water stored in the shallow aquifer exceeds a threshold value specified by the user, $w_{revap,mx}$ is the maximum amount of water moving into the soil zone in response to water deficiencies (mm H_2O), aq_{sh} is the amount of water stored in the shallow aquifer at the beginning of day i (mm H_2O) and $aq_{shthr,rvp}$ is the threshold water level in the shallow aquifer for revap to occur (mm H_2O). A more detailed description of the model can be found in Arnold et al. (1998) and Neitsch *et al.* (2005).

2.2 Monthly to Daily weather converter (MODAWEC)

Monthly weather data are easier to obtain than daily weather data. Schuol and Abbaspour (2007) showed that in data scarce regions such as Africa, simulations using generated

weather data were superior to simulations using the available poor quality measured data. In this study daily precipitation, maximum and minimum temperature are generated from monthly precipitation, number of wet days, and maximum and minimum temperature data from the Climatic Research Unit (CRU) using Monthly to Daily Weather Converter (MODAWEC) at the data point locations shows on Figure 2. The CRU data includes monthly precipitation, monthly maximum and minimum temperature and wet days, among others, on a global scale with a spatial resolution of 30 arc-min (about 50x50 km in each grid cell near the equator) for the period 1901-2000 (Mitchell et al., 2003). While there exists some other global climate time series, besides the high spatial resolution and long temporal coverage, the CRU dataset provides the most comprehensive compilation of surface climate variables (Schuol and Abbaspour, 2007). Before using generated daily data in the SWAT model, we checked the quality of the monthly CRU data by direct comparison with station observation data from the Ethiopian Meteorological Agency. This was done by comparing the statistics of the monthly CRU data and observation gauge measuring stations with a comparatively good and long-term database. This selection was mainly based on the data availability over the whole watershed.

The correlation between the monthly CRU precipitation and station observation monthly precipitation for 10 stations in the basin ranges from 0.893 to 0.942, showing the quality and usability of the CRU data. Therefore, it is better to use the gridded CRU data than the sparsely and unevenly distributed with frequently missing and erroneous gauge station data in the Blue Nile basin.

The MODAWEC model is a parametric weather generator that converts monthly precipitation (in mm) and maximum and minimum temperature (in ^{0}C) to daily values using precipitation as deriving force. It uses monthly precipitation, monthly wet days, and monthly maximum and minimum temperature in each year as main inputs. The outputs are daily precipitation, daily maximum temperature, and daily minimum temperature. To generate daily precipitation, a two-state (dry or wet), first-order Markov Chain by Nicks (1974) is used to define the day as wet or dry. Probability of rain on a given day is conditioned on the wet or dry status of the previous day. In case of a wet day, a modified exponential distribution (Eq. 3-47) is used to give first approximations of the amount of daily precipitation. The probability of a wet day is calculated directly from the number of wet days:

$$P_{(w)} = \frac{n_w}{n} \qquad Eq.3-44$$

where $P_{(w)}$ is the probability of a wet day, n_w is the number of wet days, and n is the number of days in a month. The probability of a wet day after a dry day can be estimated as a fraction of $P_{(w)}$:

$$P_{(w/d)} = a_1 + P_{(w)} \qquad \text{Eq. 3-45}$$

where $P_{(w/d)}$ is the probability of a wet day following a dry day and a_1 is a fraction usually in the range of 0.6–0.9. The probability of a wet day following a wet day can be calculated directly by using the equation:

$$P_{(w/w)} = 1 - a_1 + P_{(w/d)} \qquad \text{Eq. 3-46}$$

where $P_{(w/w)}$ is the probability of a wet day after a wet day. For many locations, $a_1 = 0.75$ gives satisfactory estimates of P(w/d) (Liu et al., 2009). In this study the default value of $a_1 = 0.75$ is used. When a day is wet, daily precipitation is generated from a modified exponential equation:

$$R_d = R_w \,.\, (-\ln(RN))^{1.3} \qquad \text{Eq. 3-47}$$

where R_d is the daily precipitation on day d, R_w is the mean precipitation amount for wet days in a month, and RN is a uniform random number.

$$R_w = \frac{R_m}{n_w} \qquad Eq.3-48$$

Where R_w is the mean precipitation amount for wet days in a month, R_m is the monthly total precipitation and n_w is the number of wet days. The R_d calculated in Eq. 3-47 are summed and corrected using the equation:

$$R_d^* = R_d \,.\, \frac{R_m}{Z} \qquad \text{Eq. 3-49}$$

where R_d^* is the corrected daily precipitation on day d, R_m is the measured monthly precipitation, and Z is the sum of the generated precipitation amounts for a month. MODAWEC uses Richardson (1981) to give first approximations of daily temperature because it correlates temperature with rainfall. The residuals of daily maximum and minimum air temperature are generated from a multivariate normal distribution. The serial correlation between the residuals of maximum and minimum air temperature is described by a first-order linear autoregressive model. Final values of temperature are obtained by correcting the initial estimates using the average daily maximum and minimum temperatures in a month. Though the temperature model requires monthly

means of maximum and minimum temperatures and their standard deviations as inputs, if the standard deviations are not available, the long-term observed extreme monthly minimums and maximums may be substituted. The model estimates standard deviation as 0.33 of the difference between the extreme and the mean for each month. If extreme temperatures are not available, the standard deviations are estimated from the following:

$$\delta T_{max} = \max(0.5, 5.8 - 0.09 * \overline{T}_{max}) \quad \text{Eq. 3-50}$$

$$\delta T_{min} = \max(0.5, 5.2 - 0.13 * \overline{T}_{min}) \quad \text{Eq. 3-51}$$

δT_{max} is the standard deviation of daily maximum temperature for a month, $\overline{T}_{max}$ is the average daily maximum temperature in the month, δT_{min} is the standard deviation of daily minimum temperature for a month, and $\overline{T}_{min}$ is the average daily minimum temperature in the month. The maximum daily temperature is simulated to be lower in rainy days. For the mean monthly maximum temperature ($\overline{T}_{max}$) this is accomplished by assuming that wet day values are less than dry day values by some fraction of the difference between $\overline{T}_{max}$ and $\overline{T}_{max}$ given below.

$$TW_{max} = TD_{max} - a_2\left(\overline{T}_{max} - \overline{T}_{min}\right) \quad \text{Eq. 3-52}$$

where TW_{max} is the daily mean maximum temperature for wet days, TD_{max} is the daily mean maximum temperature for dry days, observed data indicate that a_2 usually lies between 0.5 and 1.0. The default value of 0.5 is used in the MODAWEC model. The daily mean maximum temperature for dry days is calculated:

$$TD_{max} = \overline{T}_{max} + a_2(\overline{T}_{max} - \overline{T}_{min}) * \frac{n_w}{w} \quad \text{Eq. 3-53}$$

where n is the number of days in a month, n_w is the number of wet days, and n_d is the number of dry days. The first approximation of maximum and minimum temperature is estimated:

$T_{max,i} = TY + \delta T_{max} * dT_{max}$ Eq. 3-54

$T_{min,i} = TZ + \delta T_{min} * dT_{min}$ Eq. 3-55

where $T_{max,i}$ and $T_{min,i}$ are the first approximations of maximum and minimum temperature on day i, dT_{max} and dT_{min} are the standard normal deviates for maximum and minimum temperature, and TY = TW_{max} on wet days while TY = TD_{max} on dry days. Daily minimum temperature is assumed not to be affected by the wet/dry conditions. TZ is equal to the mean monthly minimum temperature. The simulated $T_{max,i}$ and $T_{min,i}$ are corrected using the equations:

$$T^*_{max,i} = T_{max,i} + \overline{T}_{max} - \frac{SM_1}{n}$$ Eq. 3-56

$$T^*_{min,i} = T_{max,i} - n * T_{max,i} - T_{min,i} * \frac{(\overline{T}_{max} - \overline{T}_{min})}{SM_1 - SM_2}$$ Eq. 3-57

where $T^*_{min,i}$ and $T^*_{max,i}$ are the corrected maximum and minimum temperatures on day i, and SM1 and SM2 are the sums of $T_{max,i}$ and $T_{min,i}$ for a month. A more detailed description of the model can be found in J. Liu *et al*. (2009). The final goal of this study is to achieve an accurate representation of monthly water balance with SWAT. It is unrealistic to model daily water flows using generated daily weather data.

2.3 Calibration, validation, sensitivity analysis and uncertainty analysis

Hydrologic models are prone to various types of uncertainty issues.

a) Conceptual model uncertainty which could be uncertainties due to processes occurring in the watershed but not included in the model, simplifications in the conceptual model, processes that are included in the model but their occurrences in the watershed are unknown to the modeler, and processes unknown to the modeler and not included in the model.

b) Input uncertainty due to input data such as rainfall, temperature, and errors that arise because of using point data to large areas in distributed models.

c) Parameter uncertainties which are caused by parameter non-uniqueness in inverse-modeling. Many sets of parameters may produce the same output as processes can compensate for each other.

The Soil and Water Assessment Tool-Calibration and Uncertainty Program (SWAT-CUP) is a public domain interface that is used for calibration, validation, uncertainty analysis, and sensitivity analysis of SWAT models. The program links Sequential Uncertainty Fitting (SUFI2) (Abbaspour et al., 2004; 2007), Generalized Likelihood Uncertainty Estimation (GLUE) (Beven and Binley,1992), Parameter Solution (ParaSol) (Van Griensven and Meixner, 2003a), and Markov chain Monte Carlo (MCMC) (e.g., Kuczera and Parent, 1998; Marshall et al., 2004; Vrugt et al., 2003; Yang et al., 2007). In this study we used SUFI2 because it converges with relatively smaller number of iterations, and possibility of restarting an unfinished iteration and splitting an iteration into several runs.

2.3.1 Sequential Uncertainty Fitting (SUFI2)

SUFI-2, which is a multi-site, semi-automated global search procedure, is preferable to the other calibration and uncertainty analysis tools as it converges with a relatively small number of simulations to perform calibration and uncertainty analysis over such a computationally extensive model. All sources of uncertainties such as uncertainty in driving variables (e.g. temperature, rainfall), conceptual model, parameters and measured data are accounted by parameter uncertainty in SUFI2. SUFI2 uses P-factor, the percentage of measured data bracketed by the 95% prediction uncertainty (95PPU), to assess uncertainty analysis. The 95PPU is calculated at the 2.5% and 97.5% levels of the cumulative distribution of an output variable obtained through Latin hypercube sampling removing 5% of the very bad simulations.

SUFI2 uses R-factor, which is the average thickness of the 95PPU band divided by the standard deviation of the measured data, Eq. 3-58, to measure the strength of a calibration/ uncertainty analysis.

$$R-factor=\frac{\bar{d}_x}{\sigma_x} \qquad \text{Eq. 3-58}$$

$$\bar{d}_x=\frac{1}{k}\sum_{l=1}^{k}(X_U-X_L)_l \qquad \text{Eq. 3-59}$$

Where $\bar{d}$ is average distance between the upper and the lower 95PPU, k is the number of observed data points, σ_x is the standard deviation of the measured variable X. The best outcome is that 100% of the measurements are bracketed by the 95PPU, and d is close to zero. A value of less than 1 is a desirable measure for the *R-factor*.

SUFI2 seeks to bracket most of the measured data with the smallest uncertainty band. The value of P-factor ranges between 0 and 100%, while that of R-factor ranges between 0 and infinity. A P-factor of 1 and R-factor of zero is a simulation that exactly corresponds to measured data. The degree to which the result deviates from these numbers is used to judge the strength of the calibration. The parameter uncertainties are desired parameter ranges when acceptable values of R-factor and P-factor are reached. A larger P-factor can be reached at the expense of a larger R-factor.

After getting acceptable values of R-factor and P-factor, the goodness of fit is quantified by the coefficient of determination (R^2) (Eq. 3-60) and/ or Nash-Sutcliffe (NS) coefficient (Eq. 3-61) between the observation and the final best simulation.

$$R^2 = \frac{\left[\sum_i (Q_{m,i} - \overline{Q}_m)(Q_{s,j} - \overline{Q}_s)\right]^2}{\sum_i (Q_{m,j} - \overline{Q_m})^2 \sum_i (Q_{s,i} - \overline{Q}_s)^2} \qquad \text{Eq. 3-60}$$

$$NS = 1 - \left[\frac{\sum_i (Q_m - Q_s)_i^2}{\sum_i (Q_{m,i} - \overline{Q}_m)^2}\right] \qquad \text{Eq. 3-61}$$

Where R^2 is the coefficient of determination, NS is the Nash-Sutcliffe efficiency, Q_m is the measured discharge, Q_s is the simulated discharge, $\overline{Q}_m$ is the average measured discharge and $\overline{Q}_s$ is the average simulated discharge.

R^2 describes the proportion of the variance in measured data explained by the model. R^2 ranges from 0 to 1, with higher values indicating less error, and values greater than 0.5 are considered acceptable (Van Liew *et al.*, 2003). The NS (Nash and Sutcliffe, 1970) is a

normalized static that determines the relative magnitude of the residual variance compared to the measured data variance. It indicates how well the plot of observed versus simulated data fits the 1:1 line. It ranges between -∞ and 1.0 (1 inclusive) with NS of one being the optimal value. Values between 0.0 and 1.0 are generally considered acceptable levels of performance where as values < 0.0 are not acceptable and the mean of the measured values is better predictor than the simulated value. A more detailed description of the model can be found in Abbaspour *et al*. (2007).

2.4 Model Input

SWAT partitions the watershed into subbasins to simulate runoff. It can delineate the watershed and subbasins from a Digital Elevation Model (DEM) provided by the user. It can also use provided predefined subbasins. The fundamental working units in SWAT are hydrologic response units (HRUs) which are composed of unique land cover, slope and soil combinations. The hydrologic component of the SWAT model that uses water balance equation is based on precipitation, surface runoff, evapotranspiration, percolation and return flow data. The weather component of the model needs input data on precipitation, daily maximum and minimum air temperature, solar radiation, wind speed, and relative humidity data. The input data to the SWAT model consists of DEM, digital stream network, land use data, soil data, precipitation, daily minimum and maximum air temperature, wind speed, solar radiation and relative humidity. River discharge is used for calibration and validation purposes.

2.4.1 Digital Elevation Model (DEM)

Topography is defined by a DEM that describes the elevation of any point in a given area at a specific spatial resolution. The DEM for the study areas was downloaded from Aster Global Digital Elevation Model (GDEM)(http://www.gdem.aster.ersdac.or.jp/) at a resolution of 1 arc-second.

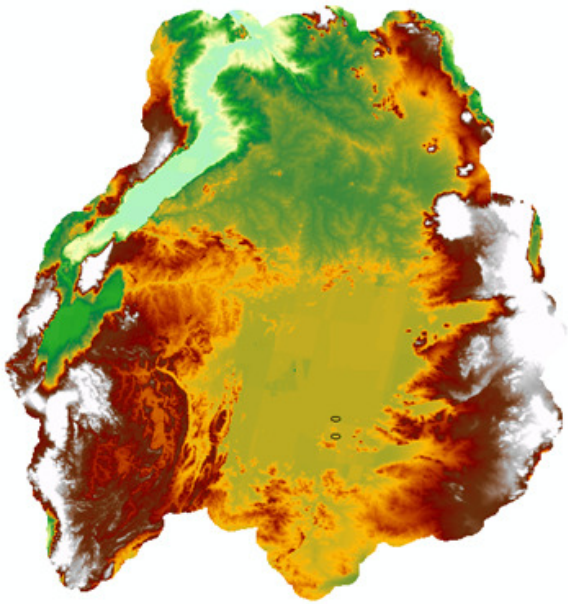

Figure 10

Equatorial Lakes Region DEM

(metres)

High : 5672

Low : 39

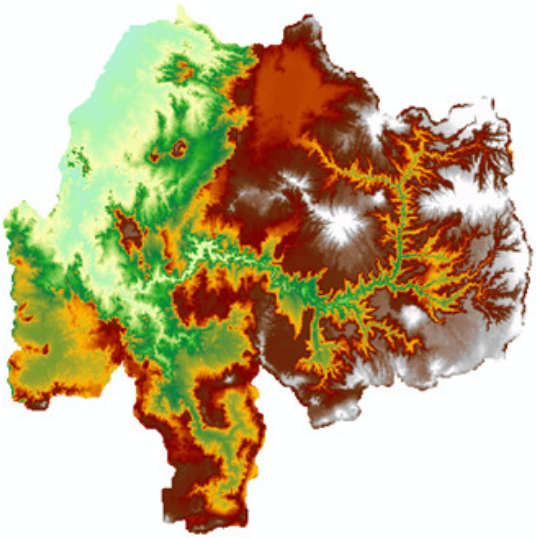

Figure 11

Blue Nile DEM

(metres)

High : 4235

Low : 436

The DEM is used at a resolution of 1 arc-second for the upper Blue Nile basin which covers an area of 174,000 km^2, but the DEM resolution of the Equatorial Lakes Region, which covers more than 410,000 km^2 is converted to 90m by 90m cell size since ArcGIS cannot handle data at higher resolution for such a large area. The DEM was used to delineate the watershed and to analyze the drainage patterns of the land surface terrain.

Subbasin parameters such as slope gradient, slope length of the terrain, and the stream network characteristics such as channel slope, length, and width are also derived from the DEM. The altitude of the Blue Nile basin varies between 436 meters above mean sea level (m.a.s.l.) to 4235 m.a.s.l. whereas the altitude of the Equatorial Lakes Region basin ranges from 39 m.a.s.l. to 5672 m.a.s.l (See Figures 10 &11).

2.4.2 Digital Stream Network

Digital stream network is taken from the US Geological Survey (USGS) public domain geographic database HYDRO1K which is derived from accumulation layer for areas with an upstream drainage area greater than 1000 km^2. A predefined digital stream network layer (See Figure 12) was imported and superimposed onto the DEM to accurately delineate the location of the streams. These data can be downloaded for free from http://eros.usgs.gov/#/Find_Data/Products_and_Data_Available/gtopo30/hydro

2.4.3 Soil Map and Data

Different soil properties such as soil texture, available water content, hydraulic conductivity and bulk density for different layers of each soil type are required as input for the SWAT hydrologic model. The required soil data for the Blue Nile and the Equatorial Lakes Region (Figures 13) are found from the Soil and Terrain Database for northeastern Africa (1995), Major Soils of the world (2002), and Digital Soil Map of the World and Derived Soil properties (1995). These data can be obtained from the Food and Agriculture Organization of the United Nations in CDROM format.

2.4.4 Land Cover/use

As land use/land cover is one of the most important factors that affect runoff, evapotranspiration and other hydrologic parameters in a watershed, it is among the necessary inputs for the SWAT model.

The land uses for the Equatorial Lakes Region and Blue Nile basins are constructed from the USGS Global Land Cover Characterization (GLCC) database (Figures 15 and 17). (http://edcsns17.cr.usgs.gov/glcc/glcc.html). The database has a spatial resolution of 1 km and 24 classes of land use representation. Land uses were reclassified to conform to the different land use/land cover types in the SWAT database (Figures 16 &18).

2.4.5 Weather data

In the Nile Basin adequate data for hydrological modeling are difficult to access or not available, and the distribution of the available observation stations is quite uneven. Moreover, the quality of the data is not reliable and there are often large amounts of missing data. The upstream riparian countries are now actively developing extensive water resources development projects. Building prediction models based on the available limited rain gauge data is not feasible. Monthly weather data are easier to obtain than daily weather data.

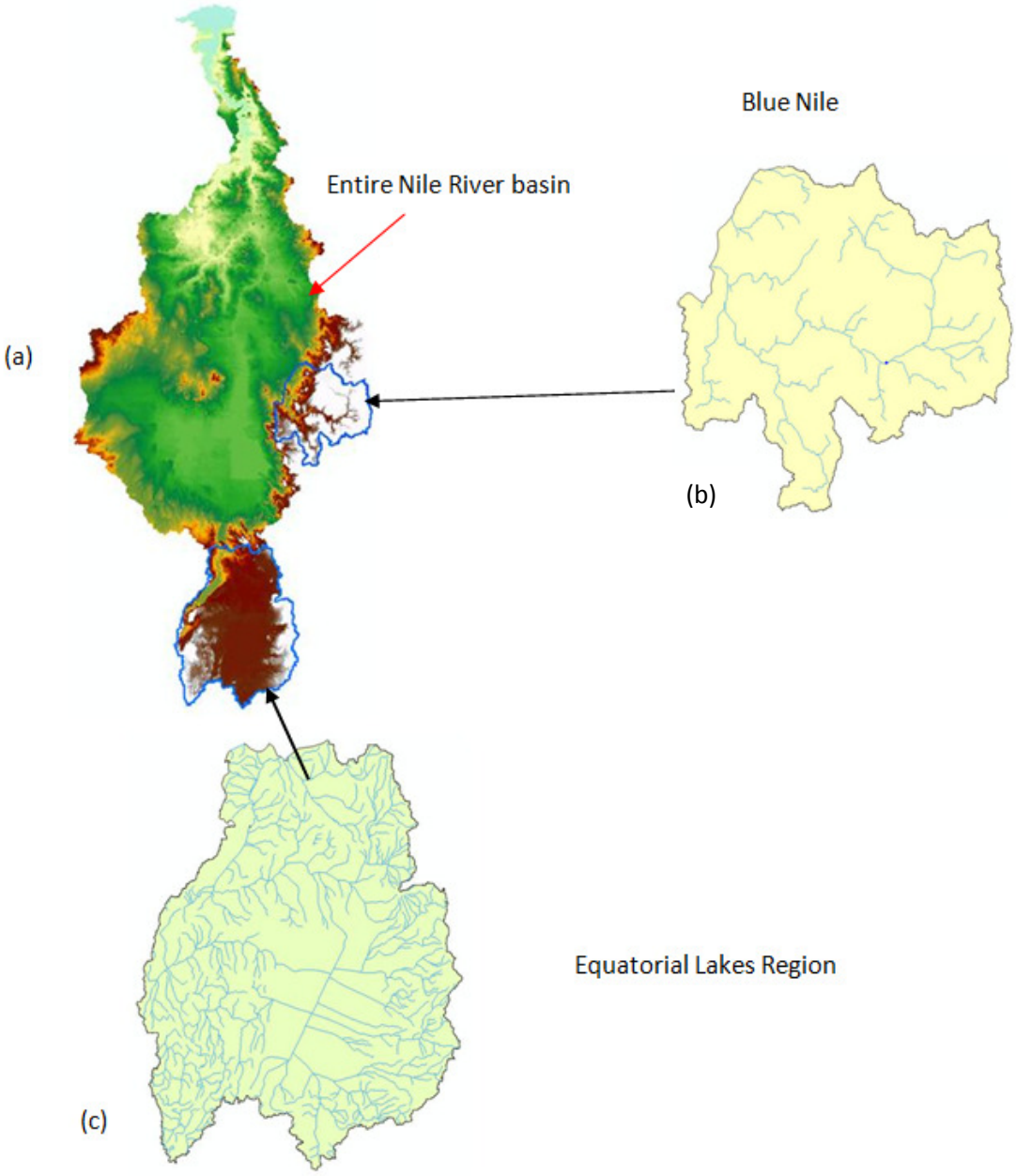

Figure 12: Streams in Blue Nile and Equatorial Lakes Region

(a)

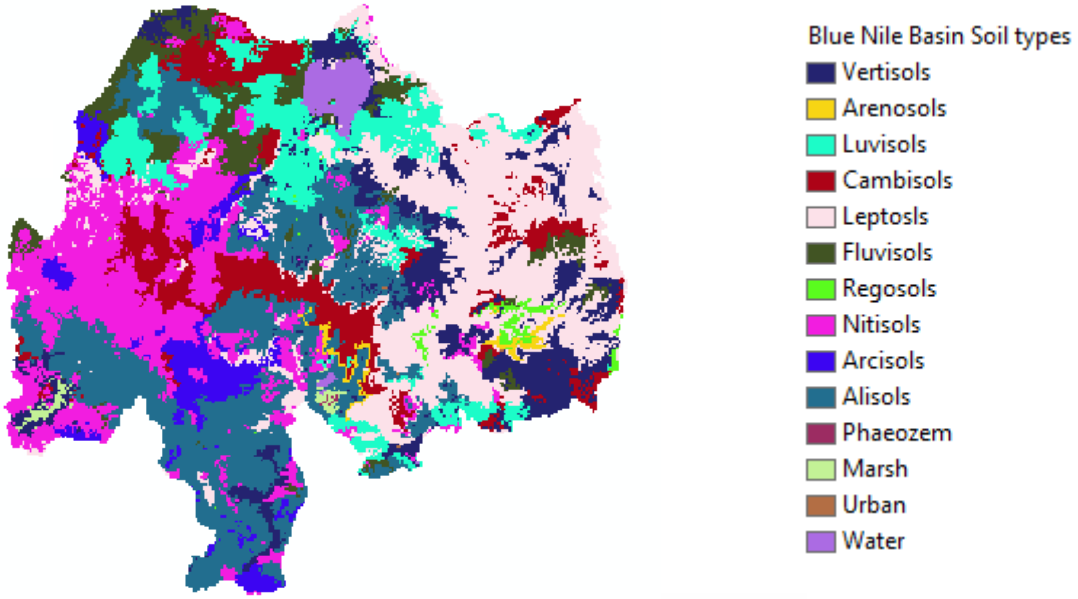

(b)

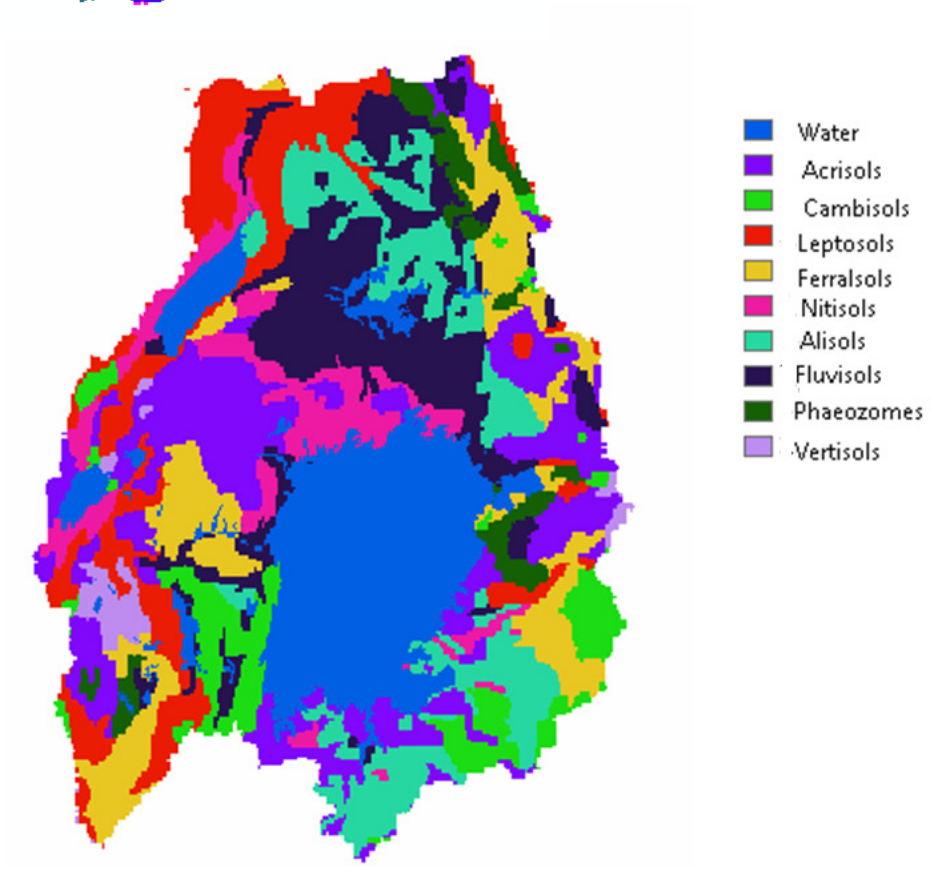

Figure 13: Soils of the Blue Nile (a), and Equatorial Lakes Region (b)

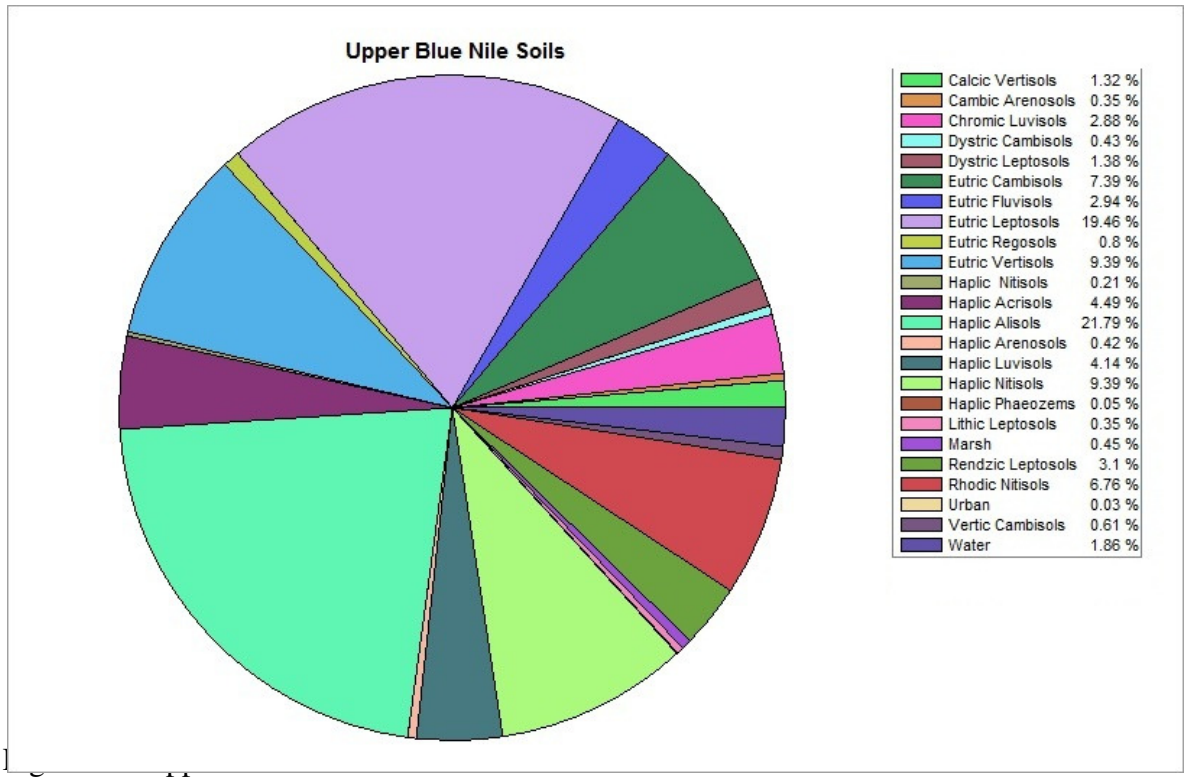

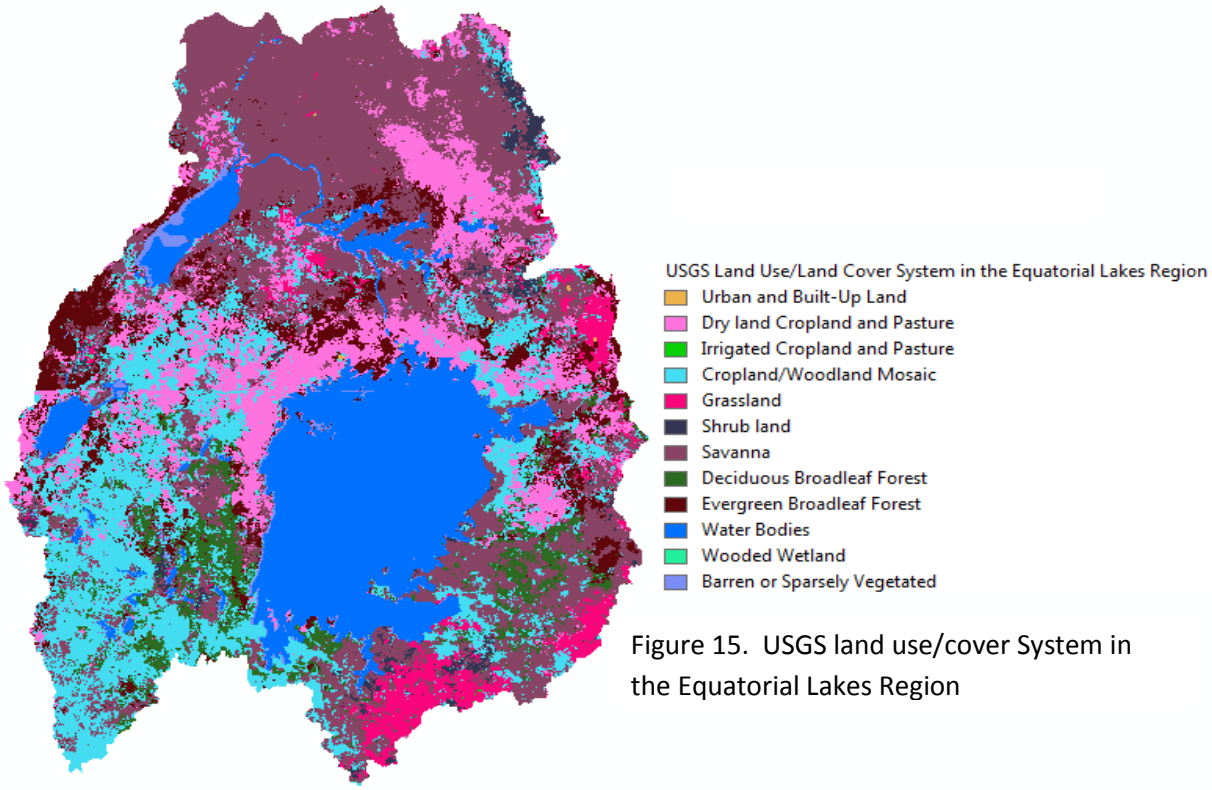

Figure 15. USGS land use/cover System in the Equatorial Lakes Region

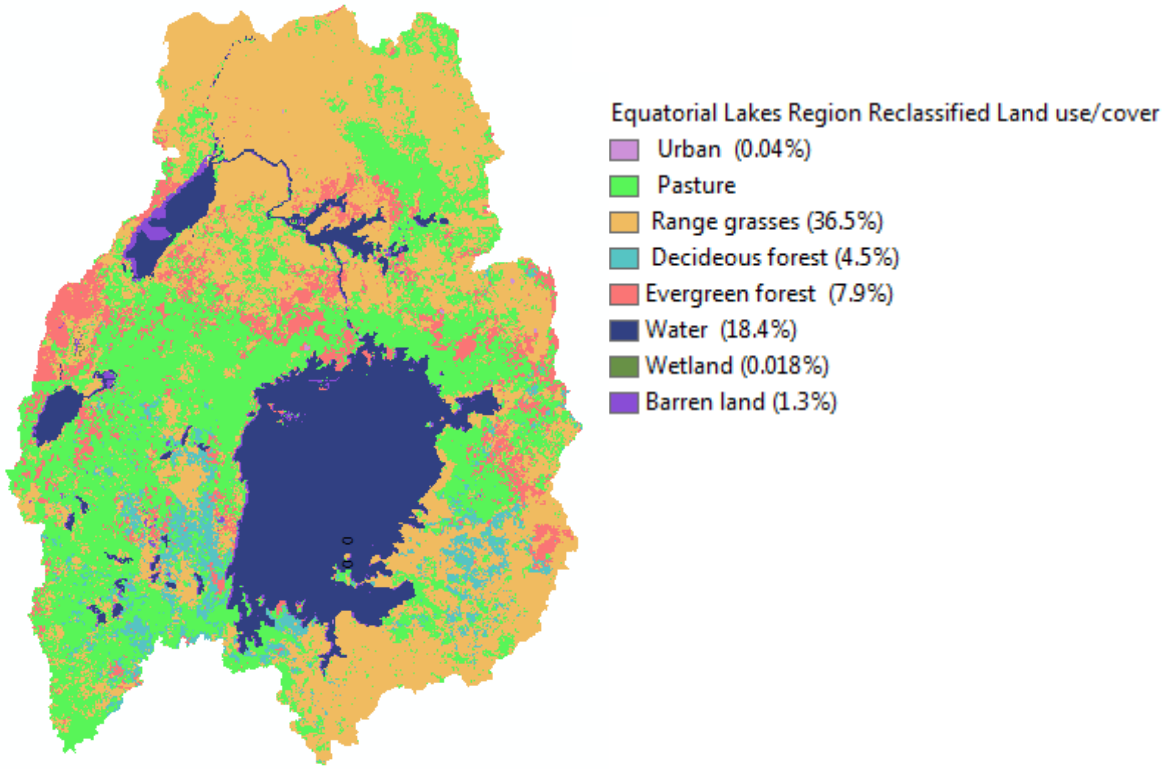

Figure 16. Equatorial Lakes Region land cover reclassified based on the SWAT model land cover/use database

Schuol and Abbaspour (2007) showed that in data scarce regions simulations using generated weather data were superior to simulations using the available poor quality measured data. Daily precipitation, daily maximum and minimum temperature are generated from monthly precipitation, number of wet days, maximum and minimum temperature data from the Climatic Research Unit (CRU) using Monthly to Daily Weather Converter (MODAWEC).

While there exist some other global climate time series, besides the high spatial resolution and long temporal coverage, the CRU dataset provides the most comprehensive compilation of surface climate variables (Schuol and Abbaspour, 2007).

Daily wind speed, relative humidity and solar radiation data to be used in the Penman-Monteith equation to get potential evapotranspiration were found from NCEP/NCAR Reanalysis1 (http://www.esrl.noaa.gov/psd/data/gridded/data.ncep.reanalysis.html). The wind speed and relative humidity data are gridded at 2.5^0 latitude/longitude resolution. The solar radiation data are gridded at about 1.91^0x1.875^0 latitude/longitude resolution. The data point locations are shown in Figure 20.

2.4.6 Wetlands and Reservoir Data

Wetlands and reservoir data are found from the Global Lakes and Wetlands Database (GLWD, Lehner and Do¨ll, 2004)(see Figure 21). The required data on the lakes and wetlands that are not available in the Global Lakes and Wetlands Database are gathered from papers and the web. Table 1 shows the main lakes that were used in the SWAT model of the Equatorial Lakes Region.

2.4.7 River Discharge Data

River discharge data for calibration and validation purposes are obtained from the Global Runoff Data Centre (GRDC, http://grdc.bafg.de).

2.5 Model Setup for the Blue Nile and Equatorial Lakes Region

The SWAT model was set up using the data described above and ArcSWAT interface. The interface helped to delineate the catchment boundary from the DEM and further subdivide the catchment into subbasins. The land cover, DEM and soil layers were used to generate HRUs. The climatic data were also integrated spatially and temporally to assign these data as the main drivers of the model to the various subbasins.

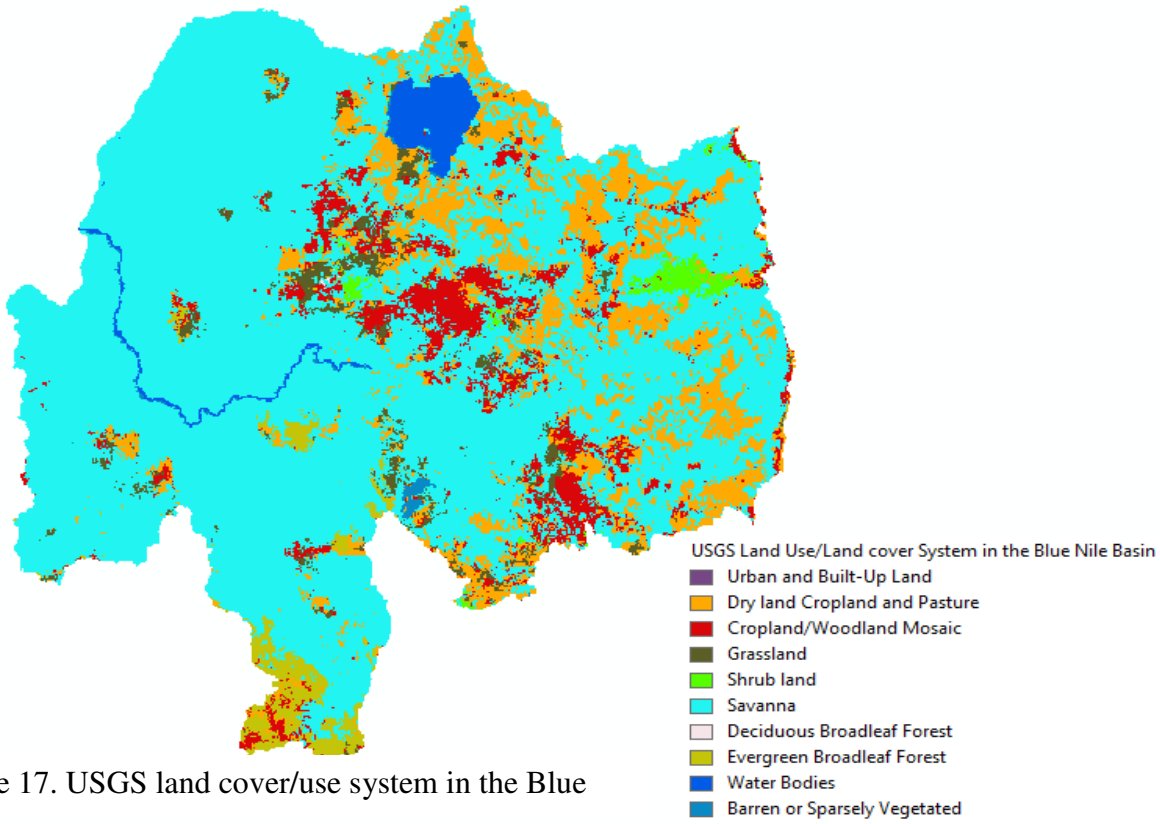

Figure 17. USGS land cover/use system in the Blue

2.5.1 Watershed Delineation

DEM was used to delineate the watershed and to analyze the drainage patterns of the land surface terrain. This tool uses and expands ArcGIS and Spatial Analyst extension functions to perform watershed delineation (Neitsch et al., 2002).

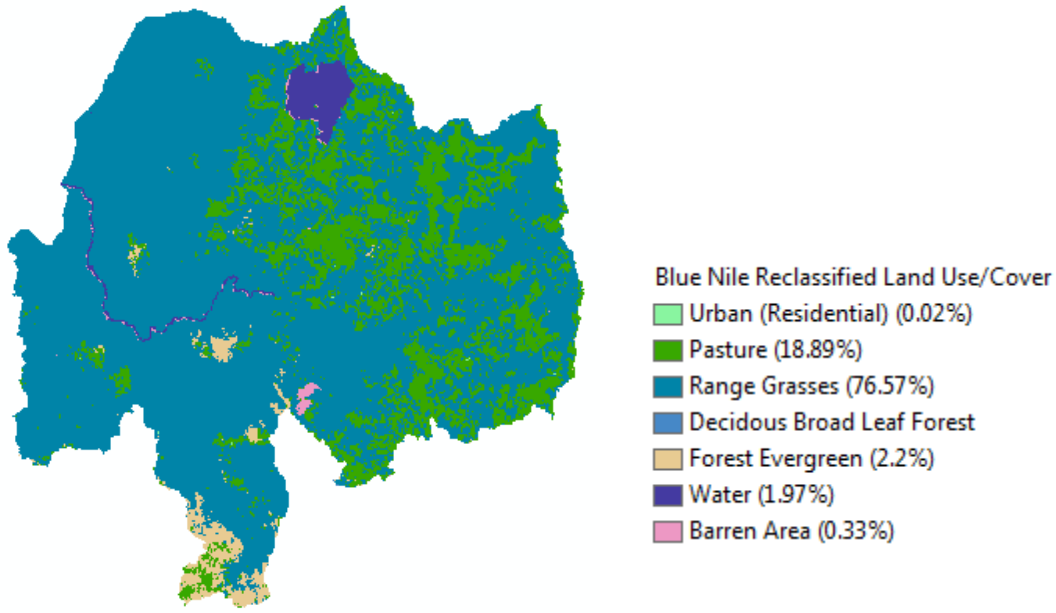

Figure 18. Blue Nile land cover/use reclassified based on the SWAT model land cover/use database

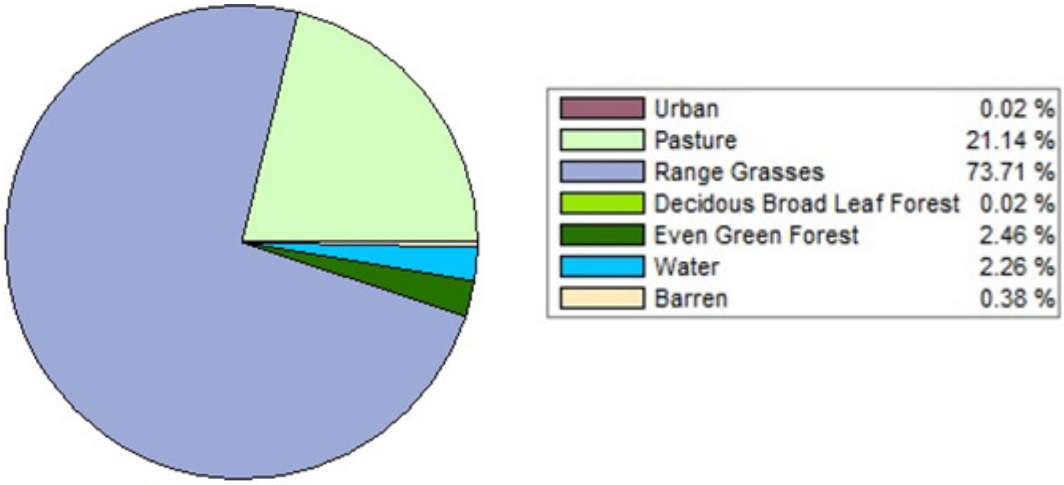

Figure 19: Upper Blue Nile land cover/land use distribution

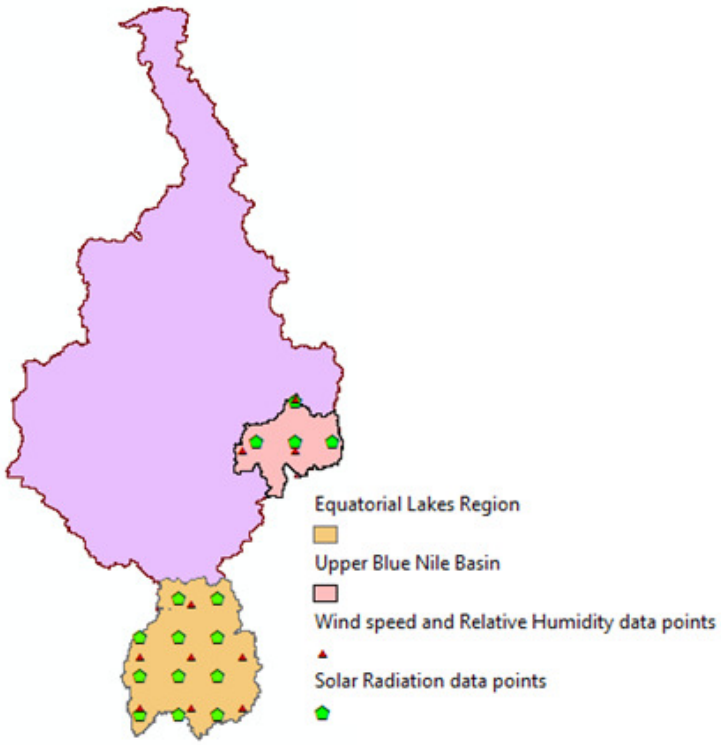

Figure 20. Data point Locations of wind speed, relative humidity and solar radiation from NCEP/NCAR Reanalysis 1

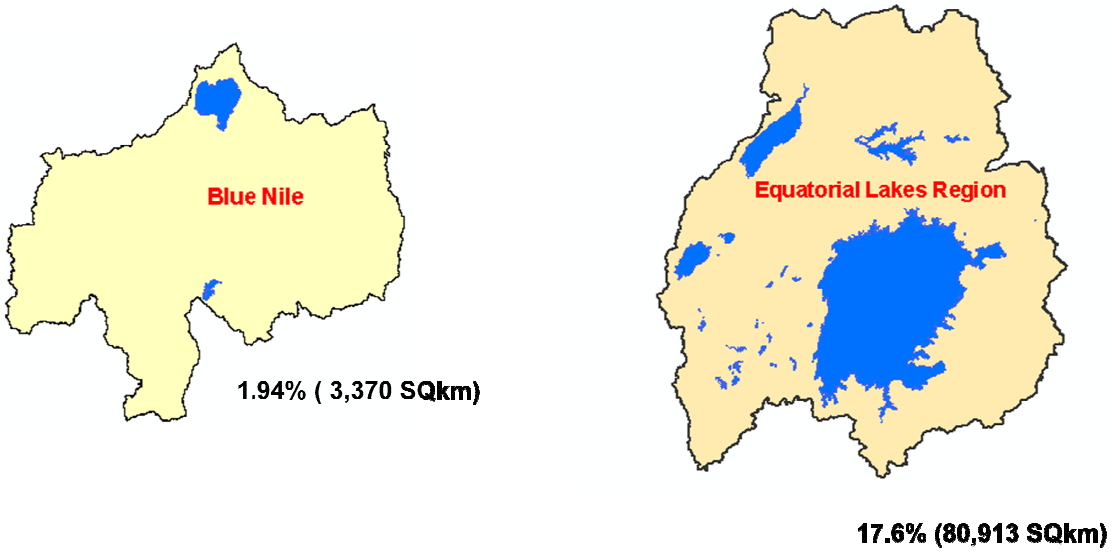

Figure 21. Major Lakes in the Blue Nile (a), and Equatorial Lakes Region (b) and their area coverage

Table 1. Major Lakes in the Equatorial Lakes Region and relevant information that were used in the SWAT2009 model

No.	LAKE_NAME	Area (km^2)	Perimeter (km)	Longitude (degree)	Latitude (degree)	Elevation (meter)
1	Lake Victoria	67075.2	6041.4	33.23	-1.30	1140
2	Albert	5401.9	508.2	30.91	1.67	629
3	Edward	2252.5	290.1	29.61	-0.39	781
4	Kyoga	1727.7	692.6	33.01	1.50	1043
5	Kwania	561.9	419.0	32.65	1.72	1043
6	George	273.4	137.7	30.17	0.00	907
7	Bisina	174.1	100.6	34.03	1.66	1043
8	Rweru	102.4	56.7	30.32	-2.39	1373
9	Nakuwa	89.8	76.4	33.49	1.19	1043
10	*	82.4	195.8	30.13	-2.44	1386
11	Ihema	78.3	63.5	30.77	-1.89	1355
12	Burigi	77.2	72.4	31.32	-2.12	1217
13	*	52.7	119.1	29.89	-1.30	2010
14	*	50.7	66.4	29.78	-1.44	1869
15	Kachira	45.8	76.7	31.13	-0.57	1315

From Global Lakes and Wetlands Database: http://www.worldwildlife.org/science/data/item1877.html); * shows names of lakes were not found.

The DEM of the basins is loaded into an ESRI (Environmental System Research Institute) grid format. DEM mask was used to dictate ArcSWAT interface to use only the masked area for stream delineation. A predefined digital stream network layer was imported and superimposed onto the DEM to accurately delineate the location of the streams. The spatial datasets used in the SWAT model were projected to the same transverse mercator projection parameters: UTM Zone 37N for Blue Nile Basin and to UTM Zone 36S for Equatorial Lakes Region, using ArcGIS 9.3. The watershed delineation process includes the following main steps: DEM setup, stream definition,

outlet and inlet definition, watershed outlets selection and definition and calculation of subbasin parameters.

On the basis of the DEM and stream network, a minimum drainage area of 1000 km^2 was used to discretize the upper Blue Nile basin into 107 subbasins and the Equatorial Lakes Region into 223 subbasins (Figure 22). SWAT model subdivides a subwatershed into areas having unique land use, soil and slope combinations. The watershed outlet is manually added and selected to finalize the watershed delineation.

2.5.2 HRU Definition

The hydrologic response units (HRUs) analysis tool in ArcSWAT helps to load land use and soil layers to the project. The USGS Land use/Land cover spatial data were reclassified into SWAT land cover/plant types. A look up table was created to identify the SWAT code for the different categories of land cover/land use on the map as per the required format. The delineated watershed by ArcSWAT and the prepared land use overlapped 97.5% for the upper Blue Nile and 99.51% for the Equatorial Lakes Region.

The soils of the Blue Nile and Equatorial Lakes Region were incorporated into the SWAT soil database prior to the SWAT model run and a look up table was created to identify the SWAT code for the different categories of soils on the map as per the required format.

The delineated watershed and soil map have an overlap of 97.9% for the upper Blue Nile basin and 98.98% for the Equatorial Lakes region. HRU analysis in ArcSWAT includes divisions of HRUs by slope classes in addition to land use and soils. The slope discretization shown in table 2 was used to discretize the slope into four classes. The

Equatorial Lakes Region has relatively flatter slopes than the Blue Nile. To reach at appropriate slope discretization, we first calculated the slopes of each basin and studied the slope patterns. To define the distributions of HRUs multiple HRU definition was used. 20 percent land use, 10 percent soil and 20% slope thresholds were used according to what the ArcSWAT user manual recommends and water and barren areas were exempted from the HRU definition threshold. Depending on the input data and HRU definition provided 595 and 1981 HRUs were created for the upper Blue Nile and Equatorial Lakes Region respectively as shown in table 3.

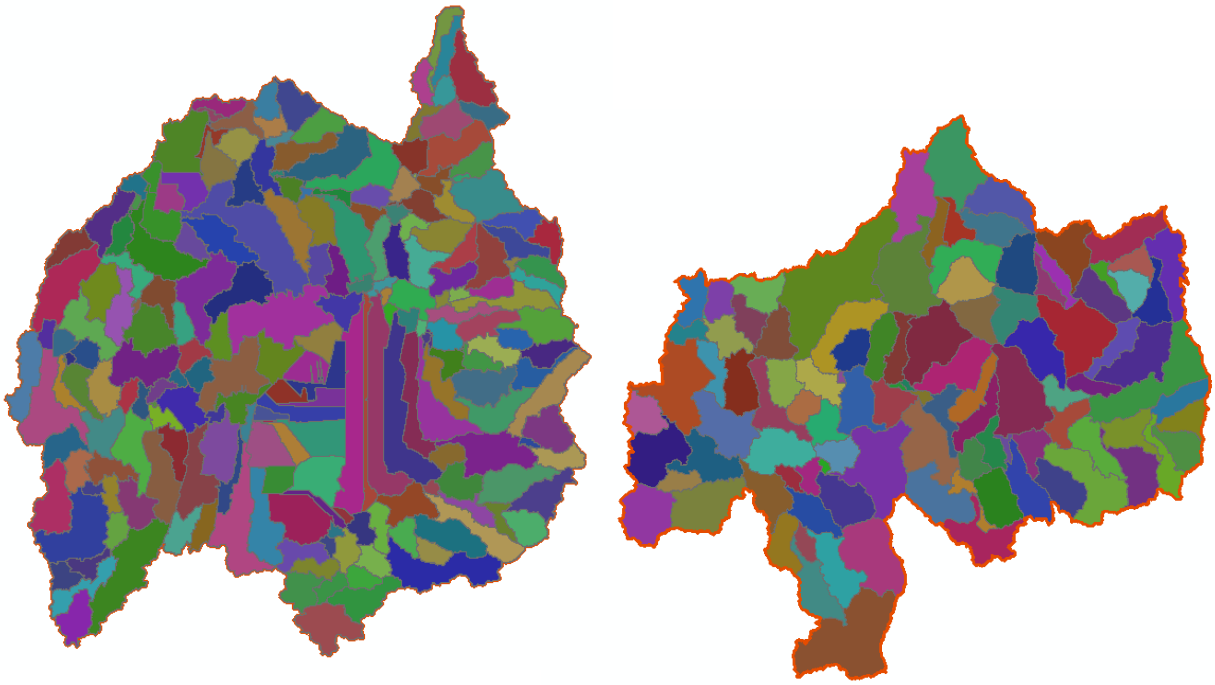

Figure 22: Upper Blue Nile and Equatorial Lakes Region SWAT subbasin discretization

Table 2. Slope discretization used for creation of HRUs in the Equatorial Lakes Region and upper Blue Nile basin

	Equatorial Lakes Region	Blue Nile Basin
Clas	Slope Range	Slope Range
1	0% - 1%	0% - 3%
2	1% - 3%	3% - 5%
3	3% - 5%	5% - 8%
4	> 5%	> 8%

Table 3. HRUs in the upper Blue Nile Basin and Equatorial Lakes Region

HRU_ID	SUBBASIN	Area_SUB	LANDUSE	Area_land use	SOIL	Area_soil	slope class	Area_slope	SLOPE	UNIQUECOMB
582	105	335424.6125	RNGE	334742.5333	ALISOL	230707.7867	8-9999	230707.787	18.2768	105_RNGE_ALISOL_8-9999
583	105	335424.6125	RNGE	334742.5333	NITISO	49847.42232	8-9999	49847.4223	16.10698	105_RNGE_NITISO_8-9999
584	105	335424.6125	RNGE	334742.5333	VERTI	54187.32425	8-9999	35553.207	15.64026	105_RNGE_VERTI_8-9999
585	105	335424.6125	RNGE	334742.5333	VERTI	54187.32425	5-8	18634.1173	6.405826	105_RNGE_VERTI_5-8
586	106	183104.8312	RNGE	93629.24326	ALISOL			549	18.24747	106_RNGE_ALISOL_8-9999
587	106	183104.8312	RNGE	93629.24326	LEPTO			3884	16.73584	106_RNGE_LEPTO_8-9999
588	106	183104.8312	FRSE	87221.30607	ALISOL	76999.14516	8-9999	76999.1452	18.0523	106_FRSE_ALISOL_8-9999
589	106	183104.8312	FRSE	87221.30607	LEPTO	10222.1609	8-9999	10222.1609	15.85056	106_FRSE_LEPTO_8-9999
590	107	548114.8475	RNGE	284795.3902	ACRISO	34154.93562	8-9999	34154.9356	20.06223	107_RNGE_ACRISO_8-9999
591	107	548114.8475	RNGE	284795.3902	ALISOL	178532.2305	8-9999	178532.231	19.38708	107_RNGE_ALISOL_8-9999
592	107	548114.8475	RNGE	284795.3902	VERTI	72108.22403	8-9999	50319.1255	16.00909	107_RNGE_VERTI_8-9999
593	107	548114.8475	RNGE	284795.3902	VERTI	72108.22403	5-8	21789.0985	6.396894	107_RNGE_VERTI_5-8
594	107	548114.8475	FRSE	254392.5164	ACRISO	87019.78673	8-9999	87019.7867	19.67965	107_FRSE_ACRISO_8-9999
595	107	548114.8475	FRSE	254392.5164	ALISOL	167372.7297	8-9999	167372.73	19.94868	107_FRSE_ALISOL_8-9999

Blue Nile Basin

HRU_ID	SUBBASIN	Area-Sub	LANDUSE	Area_Land use	SOIL	Area_soil	Slope Class	Area_slope	SLOPE	UNIQUECOMB
1969	220	595571.94	PAST	365946.3167	LEPTO	228952.114	5-9999	228952.114	14.10998	220_PAST_LEPTO_5-9999
1970	220	595571.94	PAST	365946.3167	REGOSO	136994.2027	5-9999	136994.203	17.68615	220_PAST_REGOSO_5-9999
1971	220	595571.94	FRSD	164031.1978	CAMBISO	27063.67838	5-9999	27063.6784	12.69491	220_FRSD_CAMBISO_5-9999
1972	220	595571.94	FRSD	164031.1978	LEPTO	113560.784	5-9999	113560.784	14.21851	220_FRSD_LEPTO_5-9999
1973	220	595571.94	FRSD	164031.1978	REGOSO	23406.73544	5-9999	23406.7354	15.64438	220_FRSD_REGOSO_5-9999
1974	221	265454.01	RNGE					132026.758	0.573844	221_RNGE_ALISOL_0-1
1975	221	265454.01	RNGE					131986.843	1.696757	221_RNGE_ALISOL_1-3
1976	222	211532.31	PAST	207358.3955	LEPTO	25114.31391	5-9999	25114.3139	13.71838	222_PAST_LEPTO_5-9999
1977	222	211532.31	PAST	207358.3955	REGOSO	182244.0816	5-9999	182244.082	15.74541	222_PAST_REGOSO_5-9999
1978	223	340698.96	RNGE	327710.1432	ACRISO	40212.17876	0-1	11846.3862	0.629998	223_RNGE_ACRISO_0-1
1979	223	340698.96	RNGE	327710.1432	ACRISO	40212.17876	1-3	28365.7925	1.866699	223_RNGE_ACRISO_1-3
1980	223	340698.96	RNGE	327710.1432	ALISOL	287497.9645	0-1	109664.929	0.616601	223_RNGE_ALISOL_0-1
1981	223	340698.96	RNGE	327710.1432	ALISOL	287497.9645	1-3	177833.036	1.768633	223_RNGE_ALISOL_1-3

Equatorial Lakes Region

2.5.3 Importing Weather Data

After HRU definition weather data to be used in the simulation are imported. The time series weather data are loaded using weather station locations, and for each type of weather data loaded (precipitation, temperature, solar radiation, wind speed and relative humidity), each subwatershed is linked to one gage.

2.6 Surrogate Regional Climate Change Scenarios

Surrogate climate change scenarios (SCCS), by which given changes are made to the baseline weather data, are used to assess potential impacts of climate change on the flow of the upper Blue Nile basin. SCCS are used for sensitivity experiments, but cannot provide a full picture of climate change impacts on water resources for the region of application. The surrogates are approximated using Intergovernmental Panel on Climate Change (IPCC, 2007) data. The period from 1960-2000 was used as baseline and has been used to determine the changes and the effect of the surrogate climate changes. The following Surrogate Regional Climate Change Scenarios are used:

- A2 surrogate: 25%, 3^{o}C, 2^{o}C increase for precipitation, minimum and maximum daily temperature, respectively, and CO_2 emission of 850ppm.
- A1B surrogate: 20%, 2.5^{o}C, 1.5^{o}C increase for precipitation, minimum and maximum daily temperature, respectively, and CO_2 of 700ppm.
- B1 surrogate: 10%, 2^{o}C, 1^{o}C increase for precipitation, minimum and maximum daily temperature, respectively, and CO_2 of 500ppm.

CHAPTER THREE

3.0 Results and Discussion

The results and discussion section consists of SWAT hydrologic model customization: sensitivity analysis, calibration, uncertainty analysis and validation results for both the Equatorial Lakes Region and Blue Nile basins and sensitivity of the Blue Nile to surrogate climate change scenarios. The calibration and validation results using SUFI2 over the Equatorial Lakes Region are not satisfactory at a catchment scale; therefore, we

have performed the sensitivity analysis to surrogate climate change scenarios over the Blue Nile basin only.

3.1 Blue Nile

3.1.1 Sensitivity Analysis

The comparison of default simulation output with the observed streamflow data at the gauge station at sudan border showed clear difference between the observed and simulated flows. The results from the simulation cannot be directly used for further analysis but instead the ability of the model to sufficiently predict the constituent stream flow should be evaluated through sensitivity analysis, uncertainty analysis, model calibration and validation (White and Chaubey, 2005).

Sensitivity analyses were conducted for the Blue Nile basin to determine the parameters needed to improve simulation results and thus to better understand the behavior of the hydrologic system and to evaluate the applicability of the model. Parameters for sensitivity analysis were selected by reviewing previously used calibration parameters and documentation from the SWAT manuals (e.g. Werner, 1986; Bosshart, 1997; Arnold et al., 1999 and 2000; Zeleke, 2000; Kirsch et al., 2002; White and Chaubey, 2005; Neitsch et al., 2005; Setegn et al., 2008). Out of the 27 global parameters of hydrology in the SWAT model, 19 parameters were found to be sensitive and 16 of the most sensitive parameters that are related to our project were used for calibration (Table 4). Sensitivity analysis without observed data measures the sensitivity of the output to changes in input parameters. Sensitivity analysis with observed data measures the sensitivity of the predicted output and model error to changes in input parameters. The remaining parameters had no significant effect on stream flow simulations. As changes in their

values do not cause significant changes in the model output, they were not considered for calibration.

Data from 1979 to 1983 were applied for sensitivity analysis and calibration and subsequently validate hindcasts over the period 1984-1987. The flow was sensitive to the following ground water parameters: the base flow alpha factor (Alpha_Bf) or baseflow recession constant in days, threshold depth of water in the shallow aquifer required for return flow to occur (Gwqmn) in mm, Ground water Delay (Gw_Delay) in days, threshold depth of water in the shallow aquifer for "revap" or percolation to the deep aquifer to occur (Revapmin) in mm, and Groundwater "revap" coefficient (Gw_Revap). The flow was also found to be sensitive to soil properties: soil evaporation compensation factor (Esco), available water capacity of the soil layer (Sol_Awc) in mm /mm of soil depth, saturated hydraulic conductivity (Sol_K), depth from soil surface to bottom of layer (Sol_Z) in mm and moist soil albedo (Sol_Alb). The flow was also sensitive to crop parameters: maximum canopy storage (Canmx) in mm H_2O, and plant uptake compensation factor (Epco).

3.1.2 Flow Calibration and Validation using SUFI2 Algorithm

Model calibration is the modification of parameter values and comparison of predicted output of interest to measured data until a defined objective function is achieved (James and Burges, 1982). The model was initially calibrated on annual basis followed by monthly time steps. Parameters for modification are selected from those identified by the sensitivity analysis (Table 4). To get converged solution 1800 iterations were used. The p-factor, which is the percentage of observations bracketed by the 95% prediction uncertainty (95PPU), brackets 90% of the observation and r-factor equals 0.7 for

calibration showing that the SUFI2 captured the observations very well. The R^2 and Nash-Sutcliffe (NS) coefficient, calculated between the best simulation (simulation with the largest objective function value) and the measured data, indicate very good results for calibration (over the period from 1979-1983) and validation (over the period from 1984-1987) at the Sudan Border, an outlet of the upper Blue Nile basin.

The calibration resulted in P-factor of 90%, R-factor of 0.7, R^2 of 0.93 and NS of 0.93 whereas validation resulted in R^2 of 0.92 and NS of 0.92 (Figures 24-28). Bekele and Knapp (2010) suggested that model simulation with these results can be judged as very good. The calibration process using SUFI2 algorithm gave the final fitted parameters shown in Table 5. These final fitted parameter values were incorporated into the SWAT2009 model for validation and to investigate the impact of different climate change scenarios in the Blue Nile Basin. The uncertainty of simulated flow is due to errors in input data such as rainfall and temperature as the data are stochastically generated from a gridded monthly data that uses small number of stations for interpolation in the region and/or other sources of uncertainties such as upstream dam construction for town water supply, diversion of streams for irrigation, error in the type of soil/land cover and the corresponding soil/land cover properties in the area and other unknown activities in the subbasins. SWAT model does not consider the effect of erosion on runoff but soil erosion can affect the structures, infililtration capacity and other properties of the soil which makes the predictions uncertain.

As can be seen from the cumulative distribution for calibration in Figures 29, in the calibration period the best simulation overestimates low flows. During the validation

period, one can observe that the low flows are overestimated and the peak flows are underestimated (Figure 30). The average annual discharge during calibration and validation are shown in Table 6.

Table 4. The 16 most sensitive parameters in the upper Blue Nile basin, used for calibration, based on the approach of Van Grienven *et al*., 2006

No	parameter	Description	Rank without observed data	Rank with observed data
1	Alpha_Bf	Base flow recession constant	13	3
2	Canmx	maximum canopy storage (mm H_2O)	4	7
3	Ch_k2	Effective hydraulic conductivity in main channel alluvium (mm/hr)	6	9
4	Ch_N2	mannngs's "n" value for the main channel	14	15
5	Cn2	Initial SCS runoff curve number for moisture condition II	10	14
6	Epco	plant uptake compensation factor	9	8
7	Esco	soil evaporation compensation factor	1	1
8	Gw_Delay	ground water delay (days)	11	13
9	GW_Revap	Revap Coefficient	5	6
10	Gwqmn	threshold water level in shallow aquifer for base flow (mm H_2O)	7	5
11	Revapmn	threshold depth of water in the shallow aquifer for the "revap" to occur (mm H_2O)	16	11
12	Sol_Alb	moist soil albedo	12	12
13	Sol_Awc	available water capacity of soil (mm/mm)	2	2
14	Sol_K	saturated hydraulic conductivity	8	10
15	Sol_Z	depth from soil surface to bottom of layer (mm)	3	4
16	Surlag	surface runoff lag time (days)	15	16

Table 5. SWAT flow sensitive parameters and fitted values after calibration using SUFI2 for the upper Blue Nile Basin

No	Sensitive Parameter	Lower and Upper Bound	Final Fitted Value
1	Alpha_Bf	0-1	0.005
2	Canmx	0-100	37.63
3	Ch_k2	-0.01-500	11.72
4	Ch_N2	-0.01-0.3	0.03
5	CN2	±50%	-44.5%*
6	Epco	0-1	1.0
7	Esco	0-1	0.54
8	Gw_Delay	0-500	15
9	GW-Revap	0.02-0.2	0.052
10	Gwqmn	0-5000	77
11	Revapmn	0-500	47.3
12	Sol_Alb	±25%	-4.2%*
14	Sol_Awc	±25%	9.5%*
14	Sol_K	±50%	42.3%*
15	Sol_Z	±25%	-2%*
16	Surlag	0-24	14

CN2, S_Awc, Sol_K, Sol_Z and Sol_Alb have different parameter values depending on the land cover or the soil texture type. Asterisk means relative change of the parameter value.

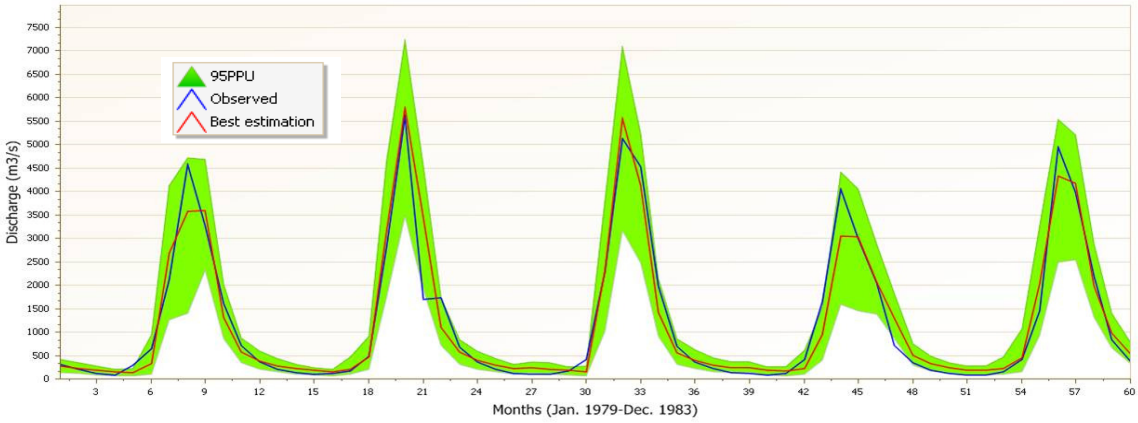

Figure 24. Calibration at Sudan Border: P-factor = 90%, R-factor = 0.7, R^2 = 0.93 and NS = 0.93.

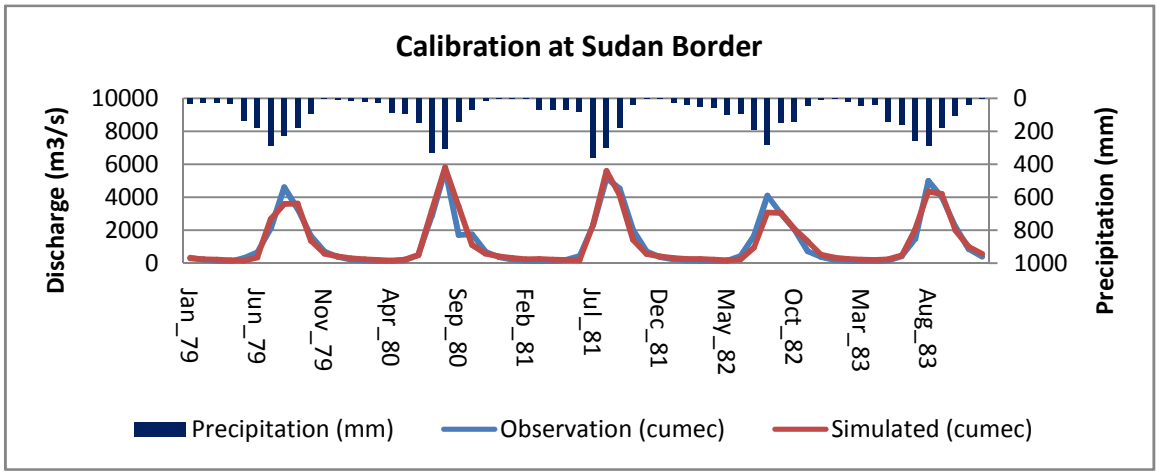

Figure 25. Time series of measured and simulated monthly flow calibration results

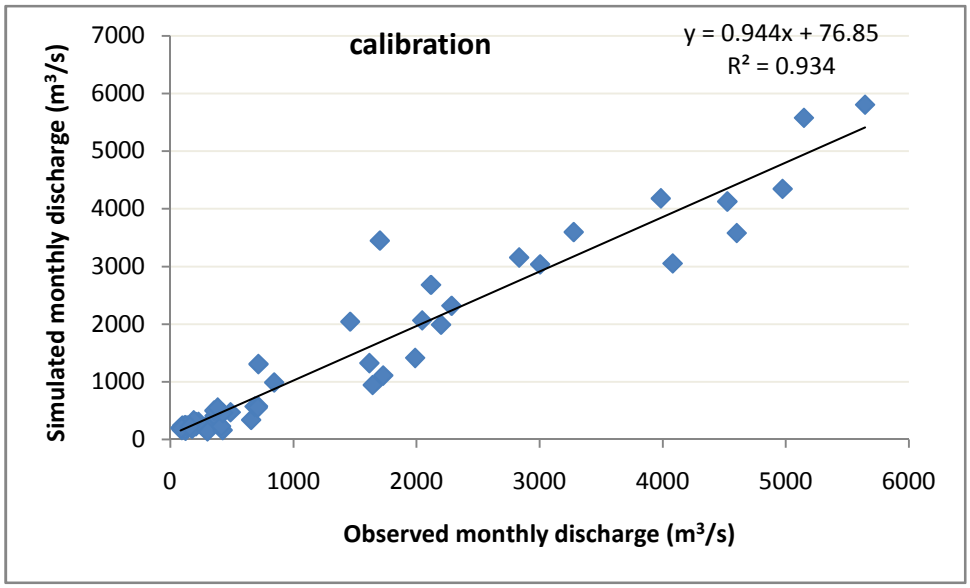

Figure 26. Flow correlation for calibration period

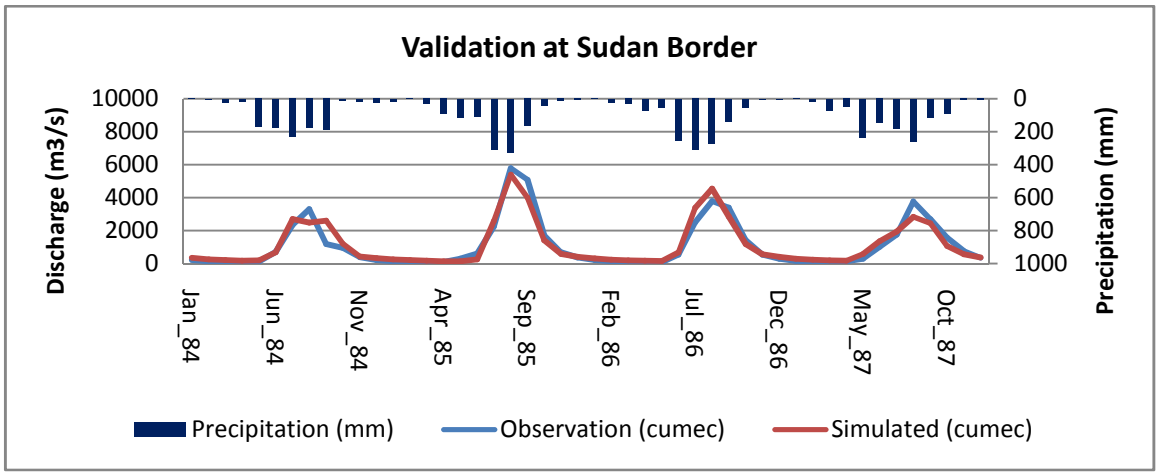

Figure 27. Time series of measured and simulated monthly flow validation results, $R^2 = 0.92$ and NS = 0.92

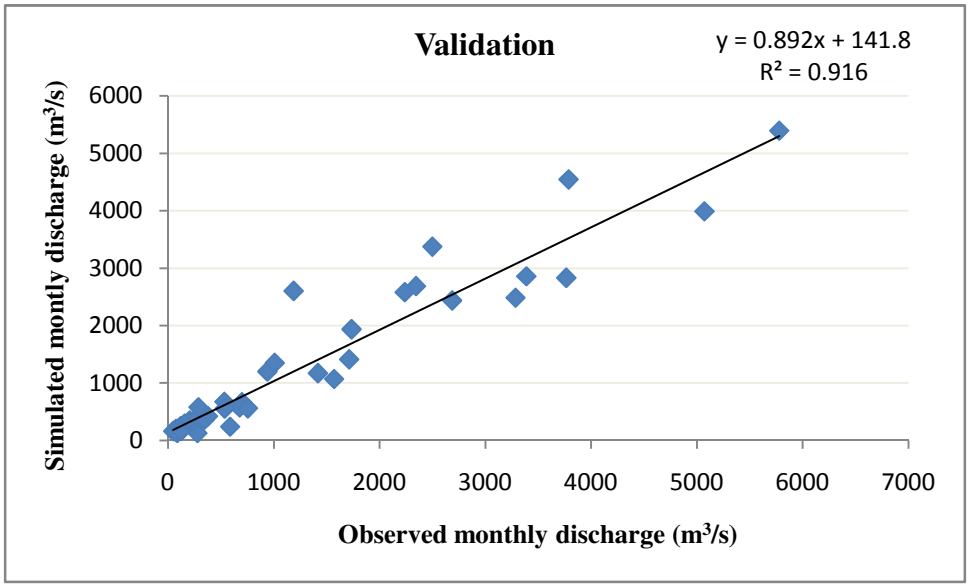

Figure 28. Flow correlation for validation period at Sudan Border Discharge station

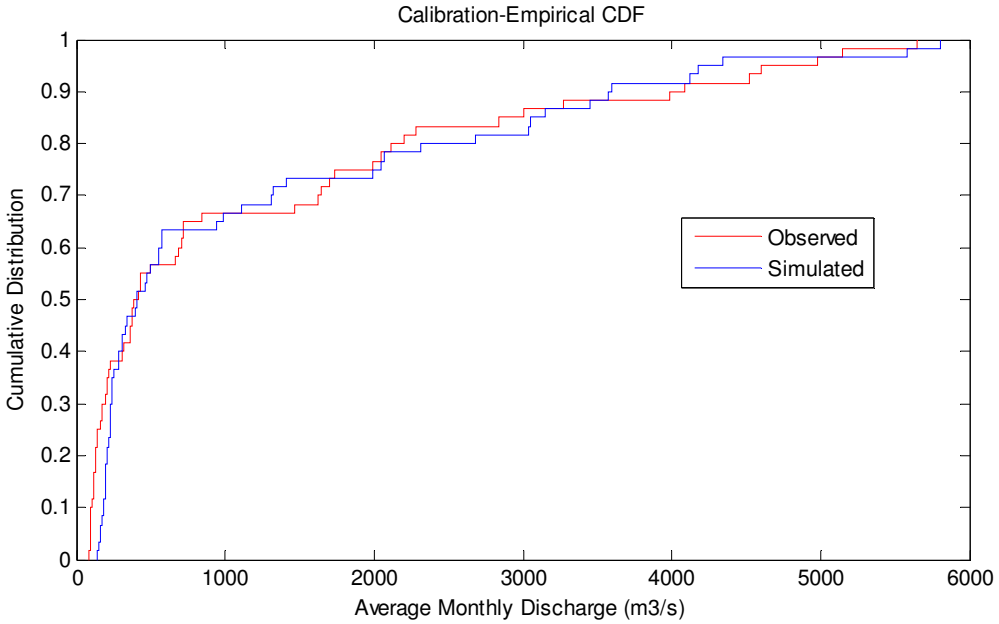

Figure 29. Cumulative distribution for calibration at Sudan Border

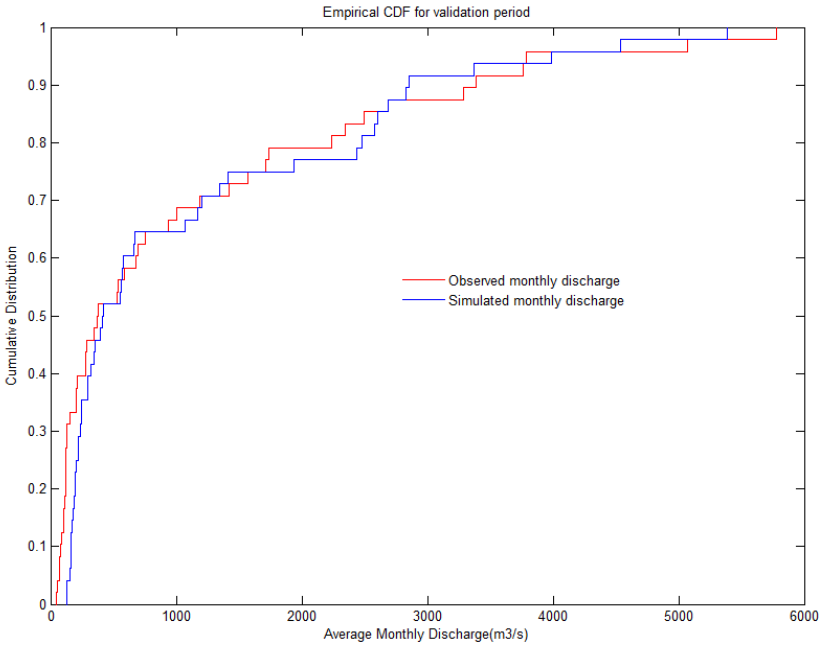

Figure 30. Cumulative distribution for validation period at Sudan Border

Table 6. Average annual discharge (m^3/s) from the upper Blue Nile Basin at Sudan border

	Calibration Period	Validation Period	Average
Observed	1211.8	1091.6	1158.4
SWAT	1221.8	1115.6	1174.6

The annual discharge from Table 6 above gives 36,555,890,215 m^3 and 37,064,644,620 m^3 for calibration and validation respectively. During this time there was reduction in discharge because of prolonged drought. The simulated average discharge from 1960-2000 for the upper Blue Nile at Sudan border is 1495.2 m^3/s which gives an annual discharge of 47,184,584,853 m^3. This amount is 56.1% of the annual 84.1 Billion m^3 at Aswan High Dam.

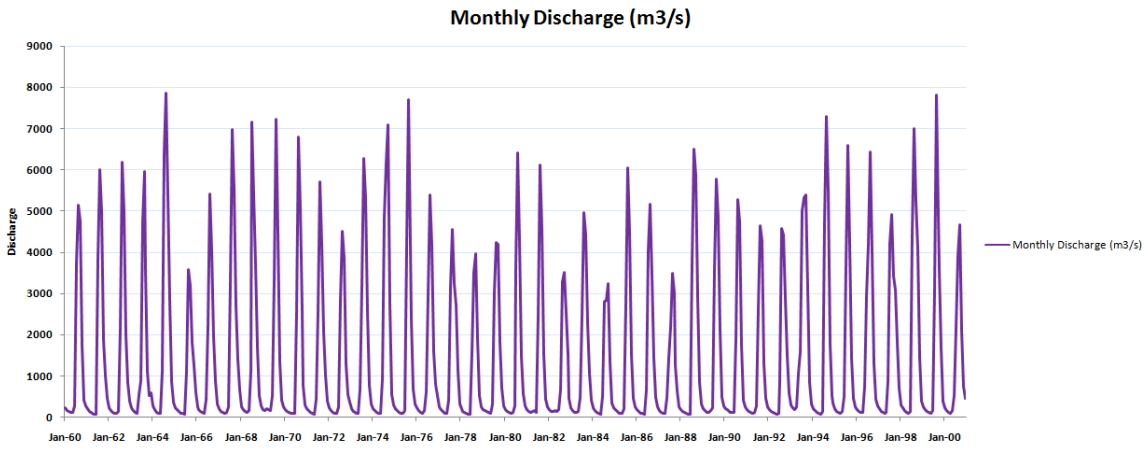

Figure 31. Simulated hydrograph of the upper Blue Nile basin for baseline Scenario (1960-200).

3.1.3 Sensitivity to potential climate change in the Blue Nile Basin

Since the objective of this work is to assess the impacts of potential climate change on hydrological and water resources, surrogate climate change scenarios (SCCS) were adopted from the Intergovernmental Panel on Climate Change (IPCC-2007) data (see section 2.6 for details) to use as input to SWAT. These SCCS are not intended to be accurate predictions of future climate conditions; rather, they are used for sensitivity experiments.

The impact of the SCCS, changed CO_2, temperature, and precipitation changes on the water balance components in the basin was estimated using a sensitivity analysis employing the calibrated SWAT model. The baseline streamflow is represented by the calibration simulation with the highest objective function. In the first part of the analysis, separate model simulations were performed for B1 surrogate, A1B surrogate and A2 surrogate. In the second part of the simulation, separate model simulations were performed for $\pm 10\%$, $\pm 20\%$ and $\pm 25\%$ precipitation changes; 550 ppm, 700ppm and 850ppm atmospheric CO_2 concentration; 1 and 2, 1.5 and 2.5, and 3 and 4 ^{o}C increments to daily maximum and minimum temperature respectively.

The average water balance components of the different scenarios were compared with the baseline hydrologic variables. Table 7 shows the average water balance components on annual basis from 1960-2000. Tables 8, 9 and 10 show the average water balance components on annual basis for B1 surrogate, A2 surrogate and A1B surrogate respectively. As Table 20 shows, surface runoff, lateral flow and water yield increase most in A2 surrogate than A1B and B1 surrogates. In A2 surrogate the average annual

surface runoff, lateral flow and water yield increased by 104%, 33% and 77% of the baseline (1960-2000) respectively (see table 20). The change in evapotranspiration from the baseline in A2 surrogate and A1B surrogate are the same. This is caused by the fact that though daily temperature increase is more in A2 surrogate than in A1B surrogate, the effect of temperature is damped by the increased atmospheric CO_2 as stomatal conductance decreases with atmospheric CO_2 increments (Fontaine et al., 2001).

Surface runoff is the most sensitive hydrologic variable to precipitation change. 10%, 20% and 25% precipitation increments to the baseline precipitation caused 38%, 82% and 106% increment to the average annual surface runoff while the average annual water yield increased by 42%, 67% and 80% respectively and the average annual evapotranspiration increased by 2%, 4% and 5% respectively (Table 20). Increasing each measured precipitation value by 10%, 20% and 25% significantly increases water yield (Table 20 and Figure 36). The simulation with 25% increase to the measured precipitation values shows 106% (49.06mm), 33% (26.77mm) and 80% (234.3 mm) increase to the annual average surface runoff, lateral flow and water yield of the baseline respectively, whereas 25% decrease to the measured precipitation values shows 67% (31.04 mm), 34% (27.46 mm) and 38% (110.21mm) decrement to the annual average surface runoff, lateral flow and water yield respectively as shown in Tables 7, 16 and 20. The hydrology is more sensitive to precipitation changes than to changes in temperature or atmospheric CO_2 (Table 20).

Increasing temperature decreases the surface runoff, lateral flow and water yield and increases evapotranspiration. Increased air temperature increases the vapor pressure deficit increasing the evaporative demand and reducing the surface runoff, lateral flow

and water yield. The basin is less sensitive to temperature change as compared to precipitation change as can be clearly observed from Table 20.

Increasing atmospheric CO_2 increases average annual runoff, lateral flow and water yield and decreases the average annual evapotranspiration (Table 11-13 and 20, Figures 33 and 35). When the atmospheric CO_2 increased to 850 ppm, average annual runoff, lateral flow and water yield increased by 22% (10.3mm), 9% (7.3 mm) and 19% (57.3 mm) respectively while evapotranspiration decreased by 12.8% (107.1 mm) (Tables 13 and 20).

Table 7. Water balance components on annual average basis from 1960-2000 over the upper Blue Nile basin

Month	Rain (mm)	Surface Runoff (mm)	Lateral Flow (mm)	Water Yield (mm)	Evapotranspiration (mm)
1	12.51	0.01	2.29	2.37	28.37
2	18.91	0.06	1.51	1.66	30.17
3	41.61	0.13	1.52	1.79	45.61
4	63.26	0.18	1.72	2.23	56.09
5	113.42	0.71	2.55	4.39	71.61
6	158.93	2.45	4.16	11.46	75.73
7	309.26	18.89	10.95	60.88	86.41
8	294.09	16.37	17.36	92.87	72.54
9	178.88	5.67	16.38	69.01	68.83
10	79.09	1.58	11.75	31.39	48.98
11	27.91	0.25	6.71	11.08	38.02
12	13.13	0.01	3.9	4.52	25.92
sum	**1311**	**46.31**	**80.8**	**293.65**	**648.28**

Table 8. Water balance components on annual average basis over the upper Blue Nile basin for B1 Surrogate

Month	Rain (mm)	Surface Runoff(mm)	Lateral Flow (mm)	Water Yield (mm)	Evapotranspiration (mm)
1	13.74	0.03	2.55	2.76	24.34
2	20.76	0.1	1.71	2.07	28.67
3	45.7	0.22	1.76	2.44	48.45
4	69.5	0.3	2.01	3.25	58.71
5	124.58	1.21	3	7.03	74.97
6	174.32	3.94	4.86	19.27	80.78
7	339.42	25.97	12.37	89.99	91.01
8	322.91	21.76	19.33	127.06	77.35
9	196.51	7.64	18.2	91.71	75.1
10	87.05	2.1	13.05	40.76	54.46
11	30.76	0.33	7.43	13.58	41.6
12	14.38	0.02	4.32	5.36	27.36
sum	**1439.63**	**63.62**	**90.59**	**405.28**	**682.8**

Table 9. Water balance components on annual average basis over the upper Blue Nile basin for A2 Surrogate

Month	Rain (mm)	Surface Runoff (mm)	Lateral Flow (mm)	Water Yield (mm)	Evapotranspiration (mm)
1	15.66	0.07	3.01	3.44	22.85
2	23.65	0.21	2.06	2.78	26.84
3	52	0.49	2.18	3.77	48.1
4	79.04	0.65	2.56	5.39	59.26
5	141.64	2.49	3.91	12.09	75.63
6	198.16	7.04	6.25	32.15	81.06
7	385.6	38.33	14.92	123.61	90.4
8	366.86	30.96	22.63	156.69	79.39
9	223.31	10.94	21.16	109.3	80.49
10	99.01	2.95	15.21	49.01	58.68
11	35.03	0.51	8.7	16.41	44.06
12	16.41	0.03	5.09	6.54	29.27
sum	**1636.37**	**94.67**	**107.68**	**521.18**	**696.03**

Table 10. Water balance components on annual average basis over the upper Blue Nile basin for A1B Surrogate

Month	Rain (mm)	Surface Runoff (mm)	Lateral Flow (mm)	Water Yield (mm)	Evapotranspiration (mm)
1	14.98	0.06	2.88	3.25	23.51
2	22.64	0.16	1.95	2.54	27.78
3	49.86	0.37	2.05	3.23	48.91
4	75.85	0.51	2.38	4.53	59.74
5	136.11	1.96	3.58	10.05	76.1
6	190.57	5.89	5.74	27.29	81.49
7	371	34.32	14	112.32	90.7
8	352.91	28.18	21.48	147.49	77.73
9	214.76	10.08	20.19	104.46	76.27
10	95.14	2.73	14.55	47.17	55.95
11	33.59	0.45	8.33	15.69	42.64
12	15.69	0.03	4.86	6.24	28.28
sum	**1573.1**	**84.74**	**101.99**	**484.26**	**689.1**

Table 11. Water balance components on annual average basis over the upper Blue Nile basin with CO_2 of 550 pmm

Month	Rain (mm)	Surface Runoff (mm)	Lateral Flow (mm)	Water yield (mm)	Evapotranspiration (mm)
1	12.51	0.02	2.35	2.46	27.1
2	18.91	0.07	1.56	1.75	29.44
3	41.61	0.16	1.58	1.94	44.01
4	63.26	0.22	1.78	2.45	53.63
5	113.42	0.88	2.65	4.97	68.42
6	158.93	2.96	4.33	13.3	71.88
7	309.26	20.37	11.26	66.01	80.68
8	294.09	16.98	17.73	96.88	67.72
9	178.88	5.91	16.72	71.37	65.17
10	79.09	1.65	12.01	32.55	46.65
11	27.91	0.27	6.87	11.58	36.6
12	13.13	0.01	4	4.71	25.48
sum	**1311**	**49.5**	**82.84**	**309.97**	**616.78**

Table 12. Water balance components on annual average basis over the upper Blue Nile basin with CO_2 of 700 pmm

Month	Rain (mm)	Surface Runoff (mm)	Lateral Flow (mm)	Water Yield (mm)	Evapotranspiration (mm)
1	12.51	0.02	2.42	2.55	25.98
2	18.91	0.08	1.6	1.85	28.47
3	41.61	0.2	1.63	2.12	42.46
4	63.26	0.26	1.86	2.72	51.28
5	113.42	1.05	2.77	5.67	65.26
6	158.93	3.45	4.52	15.31	68.19
7	309.26	21.69	11.56	70.98	75.25
8	294.09	17.56	18.09	100.57	63.17
9	178.88	6.14	17.04	73.61	61.67
10	79.09	1.72	12.26	33.81	44.4
11	27.91	0.29	7.03	12.06	35.15
12	13.13	0.01	4.1	4.92	24.97
sum	**1311**	**52.47**	**84.88**	**326.17**	**586.25**

Table 13. Water balance components on annual average basis over the upper Blue Nile basin with CO_2 of 850 pmm

Month	Rain (mm)	Surface Runoff (mm)	Lateral Flow (mm)	Water Yield (mm)	Evapotranspiration (mm)
1	12.51	0.03	2.51	2.72	24.52
2	18.91	0.1	1.68	2.03	26.75
3	41.61	0.26	1.73	2.46	39.96
4	63.26	0.33	2	3.3	47.99
5	113.42	1.35	2.98	7.01	60.53
6	158.93	4.04	4.83	18.59	62.68
7	309.26	23.48	12.05	78.25	67.38
8	294.09	18.39	18.63	105.79	56.63
9	178.88	6.47	17.51	76.98	56.58
10	79.09	1.81	12.64	35.7	41.08
11	27.91	0.32	7.27	12.81	32.96
12	13.13	0.01	4.25	5.26	24.12
sum	**1311**	**56.59**	**88.08**	**350.9**	**541.18**

Table 14. Water balance components on annual average basis over the upper Blue Nile basin with +10% precipitation

Month	Rain (mm)	Surface Runoff (mm)	Lateral Flow (mm)	Water Yield (mm)	Evapotranspiration (mm)
1	13.76	0.02	2.61	2.81	29.22
2	20.81	0.09	1.74	2.04	31.27
3	45.77	0.2	1.77	2.38	47.54
4	69.58	0.3	2.03	3.17	58.54
5	124.77	1.2	3.03	7.09	74.23
6	174.83	3.88	4.92	20.21	77.58
7	340.19	25.83	12.46	91.79	87.04
8	323.5	21.95	19.43	129.38	72.72
9	196.77	7.79	18.34	94.82	69.11
10	87	2.19	13.24	43.51	49.6
11	30.7	0.36	7.6	14.67	38.91
12	14.44	0.01	4.43	5.62	26.78
sum	**1442.12**	**63.82**	**91.6**	**417.49**	**662.54**

Table 15. Water balance components on annual average basis over the upper Blue Nile basin with +20% precipitation

Month	Rain (mm)	Surface Runoff (mm)	Lateral Flow (mm)	Water Yield (mm)	Evapotranspiration (mm)
1	15.02	0.03	2.94	3.22	30.04
2	22.7	0.13	1.96	2.39	32.37
3	49.93	0.31	2.03	2.92	49.33
4	75.91	0.44	2.35	4.07	60.76
5	136.11	1.82	3.53	9.53	76.45
6	190.72	5.71	5.69	27.13	79.06
7	371.11	33.68	13.94	111.62	87.46
8	352.91	28.34	21.44	148.86	72.81
9	214.65	10.27	20.25	107.54	69.27
10	94.91	2.91	14.7	49.97	50.03
11	33.49	0.51	8.49	16.95	39.6
12	15.76	0.02	4.97	6.48	27.52
sum	**1573.22**	**84.17**	**102.29**	**490.68**	**674.7**

Table 16. Water balance components on annual average basis over the upper Blue Nile basin with +25% precipitation

Month	Rain (mm)	Surface Runoff (mm)	Lateral Flow (mm)	Water Yield (mm)	Evapotranspiration (mm)
1	15.64	0.04	3.1	3.43	30.43
2	23.64	0.15	2.08	2.58	32.9
3	52.01	0.37	2.16	3.23	50.17
4	79.07	0.54	2.52	4.58	61.79
5	141.78	2.2	3.79	10.92	77.42
6	198.67	6.73	6.08	30.89	79.68
7	386.58	37.92	14.66	121.57	87.64
8	367.61	31.83	22.42	158.55	72.85
9	223.6	11.65	21.18	113.98	69.33
10	98.87	3.32	15.42	53.27	50.21
11	34.88	0.59	8.92	18.07	39.91
12	16.41	0.03	5.24	6.92	27.86
sum	**1638.76**	**95.37**	**107.57**	**527.99**	**680.19**

Table 17. Water balance components on annual average basis over the upper Blue Nile basin with -10% precipitation

Month	Rain (mm)	Surface Runoff (mm)	Lateral Flow (mm)	Water Yield (mm)	Evapotranspiration (mm)
1	11.26	0.01	1.96	2.04	27.35
2	17.02	0.04	1.29	1.41	28.83
3	37.45	0.07	1.28	1.5	43.5
4	56.93	0.1	1.42	1.85	53.41
5	102.08	0.37	2.09	3.54	68.64
6	143.04	1.42	3.43	9.38	73.56
7	278.33	12.91	9.41	54.28	85.79
8	264.68	11.59	15.2	90.18	72.46
9	160.99	3.91	14.36	69.33	68.68
10	71.18	1.07	10.22	30.89	48.47
11	25.11	0.16	5.8	10.35	37.19
12	11.82	0	3.35	3.99	25.04
sum	**1179.89**	**31.65**	**69.81**	**278.74**	**632.92**

Table 18. Water balance components on annual average basis over the upper Blue Nile basin with -20% precipitation

Month	Rain (mm)	Surface Runoff (mm)	Lateral Flow (mm)	Water Yield (mm)	Evapotranspiration (mm)
1	10.01	0	1.64	1.69	26.26
2	15.13	0.02	1.07	1.14	27.44
3	33.29	0.04	1.05	1.16	41.25
4	50.61	0.05	1.14	1.38	50.42
5	90.74	0.18	1.67	2.41	65.12
6	127.15	0.74	2.74	5.83	70.75
7	247.41	8.06	7.87	37.59	84.8
8	235.27	7.63	12.99	70.46	72.23
9	143.1	2.51	12.28	56.2	68.34
10	63.28	0.68	8.67	24.74	47.68
11	22.32	0.09	4.89	8.29	36.09
12	10.5	0	2.81	3.25	23.97
sum	**1048.81**	**20**	**58.82**	**214.14**	**614.35**

Table 19. Water balance components on annual average basis over the upper Blue Nile basin with -25% precipitation

Month	Rain (mm)	Surface Runoff (mm)	Lateral Flow (mm)	Water Yield (mm)	Evapotranspiration (mm)
1	9.39	0	1.49	1.52	25.68
2	14.19	0.02	0.97	1.02	26.71
3	31.21	0.02	0.94	1.01	40.04
4	47.44	0.03	1.01	1.18	48.75
5	85.07	0.11	1.47	1.98	63.13
6	119.2	0.51	2.41	4.52	69.09
7	231.95	6.09	7.09	30.1	84.16
8	220.57	5.97	11.86	60.63	72.07
9	134.16	1.93	11.23	49.48	68.12
10	59.32	0.52	7.89	21.79	47.2
11	20.93	0.07	4.44	7.32	35.44
12	9.85	0	2.54	2.89	23.38
sum	**983.28**	**15.27**	**53.34**	**183.44**	**603.77**

Table 20. Ratio of hydrologic variables of the various climate change scenarios to the Baseline climate in the upper Blue Nile Basin

Ratio	Rain	Surface Runoff	Lateral Flow	WATER YIELD	Evapotranspiration
B1/(Baseline)	1.10	1.37	1.12	1.38	1.05
A1B/(Baseline)	1.20	1.83	1.26	1.65	1.06
A2/(Baseline)	1.25	2.04	1.33	1.77	1.07
+10 Precipitation/Baseline	1.100	1.378	1.13	1.42	1.02
+20 Precipitation/Baseline	1.200	1.818	1.27	1.67	1.04
+25% Precipitation/Baseline	1.250	2.059	1.33	1.80	1.05
-10% Precipitation/Baseline	0.900	0.683	0.86	0.95	0.98
-20% Precipitation/Baseline	0.800	0.432	0.73	0.73	0.95
-25% Precipitation/Baseline	0.750	0.330	0.66	0.62	0.93
(+1^{o}C and +2^{o}C to daily Tmax and Tmin)/Baseline	1.00	0.94	0.97	0.93	1.07
(+1.5^{o}C and +2.5^{o}C to daily Tmax and Tmin)/Baseline	1.00	0.92	0.96	0.91	1.08
(+3^{o}C and +4^{o}C to daily Tmax and Tmin)/Baseline	1.00	0.88	0.95	0.88	1.11
Co_2 of 550 ppm/Baseline	1.000	1.069	1.03	1.06	0.95
Co_2 of 700 ppm/Baseline	1.000	1.133	1.05	1.11	0.90
Co_2 of 850 ppm/Baseline	1.000	1.222	1.09	1.19	0.83

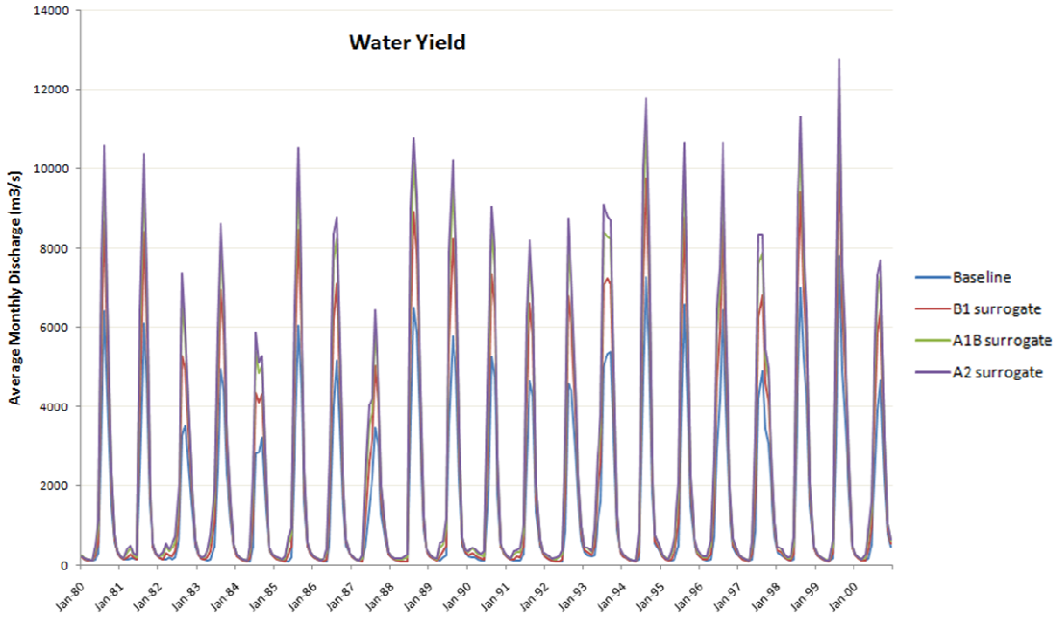

Figure 32. Response of water yield to the regional surrogate climate change scenarios in the upper Blue Nile with the data from 1980-2000.

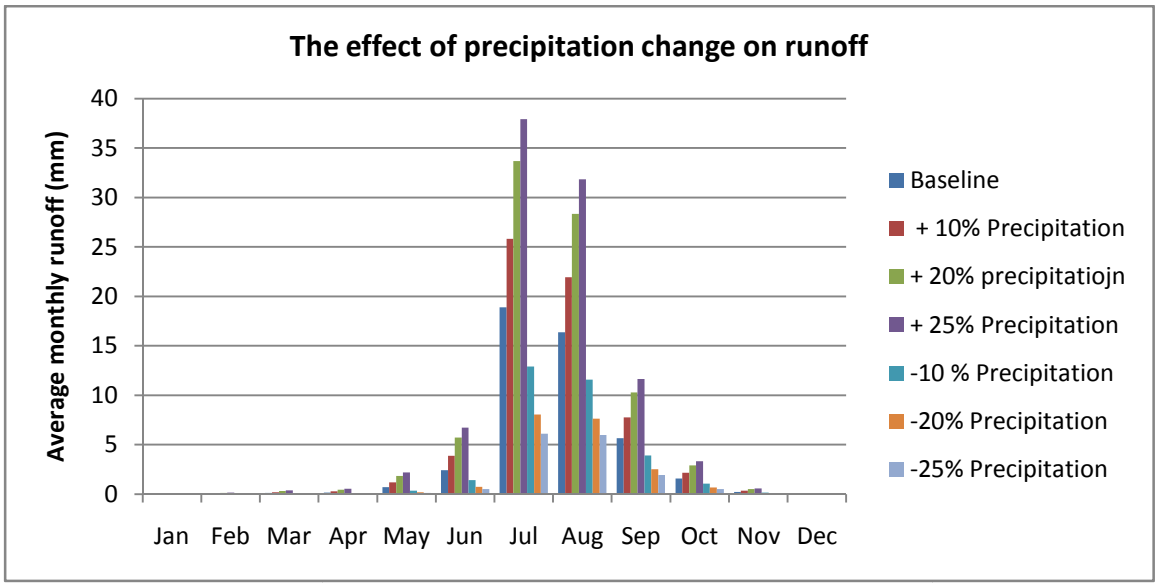

Figure 33. Effect of precipitation change on runoff in the upper Blue Nile Basin

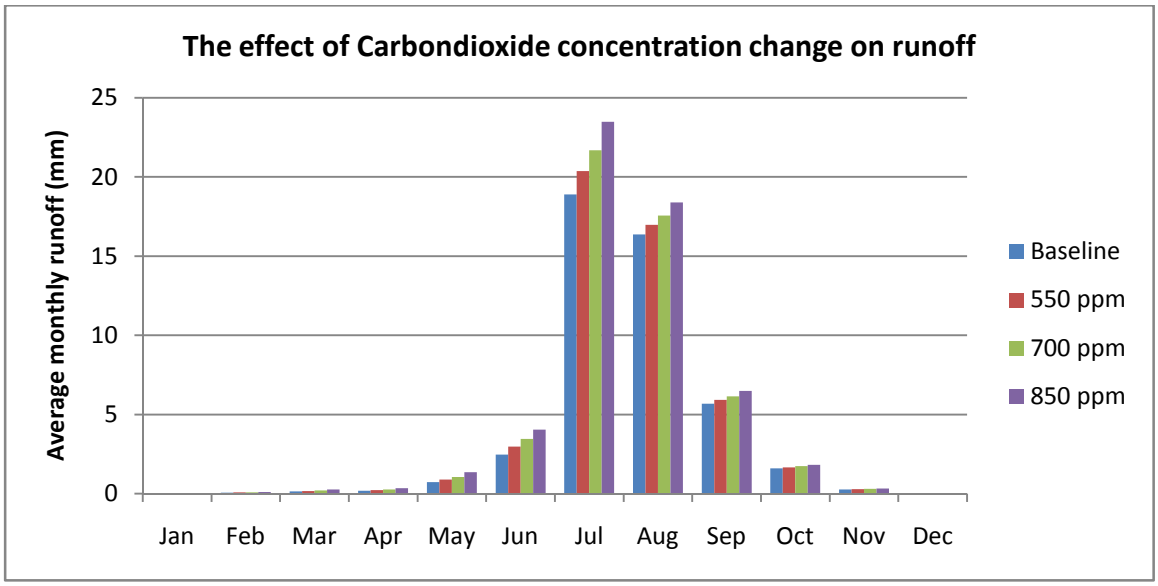

Figure 34. Response of runoff to CO_2 change in the upper Blue Nile Basin

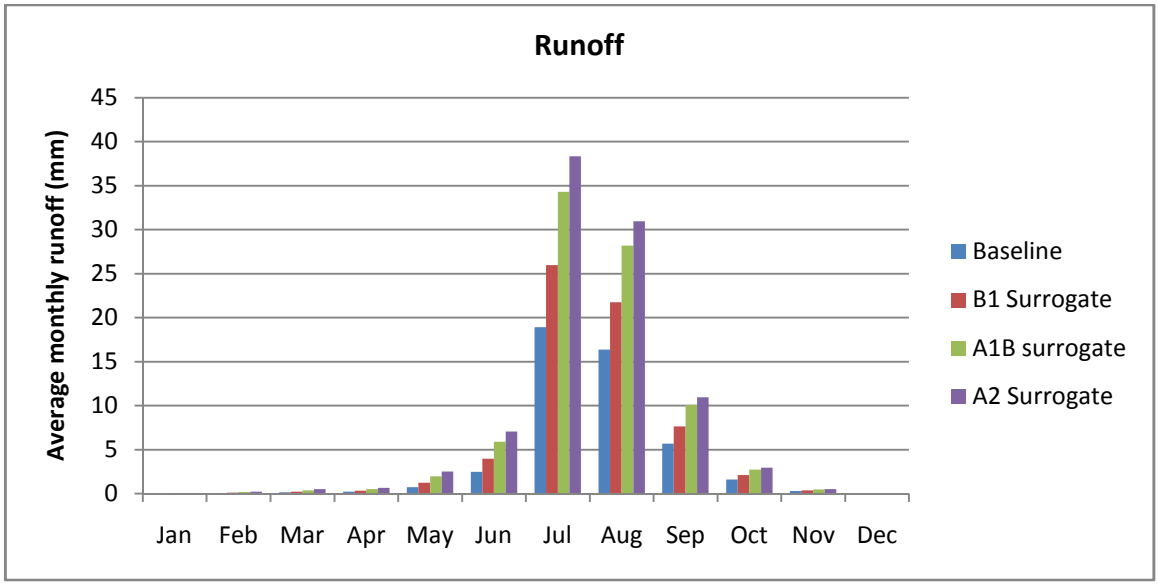

Figure 35. Runoff in the different regional climate change scenarios in the upper Blue Nile Basin

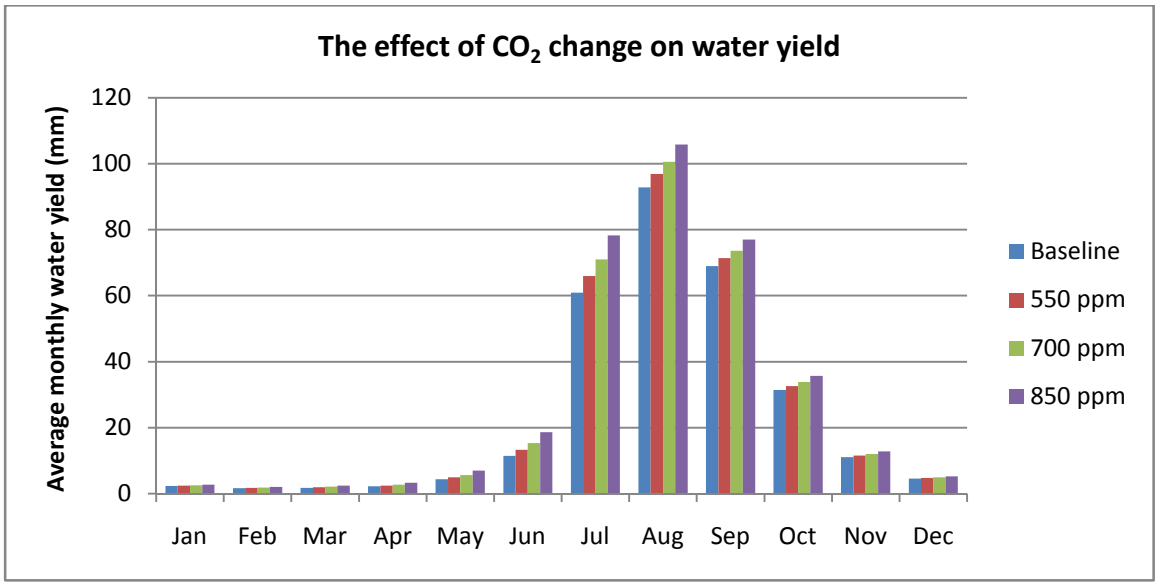

Figure 36. Response of water yield to CO_2 change in the upper Blue Nile Basin

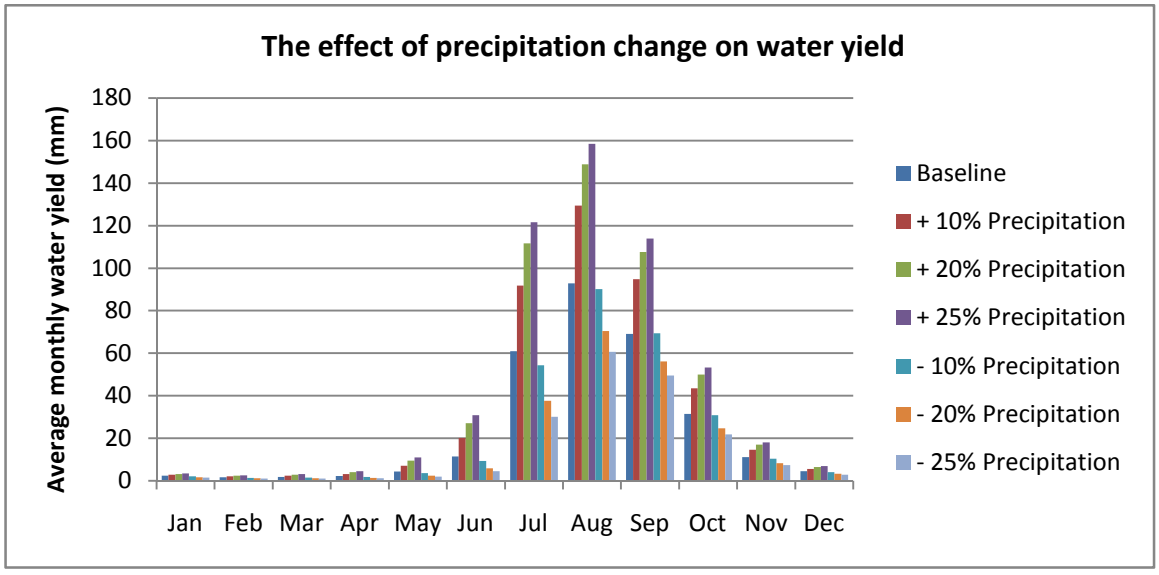

Figure 37. Response of water yield to Precipitation increments in the upper Blue Nile Basin

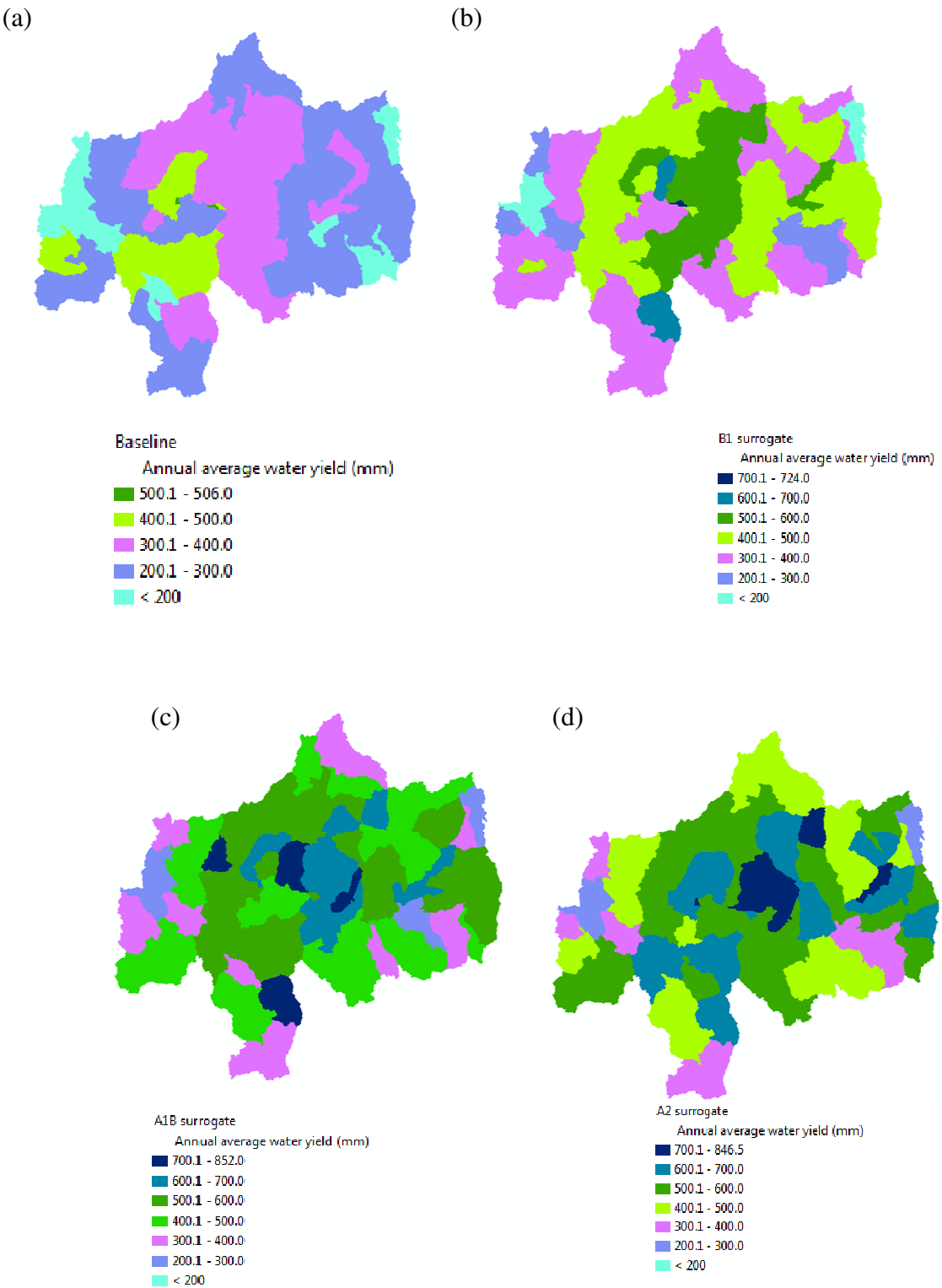

Figure 38. Spatial variability of average annual water yield in the upper Blue Nile Basin (mm) from 1960-2000 (a); B1 surrogate (b); A1B surrogate (c) and A2 surrogate (d)

3.2 Equatorial Lakes Region

Table (21) shows the sensitive parameters that were used for calibration in the Equatorial Lakes Region and their relative sensitivity ranks and values. We tried to calibrate the flow at Lake Albert outlet and Paara stations using SUFI-2 algorithm, but it was not successful. This is consistent with earlier attempts by Schuol et al. (2008). This is because about 20% of the Equatorial Lakes Region area is water and we could not get important lake information such as the outflow from Lake Victoria, which is a regulated Lake with the 4th largest surface area in the world.

We modeled an upper subbasin of the Equatorial Lakes Region, the Rusumo watershed which comprises an area of 30,691 km^2, to see the applicability and feasibility of the SWAT2009 model in the region. It is a subbasin of the Kagera basin. It has subwatersheds of area 2336.9 km^2, 13564.2 km^2, 14500.6 km^2, 57.4 km^2, and 232.2 km^2 in Tanzania, Burundi, Rwanda, the Democratic Republic of the Congo, and Uganda, respectively (Figure 39). Tables 22 and 23 show the sensitive parameters that were used for calibration and validation and their relative sensitivity rank without and with observed data in the Rusumo subbasin. Sensitivity analysis without observed data measures the sensitivity of the output to changes in input parameters.

Sensitivity analysis with observed data measures the sensitivity of the predicted output and model error to changes in input parameters. The remaining parameters had no significant effect on stream flow simulations. As changes in their values do not cause significant changes in the model output, they were not considered for calibration.

3.2.1 Calibration and Validation Results for Rusumo using SUFI2

Figures 40 and 41 show the calibration results and Figure 42 shows the validation results. As shown from the cumulative distribution for calibration and validation (Figures 43 and 44), SWAT2009 underestimated the peak flows and low flows during the calibration period, and the peak flows during the validation period. It overestimates low flows during the validation period (Figure 44). The coefficient of determination R^2 for calibration and validation is, respectively, 0.49 and 0.58, as shown from Figures 40, 41 and 42. The Nash-Sutcliffe coefficient was found to be 0.49 and 0.51 for calibration and validation, respectively (Figures 40, 41 and 42). The 95PPU bracketed 90% of the observed data but the r-factor is 1.56 (Figure 40). This shows that the model of Rusumo is more uncertain than that of the Blue Nile Basin.

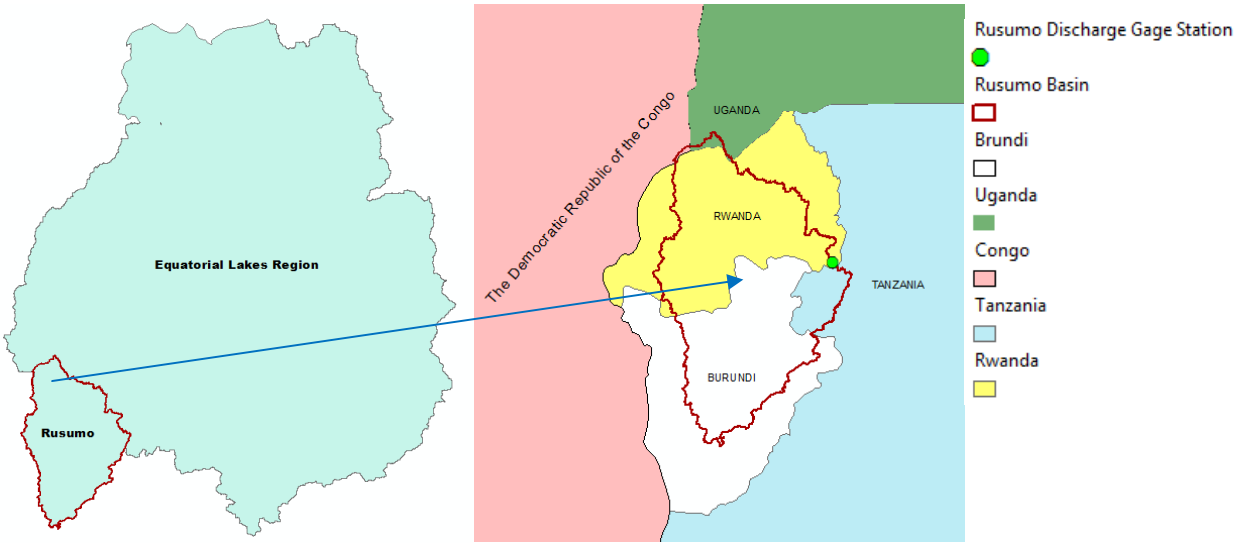

Figure 39. The location of the Rusumo subwatershed

Table 21. Sensitivity results for the Equatorial Lakes region without observed data, based on the approach of Van Grienven *et al*.(2006)

Parameter	Rank	mean	Description
Alpha_Bf	7	1.34E-01	Base flow alpha factor (days)
Canmx	11	4.39E-02	maximum canopy storage (mm H_2O)
Ch_K2	12	1.96E-02	Effective hydraulic conductivity in main channel alluvium
Ch_N2	16	2.32E-03	mannngs's "n" value for the main channel
Cn2	1	1.28E+00	Initial SCS runoff curve number for moisture condition II
Epco	10	7.34E-02	plant uptake compensation factor
Esco	2	9.53E-01	soil evaporation compensation factor
Gw_Delay	14	9.86E-03	ground water delay (days)
Gw_Revap	6	1.70E-01	Revap Coefficient
Gwqmn	3	3.24E-01	threshold water level in shallow aquifer for base flow (mm H_2O)
Revapmn	9	7.53E-02	threshold depth of water in the shallow aquifer for the "revap" to occur (mm H_2O)
Sol_Alb	13	1.35E-02	moist soil albedo
Sol_Awc	5	2.73E-01	available water capacity of soil (mm/mm)
Sol_K	8	8.88E-02	saturated hydraulic conductivity
Sol_Z	4	3.12E-01	depth from soil surface to bottom of layer (mm)
Surlag	15	2.46E-03	surface runoff lag time (days)

Table 22. Sensitivity results for Rusumo basin without observed data, based on the approach of Van Grienven *et al*. (2006)

	Parameter	Rank without Observed Data	mean
1	Alpha_Bf	12	1.26E-02
2	Canmx	6	2.02E-01
3	Ch_K2	9	7.17E-02
4	Ch_N2	11	1.89E-02
5	Cn2	13	7.20E-03
6	Epco	7	1.39E-01
7	Esco	1	5.93E-01
8	Gw_Delay	14	3.97E-03
9	Gw_Revap	3	4.64E-01
10	Gwqmn	5	3.43E-01
11	Revapmn	15	3.11E-03
12	Sol_Alb	10	3.62E-02
13	Sol_Awc	4	4.31E-01
14	Sol_K	8	9.78E-02
15	Sol_Z	2	5.42E-01
16	Surlag	16	3.32E-04

Table 23. Sensitivity results for Rusumo basin with observed data, based on the approach of Van Grienven *et al*.(2006)

	Parameter	Rank with observed data	mean
1	Alpha_Bf	4	1.37E-01
2	Canmx	5	1.22E-01
3	Ch_K2	8	4.61E-02
4	Ch_N2	13	2.04E-02
5	Cn2	15	3.12E-03
6	Epco	7	8.45E-02
7	Esco	1	3.82E-01
8	Gw_Delay	14	6.62E-03
9	Gw_Revap	6	1.01E-01
10	Gwqmn	10	3.84E-02
11	Revapmn	11	2.72E-02
12	Sol_Alb	12	2.14E-02
13	Sol_Awc	3	2.70E-01
14	Sol_K	9	4.33E-02
15	Sol_Z	2	2.91E-01
16	Surlag	16	4.75E-04

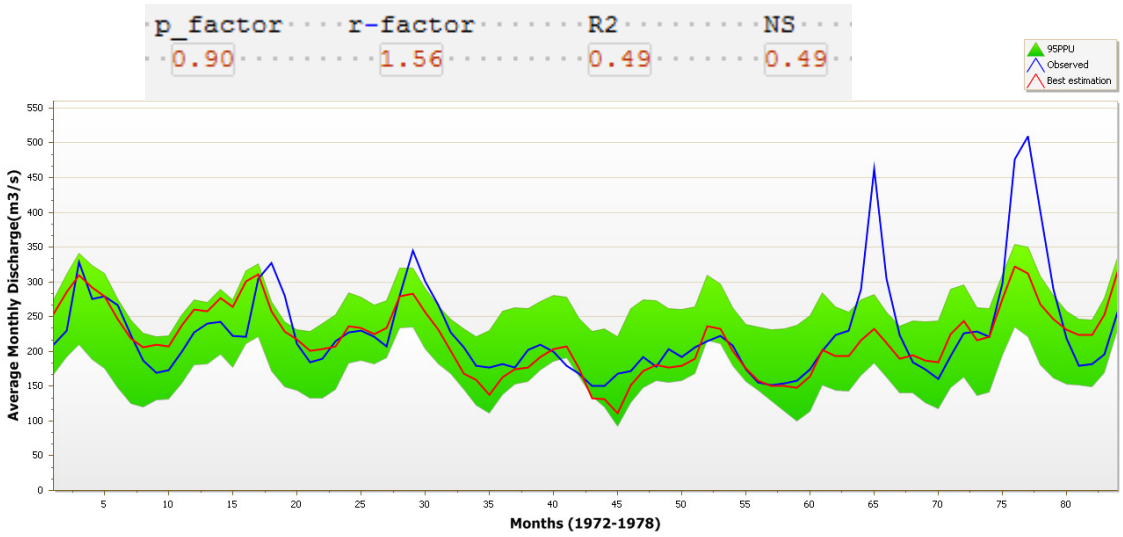

Figure 40. Calibration at Rusumo outlet

Table 24. Average Annual Discharge (m^3/s) from Rusumo Basin

	Calibration Period	Validation Period	Average
Observed	228.0	222.0	225.3
SWAT	217.9	240.9	230.9

Table 25. SWAT flow sensitive parameters and fitted values after Calibration using SUFI2 for Rusumo Basin

No	Sensitive Parameter	Lower and Upper Bound	Final Fitted Value
1	Alpha_Bf	0-1	0.072
2	Canmx	0-100	12.250
3	Ch_k2	-0.01-500	4.540
4	Ch_N2	-0.01-0.3	0.108
5	CN2	±10%	-2.56%*
6	Epco	0-1	0.21
7	Esco	0-1	0.74
8	Gw_Delay	0-500	15
9	GW-Revap	0.02-0.2	0.052
10	Gwqmn	0-5000	77
11	Revapmn	0-500	47.3
12	Sol_Alb	0-0.25	0.24
14	Sol_Awc	±25%	10.48%*
14	Sol_K	±25%	-8.31%*
15	Sol_Z	±25%	9.58%*
16	Surlag	0-24	14

CN2, S_Awc, Sol-K Sol_Z and Sol_Alb have different parameter values depending on the land cover or the soil texture type. * means relative change of the parameter value.

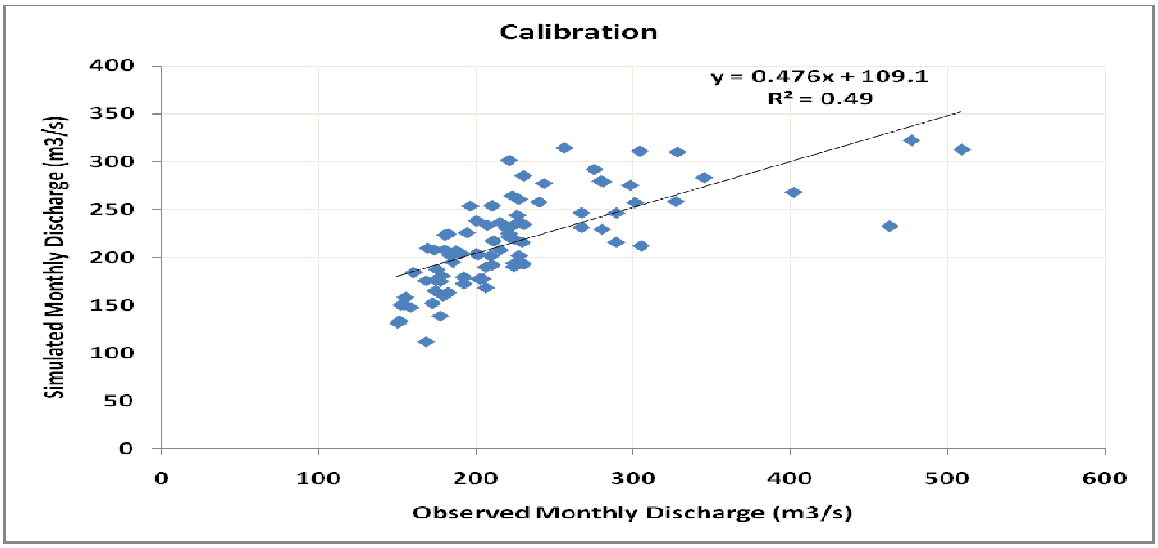

Figure 41. Correlation of monthly measured and simulated discharge at Rusumo station during calibration period (1972-1984)

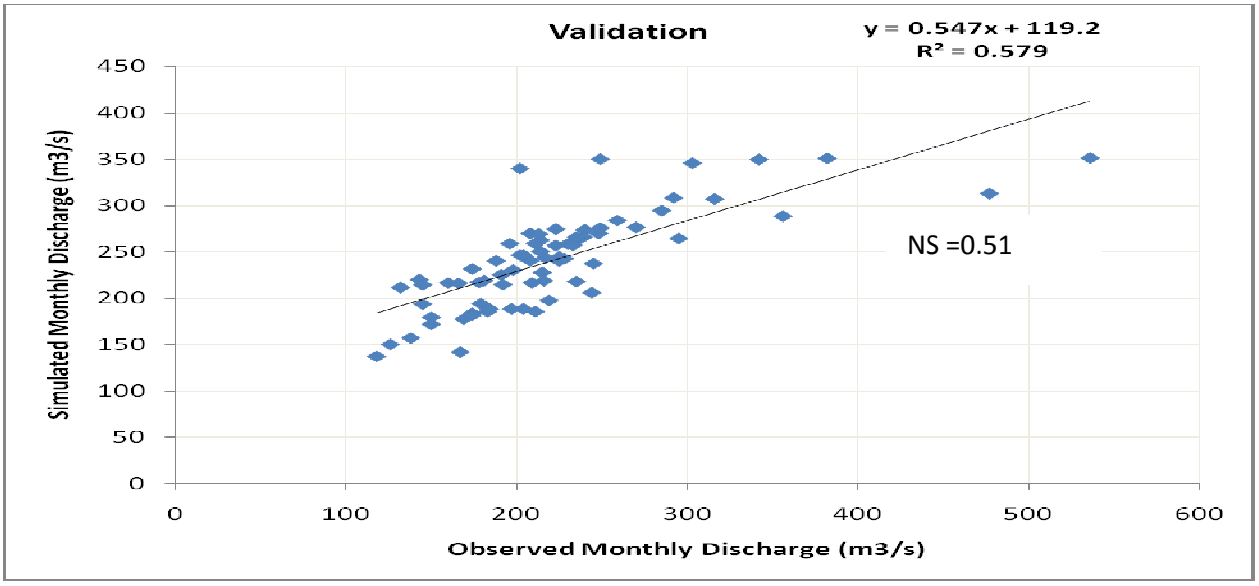

Figure 42. Correlation of monthly measured and simulated discharge at Rusumo station during validation period (1972-1984)

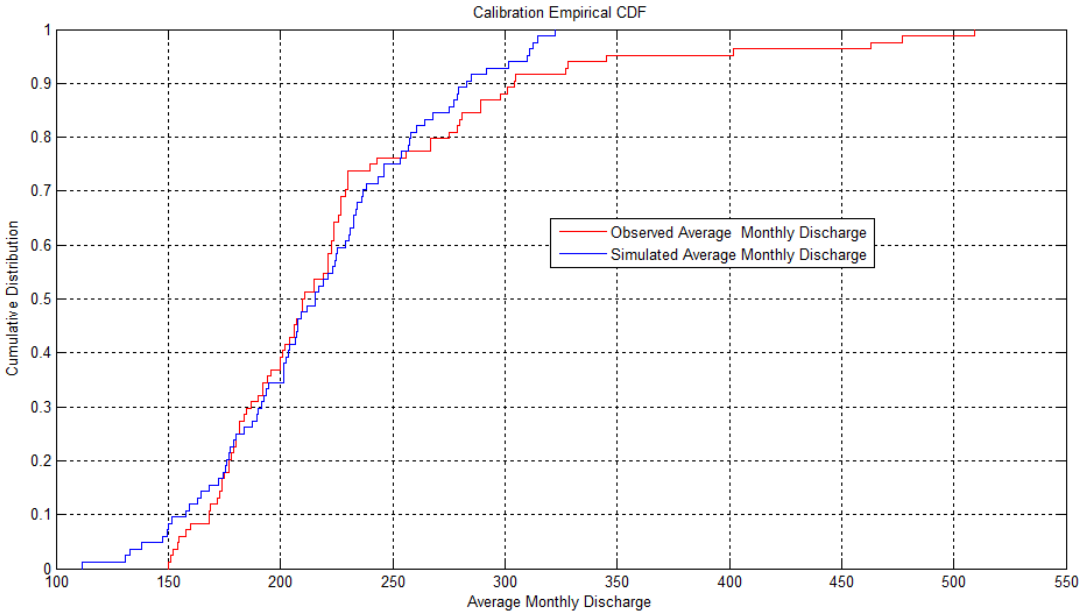

Figure 43. Cumulative distribution for calibration at Rusumo gage station

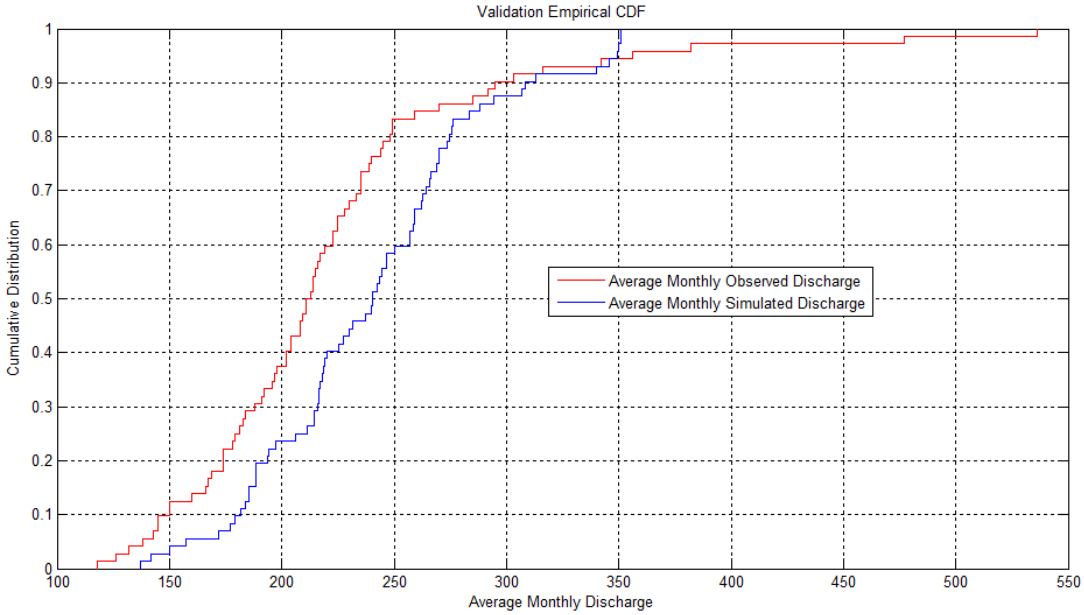

Figure 44. Cumulative distribution for validation at Rusumo gage station

CHAPTER 4

4.0 Summary and Conclusions

This thesis research studied the applicability of the semi-distributed hydrologic model SWAT2009, using downscaled gridded monthly weather data, in the main sources of the Nile River: Blue Nile and Equatorial Lakes Region. SWAT requires daily input weather data, but the gage stations in the Nile basin are scarce and unevenly distributed, sometimes with many missing and erroneous data. Schuol and Abbaspour (2007) showed that in data scarce regions such as Africa simulations using generated weather data were superior to simulations using the available poor quality measured data. Among the required weather data for SWAT model: daily precipitation, daily maximum and minimum temperature were stochastically generated from the Climate Research Unit (CRU) gridded monthly weather dataset using Monthly to Daily Weather Converter (MODAWEC). The data points are at a spatial resolution of 30 arc-min latitude/longitude. Before using generated daily data in the SWAT model, we checked the quality of the monthly CRU data by direct comparison with station observation data from the Ethiopian Meteorological Agency. High correlation between the monthly CRU precipitation and station observation monthly precipitation shows the usability of the gridded CRU data.

The sensitive parameters were identified for calibration and validation. Calibration, validation and uncertainty analysis was performed using Sequential Uncertainty Fitting (SUFI-2) algorithm. Calibration was done on annual basis followed by monthly intervals. The monthly calibration and validation results over the Blue Nile are very good with R^2

and Nash-Sutcliffe coefficients of 0.93 and 0.93 respectively for calibration and 0.92 and 0.92 respectively for validation with 90% of the observed data bracketed by the 95PPU (95% Prediction Uncertainty Band) and R-factor of 0.7. But, the model over the Equatorial Lakes Region was not successful because about 20% of the basin is covered by water bodies (Table 1 and Figure 21), and we could not get the required information especially the discharge from Lake Victoria which is a regulated lake with the 4th largest surface area in the world. The model of Rusumo using SWAT2009 is more uncertain than that of the Blue Nile Basin.

The study showed that downscaled gridded monthly weather data can be used in data scare areas like the Nile basin where the measuring gages are small in number (not with the recommended density of observation stations), unevenly distributed and sometimes with much missing and erroneous data. The final goal of this study is to achieve an accurate representation of the monthly water balance with SWAT. It is unrealistic to model daily water flows using generated daily weather data. The study showed that SWAT can be used to study environmental change impacts on water resources and the competition for water resources by different sectors in the basins.

The uncertainty of simulated flow is due to errors in input data such as rainfall and temperature as the data are stochastically generated from a gridded monthly data that uses small number of stations for interpolation in the region, and/or other sources of uncertainties such as upstream dam/reservoir construction for town water supply, diversion of streams for irrigation, error in the type of soil/land cover and the corresponding soil/land cover properties in the area and other unknown activities in the

sub-basins. SWAT model does not consider the effect of erosion on runoff but soil erosion can affect the structures, infililtration capacity and other properties of the soil which makes the predictions uncertain. The data points downscaled from the monthly CRU weather data are at a resolution of 0.5^0 latitude/longitude. SWAT takes one data point location for each subbasin, which is a less realistic representation.

The study investigated the sensitivity of the Blue Nile to potential climate change scenarios. It showed that the Blue Nile is sensitive to potential climate change and Surface runoff is the most sensitive hydrologic variable to precipitation change. The Surrogate Climate Change Scenarios (SCCS) are used for sensitivity experiments, but can't provide a full picture of climate change impacts on water resources for the region of application.

4.1 Recommendations

To accurately model the water resources at a subwatershed scale, using many discharge stations for calibration and validation is important. But, in our study due to the scarcity of discharge gage stations in the basins and inaccessibility of the data from some of them , we used one discharge station each at the outlet of the Blue Nile and Rusumo basins. Many gage stations need to be established in the Nile basin to more appropriately study the ecohydrology and hydroclimatology of the basin. Getting data even for the few available observation stations is difficult. There must be secure data archiving and data transfer among researchers. Some of the data that are available from online sources are unrealistic, so data quality assessment is crucial.

The low level of model performance on the Equatorial Lakes Region can be improved by using high density observation stations and lake data especially information about lake Victoria which is a regulated lake is important. The sensitivity analysis showed that the Equatorial Lakes Region and Blue Nile are sensitive to ground water parameters such as the base flow recession constant (Alpha_Bf), threshold depth of water in the shallow aquifer required for return flow to occur (Gwqmn), Ground water Delay (Gw_Delay), threshold depth of water in the shallow aquifer for "revap" or percolation to the deep aquifer to occur (Revapmin), and Groundwater "revap" coefficient (Gw_Revap), therefore, more detailed ground water information of the basins is vital for water resources study of the basins. To model the hydrology more accurately, using distributed weather data especially precipitation is important.

References

Abbaspour, K. C., 2005, Calibration of hydrologic models: When is a model calibrated, p. 2449–2455.

-, 2007, User Manual for SWAT-CUP, SWAT Calibration and Uncertainty Analysis Programs: Swiss Federal Institute of Aquatic Science and Technology, Eawag, Duebendorf, Switzerland.

-, 2009, SWAT-CUP2.

Abbaspour, K. C., Faramarzi, M., Ghasemi, S. S., and Yang, H., 2009, Assessing the impact of climate change on water resources in Iran: Water Resources Research, v. 45, p. W10434.

Abbaspour, K. C., Yang, J., Maximov, I., Siber, R., Bogner, K., Mieleitner, J., Zobrist, J., and Srinivasan, R., 2007, Modelling hydrology and water quality in the pre-alpine/alpine Thur watershed using SWAT: Journal of Hydrology, v. 333, p. 413-430.

Arnold, J. G., Muttiah, R. S., Srinivasan, R., and Allen, P. M., 2000, Regional estimation of base flow and groundwater recharge in the Upper Mississippi river basin: Journal of Hydrology, v. 227, p. 21-40.

Arnold, J. G., Srinivasan, R., Muttiah, R. S., and Allen, P. M., 1999, CONTINENTAL SCALE SIMULATION OF THE HYDROLOGIC BALANCE1: JAWRA Journal of the American Water Resources Association, v. 35, p. 1037-1051.

Arnold, J. G., Srinivasan, R., Muttiah, R. S., and Williams, J. R., 1998, LARGE AREA HYDROLOGIC MODELING AND ASSESSMENT PART I: MODEL

DEVELOPMENT1: JAWRA Journal of the American Water Resources Association, v. 34, p. 73-89.

Arnold, J. G., Williams, J. R., Nicks, A. D., and Sammons, N. B., 1990, SWRRB; a basin scale simulation model for soil and water resources management, Texas A & M University Press.

Batjes, N. H., 2002, Revised soil parameter estimates for the soil types of the world: Soil Use and Management, v. 18, p. 232-235.

Bayabil, H. K., Tilahun, S. A., Collick, A. S., Yitaferu, B., and Steenhuis, T. S., Are runoff processes ecologically or topographically driven in the (sub) humid Ethiopian highlands? The case of the Maybar watershed: Ecohydrology, v. 3, p. 457-466.

Bekoe, E. O., 2005, Application of a hydrological model in a data-poor tropical West African catchment: a case study of the Densu Basin of Ghana.

Benaman, J., Shoemaker, C. A., and Haith, D. A., 2005, Calibration and validation of soil and water assessment tool on an agricultural watershed in upstate New York: Journal of Hydrologic Engineering, v. 10, p. 363.

Beven, K., and Binley, A., 1992, Future of distributed models: Model calibration and uncertainty prediction: Hydrological processes, v. 6, p. 279-298.

Bewket, W., and Sterk, G., 2005, Dynamics in land cover and its effect on stream flow in the Chemoga watershed, Blue Nile basin, Ethiopia: Hydrological Processes, v. 19, p. 445-458.

Beyene, T., Lettenmaier, D. P., and Kabat, P., Hydrologic impacts of climate change on the Nile River Basin: implications of the 2007 IPCC scenarios: Climatic change, v. 100, p. 433-461.

Birhanu, B. Z., Hydrological modeling of the Kihansi river catchment in South Central Tanzania using SWAT model.

Bouraoui, F., Benabdallah, S., Jrad, A., and Bidoglio, G., 2005, Application of the SWAT model on the Medjerda river basin (Tunisia): Physics and Chemistry of the Earth, Parts A/B/C, v. 30, p. 497-507.

Cao, W., Bowden, W. B., Davie, T., and Fenemor, A., 2006, Multi variable and multi site calibration and validation of SWAT in a large mountainous catchment with high spatial variability: Hydrological Processes, v. 20, p. 1057-1073.

Change, I., 2007, Climate change 2007: Impacts, adaptation and vulnerability: Contribution of the Working Group II to the Fourth Assessment report of the Intergovernmental Panel on Climate Change.

Conan, C., de Marsily, G., Bouraoui, F., and Bidoglio, G., 2003, A long-term hydrological modelling of the Upper Guadiana river basin (Spain): Physics and Chemistry of the Earth, Parts A/B/C, v. 28, p. 193-200.

Conway, D., 1996, The impacts of climate variability and future climate change in the Nile Basin on water resources in Egypt: International Journal of Water Resources Development, v. 12, p. 277-296.

-, 2000, The climate and hydrology of the Upper Blue Nile River: Geographical Journal, v. 166, p. 49-62.

-, 2005, From headwater tributaries to international river: observing and adapting to climate variability and change in the Nile basin: Global Environmental Change Part A, v. 15, p. 99-114.

Conway, D., Hanson, C. E., Doherty, R., and Persechino, A., 2007, GCM simulations of the Indian Ocean dipole influence on East African rainfall: Present and future: Geophysical Research Letters, v. 34, p. L03705.

Conway, D., and Hulme, M., 1993, Recent fluctuations in precipitation and runoff over the Nile sub-basins and their impact on main Nile discharge: Climatic Change, v. 25, p. 127-151.

Conway, D., Krol, M., Alcamo, J., and Hulme, M., 1996, Future availability of water in Egypt: The interaction of global, regional, and basin scale driving forces in the Nile Basin: Ambio, v. 25, p. 336-342.

Dhar, S., and Mazumdar, A., 2009, Hydrological modelling of the Kangsabati river under changed climate scenario: case study in India: Hydrological Processes, v. 23, p. 2394-2406.

Diaz-Nieto, J., and Wilby, R. L., 2005, A comparison of statistical downscaling and climate change factor methods: Impacts on low flows in the River Thames, United Kingdom: Climatic Change, v. 69, p. 245-268.

Easton, Z. M., Fuka, D. R., White, E. D., Collick, A. S., Asharge, B. B., McCartney, M., Awulachew, S. B., Ahmed, A. A., and Steenhuis, T. S., A multi basin SWAT model analysis of runoff and sedimentation in the Blue Nile, Ethiopia: Hydrology and Earth System Sciences Discussions, v. 7, p. 3837-3878.

Eckhardt, K., and Ulbrich, U., 2003, Potential impacts of climate change on groundwater recharge and streamflow in a central European low mountain range: Journal of Hydrology, v. 284, p. 244-252.

Elshamy, M. E., Seierstad, I. A., and Sorteberg, A., 2009, Impacts of climate change on Blue Nile flows using bias-corrected GCM scenarios: Hydrology and Earth System Sciences, v. 13, p. 551-565.

Fao, I., and Italiana, C., 1998, The Soil and Terrain Database for northeastern Africa: Crop Production System Zones of the IGAD subregion (scale 1: 1 M): Land and Water Digital Media Series, v. 2.

Faramarzi, M., Abbaspour, K. C., Schulin, R., and Yang, H., 2009, Modelling blue and green water resources availability in Iran: Hydrological Processes, v. 23, p. 486-501.

Ficklin, D. L., Luo, Y., Luedeling, E., and Zhang, M., 2009, Climate change sensitivity assessment of a highly agricultural watershed using SWAT: Journal of Hydrology, v. 374, p. 16-29.

Fontaine, T. A., Klassen, J. F., Cruickshank, T. S., and Hotchkiss, R. H., 2001, Hydrological response to climate change in the Black Hills of South Dakota, USA/Réponse hydrologique au changement climatique dans les Collines Noires du Dakota du Sud: Hydrological Sciences Journal, v. 46, p. 27-40.

Fu, G., Charles, S. P., Viney, N. R., Chen, S., and Wu, J. Q., 2007, Impacts of climate variability on stream flow in the Yellow River: Hydrological Processes, v. 21, p. 3431-3439.

Ghaffari, G., Keesstra, S., Ghodousi, J., and Ahmadi, H., SWAT-simulated hydrological impact of land-use change in the Zanjanrood basin, Northwest Iran: Hydrological Processes, v. 24, p. 892-903.

Githui, F. W., Assessing the impacts of environmental change on the hydrology of the Nzoia catchment, in the Lake Victoria Basin.

Gosain, A. K., Rao, S., and Basuray, D., 2006, Climate change impact assessment on hydrology of Indian river basins: Current Science, v. 90, p. 346-353.

Griggs, D. J., and Noguer, M., 2002, Climate change 2001: the scientific basis. Contribution of Working Group I to the third assessment report of the Intergovernmental Panel on Climate Change: Weather, v. 57, p. 267-269.

Jones, C. A., Dyke, P. T., Williams, J. R., Kiniry, J. R., Benson, V. W., and Griggs, R. H., 1991, EPIC: an operational model for evaluation of agricultural sustainability: Agricultural Systems, v. 37, p. 341-350.

Kebede, S., Travi, Y., Alemayehu, T., and Marc, V., 2006, Water balance of Lake Tana and its sensitivity to fluctuations in rainfall, Blue Nile basin, Ethiopia: Journal of hydrology, v. 316, p. 233-247.

Kilsby, C. G., Tellier, S. S., Fowler, H. J., and Howels, T. R., 2007, Hydrological impacts of climate change on the Tejo and Guadiana Rivers: Hydrology and Earth System Sciences, v. 11, p. 1175-1189.

Kim, U., Kaluarachchi, J. J., and Smakhtin, V. U., Climate change impacts on hydrology and water resources of the Upper Blue Nile River Basin, Ethiopia, Iwmi.

Kirsch, K., Kirsch, A., and Arnold, J. G., Predicting sediment and phosphorus loads in the Rock River basin using SWAT.

Kuczera, G., and Parent, E., 1998, Monte Carlo assessment of parameter uncertainty in conceptual catchment models: the Metropolis algorithm: Journal of Hydrology, v. 211, p. 69-85.

Legesse, D., Vallet-Coulomb, C., and Gasse, F., 2003, Hydrological response of a catchment to climate and land use changes in Tropical Africa: case study South Central Ethiopia: Journal of Hydrology, v. 275, p. 67-85.

Legesse, E. S., 2009, Modeling Rainfall-runoff Relationships for the Anjeni Watershed in the Blue Nile Basin, Cornell University.

Leonard, R. A., Knisel, W. G., and Still, D. A., 1987, GLEAMS: Groundwater loading effects of agricultural management systems: Trans. ASAE, v. 30, p. 1403-1428.

Liew, M. W., and Garbrecht, J., 2003, HYDROLOGIC SIMULATION OF THE LITTLE WASHITA RIVER EXPERIMENTAL WATERSHED USING SWAT1: JAWRA Journal of the American Water Resources Association, v. 39, p. 413-426.

Liu, B. M., Collick, A. S., Zeleke, G., Adgo, E., Easton, Z. M., and Steenhuis, T. S., 2008, Rainfall discharge relationships for a monsoonal climate in the Ethiopian highlands: Hydrological Processes, v. 22, p. 1059-1067.

Liu, J., Williams, J. R., Wang, X., and Yang, H., 2009, Using MODAWEC to generate daily weather data for the EPIC model: Environmental Modelling & Software, v. 24, p. 655-664.

Mekonnen, M. A., Wörman, A., Dargahi, B., and Gebeyehu, A., 2009, Hydrological modelling of Ethiopian catchments using limited data: Hydrological Processes, v. 23, p. 3401-3408.

Mitchell, T. D., Carter, T. R., Jones, P. D., Hulme, M., and New, M., 2003, A comprehensive set of high-resolution grids of monthly climate for Europe and the globe: the observed record (1901–2000) and 16 scenarios (2001–2100): Journal of Climate.

Mohamed, Y. A., Van Den Hurk, B., Savenije, H. H. G., and Bastiaanssen, W. G. M., 2005, Hydroclimatology of the Nile: results from a regional climate model: Hydrology and Earth System Sciences Discussions, v. 2, p. 319-364.

Moriasi, D. N., and Arnhold, J. G., & Van Liew, MW & Bingner, RL & Harmel, RD & Veith, TL (2007): Model evaluation guidelines for systematic quantification of accuracy in watershed simulations: American Society of Agricultural and Biological Engineer, v. 50, p. 885–900.

Mulungu, D. M. M., and Munishi, S. E., 2007, Simiyu River catchment parameterization using SWAT model: Physics and Chemistry of the Earth, Parts A/B/C, v. 32, p. 1032-1039.

Nash, J. E., and Sutcliffe, J. V., 1970, River flow forecasting through conceptual models part I--A discussion of principles: Journal of hydrology, v. 10, p. 282-290.

Ndomba, P., Mtalo, F., and Killingtveit, A., 2008, SWAT model application in a data scarce tropical complex catchment in Tanzania: Physics and Chemistry of the Earth, Parts A/B/C, v. 33, p. 626-632.

Neitsch, S. L., Arnold, J. G., Kiniry, J. R., Srinivasan, R., and Williams, J. R., 2004, Soil and Water Assessment Tool Input/Output File Documentation. Version 2005: Temple, TX: Blackland Research Center, USDA Agricultural Research Service.

Neitsch, S. L., Arnold, J. G., Kiniry, J. R., Williams, J. R., and King, K. W., 2001, Soil and water assessment tool theoretical documentation version 2000: Grassland, Soil and Water Research Laboratory, Temple, Texas.

Nicks, A. D., 1974, Stochastic generation of the occurrence, pattern, and location of maximum amount of daily rainfall, Agricultural Research Service, US Dept. of Agriculture: for sale by the Supt. of Docs., US Govt. Print. Off., p. 154.

Peterson, J. R., and Hamlett, J. M., 1998, HYDROLOGIC CALIBRATION OF THE SWAT MODEL IN A WATERSHED CONTAINING FRAGIPAN SOILS1: JAWRA Journal of the American Water Resources Association, v. 34, p. 531-544.

Rahman, M., Bolisetti, T., and Balachandar, R., Effect of climate change on low-flow conditions in the Ruscom River watershed, Ontario.

Richardson, C.W.: Stochastic simulation of daily precipitation, temperature, and solar radiation. WATER RESOUR RES, 17, 182-190, 1981.

Rossi, C. G., Dybala, T. J., Moriasi, D. N., Arnold, J. G., Amonett, C., and Marek, T., 2008, Hydrologic calibration and validation of the Soil and Water Assessment Tool for the Leon River watershed: Journal of Soil and Water Conservation, v. 63, p. 533.

Santhi, C., Arnold, J. G., Williams, J. R., Dugas, W. A., Srinivasan, R., and Hauck, L. M., 2001, VALIDATION OF THE SWAT MODEL ON A LARGE RWER BASIN WITH POINT AND NONPOINT SOURCES1: JAWRA Journal of the American Water Resources Association, v. 37, p. 1169-1188.

Schuol, J., and Abbaspour, K. C., 2006, Calibration and uncertainty issues of a hydrological model(SWAT) applied to West Africa: Advances in Geosciences, v. 9, p. 137-143.

-, 2007, Using monthly weather statistics to generate daily data in a SWAT model application to West Africa: Ecological Modelling, v. 201, p. 301-311.

Schuol, J., Abbaspour, K. C., Srinivasan, R., and Yang, H., 2008a, Estimation of freshwater availability in the West African sub-continent using the SWAT hydrologic model: Journal of Hydrology, v. 352, p. 30-49.

Schuol, J., Abbaspour, K. C., Yang, H., Srinivasan, R., and Zehnder, A. J. B., 2008b, Modeling blue and green water availability in Africa: Water Resour. Res, v. 44, p. 1-18.

Setegn, S. G., 2008, Hydrological and sediment Yield modelling in Lake Tana Basin, Blue Nile Ethiopia, Mark-och vattenteknik, Land and Water Resource Engineering, Kungliga Tekniska högskolan.

Setegn, S. G., Dargahi, B., Srinivasan, R., and Melesse, A. M., Modeling of Sediment Yield From Anjeni Gauged Watershed, Ethiopia Using SWAT Model1: JAWRA Journal of the American Water Resources Association, v. 46, p. 514-526.

Setegn, S. G., Srinivasan, R., and Dargahi, B., 2008, Hydrological modelling in the Lake Tana Basin, Ethiopia using SWAT model: Open Hydrology Journal, v. 2, p. 49-62.

Solomon, S., Qin, D., Manning, M., Chen, Z., Marquis, M., Averyt, K. B., Tignor, M., and Miller, H. L., 2007, IPCC, 2007: Climate change 2007: The physical science basis. Contribution of Working Group I to the fourth assessment report of the

Intergovernmental Panel on Climate Change, New York: Cambridge University Press.

Srinivasan, R., Ramanarayanan, T. S., Arnold, J. G., and Bednarz, S. T., 1998, LARGE AREA HYDROLOGIC MODELING AND ASSESSMENT PART II: MODEL APPLICATION1: JAWRA Journal of the American Water Resources Association, v. 34, p. 91-101.

Stone, M. C., Hotchkiss, R. H., Hubbard, C. M., Fontaine, T. A., Mearns, L. O., and Arnold, J. G., 2001, IMPACTS OF CLIMATE CHANGE ON MISSOURI RWER BASIN WATER YIELD1: JAWRA Journal of the American Water Resources Association, v. 37, p. 1119-1129.

Taye, M. T., Ntegeka, V., Ogiramoi, N. P., and Willems, P., Assessment of climate change impact on hydrological extremes in two source regions of the Nile River Basin: Hydrology and Earth System Sciences Discussions, v. 7.

Van Griensven, A., and Bauwens, W., 2003, Multiobjective autocalibration for semidistributed water quality models: Water Resources Research, v. 39, p. 1348.

Van Liew, M. W., Arnold, J. G., and Garbrecht, J. D., 2003, Hydrologic simulation on agricultural watersheds: choosing between two models: Transactions of the ASAE, v. 46, p. 1539-1551.

Van Liew, M. W., and Garbrecht, J., 2003, Hydrologic simulation of the Little Washita River experimental watershed using SWAT: Journal of the American Water Resources Association, v. 39, p. 413-426.

Vrugt, J. A., Gupta, H. V., Bouten, W., and Sorooshian, S., 2003, A Shuffled Complex Evolution Metropolis algorithm for optimization and uncertainty assessment of hydrologic model parameters: Water Resour. Res, v. 39, p. 1201.

Vrugt, J. A., ter Braak, C. J. F., Clark, M. P., Hyman, J. M., and Robinson, B. A., 2008, Treatment of input uncertainty in hydrologic modeling: Doing hydrology backward with Markov chain Monte Carlo simulation: Water Resources Research, v. 44, p. W00B09.

Wang, S., Kang, S., Zhang, L., and Li, F., 2008, Modelling hydrological response to different land use and climate change scenarios in the Zamu River basin of northwest China: Hydrological Processes, v. 22, p. 2502-2510.

Watson, R. T., Zinyowera, M. C., and Moss, R. H., 1998, The regional impacts of climate change: an assessment of vulnerability, Cambridge Univ Pr.

White, K. L., and Chaubey, I., 2005, Sensitivity analysis, calibration, and validations for a multisite and multivariable SWAT model: Journal of the American Water Resources Association, v. 41, p. 1077-1089.

Wilby, R. L., Hassan, H., and Hanaki, K., 1998, Statistical downscaling of hydrometeorological variables using general circulation model output: Journal of Hydrology, v. 205, p. 1-19.

Williams, J. R., Nicks, A. D., and Arnold, J. G., 1985, Simulator for water resources in rural basins: Journal of Hydraulic Engineering, v. 111, p. 970-986.

Williams, J. R., 1990, The erosion-productivity impact calculator (EPIC) model: A case history: Philosophical Transactions: Biological Sciences, v. 329, p. 421-428.

Williams, J. R.: The EPIC model, In Singh, V. P. (Ed)., Computer models of watershed hydrology., Water resources publications, Highlands Ranch, CO, Chapter 25, 909-1000, 1995.

Xu, H., Taylor, R. G., Kingston, D. G., Jiang, T., Thompson, J. R., and Todd, M. C., 2009, Hydrological modeling of River Xiangxi using SWAT2005: A comparison of model parameterizations using station and gridded meteorological observations: Quaternary International.

Yang, J., Reichert, P., Abbaspour, K. C., Xia, J., and Yang, H., 2008, Comparing uncertainty analysis techniques for a SWAT application to the Chaohe Basin in China: Journal of Hydrology, v. 358, p. 1-23.

Yang, J., Reichert, P., Abbaspour, K. C., and Yang, H., 2007, Hydrological modelling of the Chaohe Basin in China: Statistical model formulation and Bayesian inference: Journal of Hydrology, v. 340, p. 167-182.

Yates, D. N., and Strzepek, K. M., 1998, Modeling the Nile Basin under climatic change: Journal of Hydrologic Engineering, v. 3, p. 98.

Zeleke, G., 2000, Landscape Dynamics and Soil Erosion Process Modeling in the North-Western Ethiopian Highlands, African Studies Series A 16: Geographica Bernensia: Berne.

Zeleke, G., and Hurni, H., 2001, Implications of land use and land cover dynamics for mountain resource degradation in the northwestern Ethiopian highlands: Mountain research and development, v. 21, p. 184-191.

Zhang, X., Srinivasan, R., and Hao, F., Predicting hydrologic response to climate change in the Luohe River basin using the SWAT model.